Regulation of the General Stress Response of *Bacillus subtilis*

Dissertation

zur

Erlangung des akademischen Grades

Doktor-Ingenieur (Dr.-Ing.)

Promotionsgebiet Systembiologie

Fakultät für Informatik und Elektrotechnik

Universität Rostock

vorgelegt von

Ulf W. Liebal, geboren am 15. September 1981 in Magdeburg/Elbe

Rostock/Warnow, 27. Februar 2013

urn:nbn:de:gbv:28-diss2014-0073-2

Erstgutachter:	Prof. Olaf Wolkenhauer	Universität Rostock
Gutachter:	Prof. Rui Alves	Universitat de Lleida
	Prof. Uwe Völker	Ernst-Moritz-Arndt-Universität Greifswald
Tag der Verteidigung:	4. Februar 2013	

Für Uta Nast

The cover picture is the truncated icosahedron by Luca Pacioli, *De divina proportione*, 1509, on page XXIIII. The truncated icosahedron is the geometric structure underlying the stressosome protein complex, and which provides the basis of the cellular automata developed in *Chapter 3* and *Chapter 4*.

Ich wollte ihn auf die Probe stellen: “und was ist Zwei mal Zwei?” Er: “Der Lügner würde behaupten fünf - der Neutrale weder zwei noch sechs - der vorsichtige Esoteriker würde sich äußern: Logarithmus 10 000 oder so.”
“Wie wäre es mit 4”, schlug ich verächtlich vor.
“Das sind die ausgesprochenen Fanatiker. Klavki! Rationalismus ist: Wahrheitskonsum.”

Der Wolkenhändler, Klavki

Errata

The following changes have been applied to the document with respect to the original submission.

Page	Original	Corrected
10	This work has been published in Liebal et al. [2012].	This work has been published in Liebal et al. [2012], and reproduced by permission of the Royal Society of Chemistry.
11	... Tindall et al. [2008] gave a thorough overview of the mathematical approaches.	... Tindall et al. [2008] gave a thorough overview of the mathematical approaches to simulate chemotaxis.
13	The phosphorelay phenotype hub	The Spo0-phosphorelay phenotype hub
16	A more detailed examination of the phosphorelay mechanism...	A more detailed model of the phosphorelay mechanism...
16	The authors examined the steady-state levels of Spo0A-P...	They examined the steady-state levels of Spo0A-P...
16	...and thus unable to measure the 'food per cell'.	...and it would thus be unable to measure the 'food per cell'.
23	...or there are of yet unknown negative feedbacks.	...or there are as of yet unknown negative feedbacks.
34-Table 3.2.	Phosphorylation of RsbR	Phosphorylation of RsbS
38	...it was thus reported by these authors that RsbC and RsbD can sense energy stress.	...it was thus reported by these authors that RsbRC and RsbRD can sense energy stress.
42	Conclusion	Conclusions
45	The multiple RsbR paralogues of *B. subtilis* possess a conserved C-termianl STAS domain	The multiple RsbR paralogues of *B. subtilis* possess a conserved C-terminal STAS domain

Page	Original	Corrected
46-Figure 4.1.	...their organisation as trimer of dimers, a traingle structure.	...their organisation as trimer of dimers, a triangle structure.
63-footnote		The original work of Liebal et al. (2012) is reproduced by permission of the Royal Society of Chemistry.
75	Conclusion	Conclusions
90	U. Liebal ... submitted, 2012a.	U. Liebal ... *BMC Syst Biol*, 7(3), 2013.

Danksagung

Es war eine erfüllende Zeit in Rostock und am Lehrstuhl Systembiologie und Bioinformatik. Diese Möglichkeit verdanke ich Olaf Wolkenhauer, der mir die Gelegenheit und das Vertrauen gegeben hat in seiner Gruppe zu forschen. Ich danke dir für die Freiheit, mit der ich meine, nicht immer zielgerichteten, Ideen verfolgen konnte. Deine Geduld und dein Vertrauen mit meinem 'Verfolgen' waren formend für meine Entwicklung.

Thomas Millat hat die wichtige tägliche Arbeit verrichtet, mich mit der Realität zu verbinden. Deine strengen Anforderungen an eine wissenschaftliche Arbeitsweise waren eine Herausforderung für mich, aber sie haben meine Aufmerksamkeit für das Detail geschärft. Du warst immer erreichbar, und wir konnten über viele Themen diskutieren.

Die Zeit mit Peter Raasch war zu kurz. So viele Themen schwebten zwischen unseren Tischen ... Deine Partikel Simulation ist bisher unerreicht und ein wichtiger Bestandteil meiner Arbeit. Das Orpheusprojekt war leider erfolglos und ich hoffe, dass du ein anderes Rad zur Schwingung findest. Ich hoffe auch wieder einen Tango mit Yvonne Schmitz zu tanzen, doch fürchte ich, dass du nur einfach wieder deinen Kopf wegdrehst, gerade wenn ich dich anspreche. Viele Ulfs gibt es nicht, und dann gleich zwei in einer Gruppe ... ohne unsere Wettstreits wären es einige Schmunzler weniger gewesen. Felix Winter stimulierte die Entwicklung der Zellulären Automaten und ich danke Stefan Pauleweit für die gelungenen Photos der Papierstressosoms.

Herr Uwe Völker hat das Gesamtprojekt aus Greifswald koordiniert. Seine Objektivität, und Geradlinigkeit sind bewundernswert. Die von ihm geleiteten Diskusionen endeten immer in einem konkreten Ergebnis. Die verständnisvolle Art und ruhige Aura von Leif Steil hat die Zusammenarbeit mit ihm besonders angenehm gestaltet.

For a while, I was sitting two armlengths apart from Julio Vera González. It was wonderful to listen to your stories, the revolutions, and conspiracies all around. With Anuradha Chauhan I had the most challenging discussions, but it was good to relax during your group-Yoga initiative. It was very stimulating that each of us, Angie Lao, Xin Lai, and me prepared our theses simultaneously, but more will I remember our tranquil gatherings in the kitchen when time seemed to stop. Praveen K. Sappa and in the beginning Hendrikje Hildisch provided the experiments for my models, resulting in the Chapter 5. Praveen, we had good times on the conferences, I hope we don't get too old for Amsterdam. Newcastle is among the best cities I have seen, but that is for a big part because of Rick Lewis and Jon-Marles Wright. I enjoyed the time there so much, you gave me such a great hospitality! But also in distance, working with you was fabulous, your comments on the

manuscripts were staggeringly precise and your responses rapid. Oscar Kuipers, Imke van Baarle, and Georg Homuth, as well as Anja Möller and Dinto José helped me to improve my manuscripts. I am indebted to helpful corrections on the thesis to Anuradha Chauhan, Wiebke Chemnitz Galal, Sherry Freiesleben, Jiri Jablonski, Thomas Millat, Julio Vera, and Florian Wendland.

Wissenschaft darf nicht im Elfenbeinturm bleiben, und ich bin Wolfang Thiel dankbar, dass wir zusammen einen allgemeinen Artikel an die Zeitungen brachten. Die Bastelkunst der Geigenbauerin Theresa Lücking hat mich auf die Origammitechnik für Ikosaheder aufmerksam gemacht. Das war eine wichtige Ambition für die Entwicklung der Stressosom-Modelle. Die Zeit in Rostock war vorallem auch so schön durch das Musizieren im FSOR. Ich danke Ines Steinhagen, Juliane Werlich, Christina Flägel, Martin Wollmann, Konrad Jakobi für die Vorstandssitzungen und Maria Dreier für das gemeinsame Musizieren am Fagott.

Ich danke meiner Familie für die Unterstützung. Dafür, dass ich bei Familie Schöning entspannen kann, und die Hausmusiken bei Winfried Liebal. Der tiefste Dank geht an Uta Nast-Schneider. Es hat gedauert, bis ich begriff, dass man kann kein Lieblingstier haben kann, da alles ineinandergreift.

Die erstrebenswerte Aufopferung im Professionellen wie im Privaten von Ludwig Nast sind verbunden mit einer sympatischen Ausgeglichenheit, Gutmütigkeit und geistigen Stärke. Es war eines seiner Herzenswünsche die Fertigstellung dieser Arbeit mitzuerleben. Leider blieb Ludwig Nast dazu nicht die Zeit.

Ich danke dem BMBF für die Finanzierung durch die BaCell und BaCell2 SysMO Projekte (FKZ: 0313978 and 0315784).

Abstract

The bacterium *Bacillus subtilis* lives in the environmentally diverse soil habitat. Various stresses challenge *B. subtilis*, and its stressosome is one of the sensors for physical and chemical insults. This pseudo-icosahedral complex is composed of three protein classes: 1) the sensor RsbR, 2) the scaffold RsbS, and 3) the kinase RsbT. Stimulation of the stressosome modifies its phosphorylation patterns and protein interactions, and results in the dissociation of RsbT. Cytoplasmic RsbT activates an additional cascade, ultimately releasing the general stress response transcription factor σ^{B}. Biochemical and molecular biological experiments have identified the reactions and interactions of the proteins, but these techniques are currently unable to identify structure-related functions. By contrast, computational models can consider the geometry of the stressosome, but despite this advantage, no such model exists for the stressosome. Using cellular automata, I introduce here the first computational models for the stressosome. Futhermore, the icosahedral structure enables the construction of a geometric model by modular origami folding that highlights motions within icosahedral structures. The conditions associated with the release of σ^{B} are amenable to ordinary differential equation models, which I used to reproduce the dynamics of a reporter protein. My analysis shows that different stimuli are processed identically, suggesting their identical perception. Theoretical reproduction of the dynamics of a reporter protein show that the proteolytic decay of the reporter protein is part of the σ^{B}-mediated general stress response, which was confirmed by subsequent experiments. The thesis confirms the activation effect of RsbR-P on the kinase activity of RsbT and the preferential dephosphorylation of RsbS-P over RsbR-P by RsbX. The Collapse Hypothesis suggested in this thesis, concerns information transmission between RsbR and RsbT and suggests a coordinated motion of three dimers. The modelling process emphasizes an activation loop for RsbT that disconnects the duration of response from that of the stimulus. Overall, the new insights enhance our understanding of the σ^{B}-mediated general stress response and raise our awareness of the environmental integration of *B. subtilis*.

Zusammenfassung

Das Bakterium *Bacillus subtilis* lebt im Boden und ist dort verschiedenen Umweltreizen ausgesetzt. Ein Teil dieser Reize wird durch das Stressosom aufgenommen. Diese komplexe Struktur von pseudo-ikosahedraler Geometrie besteht aus drei Proteinklassen: 1) dem Sensor RsbR, 2) dem Gerüstprotein RsbS und 3) der Kinase RsbT. Durch Stimulation des Stressosoms verändert sich sein Phosphorylierungsmuster, was die Interaktionen der Proteine verändert und zur Dissoziation von RsbT führt. Das frei-werdende, cytoplasmatische RsbT aktiviert eine weitere Signalkaskade, die schließlich zur Freisetzung des Transkriptionsfaktors σ^{B} und zur allgemeinen Stressantwort führt. Durch biochemische und molekularbiologische Ansätze konnten die Reaktionen und Interaktionen aufgeklärt werden, jedoch sind diese Techniken ungeeignet, Informationen zu strukturbezogenen Funktionen zu liefern. Obwohl im Gegensatz mathematische Modelle die Geometrie des Stressosoms berücksichtigen können, gab es bisher noch kein Modell zum Stressosom. In dieser Arbeit stelle ich die ersten rechnerbasierten Modelle zum Stressosom auf Basis zellulärer Automaten vor. Zusätzlich kann dessen ikosahedrale Struktur durch ein geometrisches Model auf Basis von Origammi-Falttechniken reproduziert werden, was Informationen zu Domänenbewegungen liefert. Die Bedingungen der Freisetzung von σ^{B} erlauben die Anwendung von Differentialgleichungen, mit denen ich die Dynamik eines Reporterproteins nachvollziehe. Meine Analysen zeigen, dass unterschiedliche Signale identisch verarbeitet werden, was nahelegt, dass diese Signale auch identisch aufgenommen werden. Die theoretische Reproduktion einer Reporterproteindynamik zeigt, dass der proteolytische Abbau des Reporterproteins Teil der σ^{B} induzierten allgemeinen Stressantwort ist, was durch nachfolgende Experimente bestätigt wurde. Die vorgestellte Kollapshypothese beschreibt den Informationstransfer zwischen RsbR und RsbT, und legt eine koordinierte Bewegung von drei Proteindimeren nahe. Die Modellierungsarbeiten verdeutlichen eine Aktivierungsschleife von RsbT, die eine Trennung der Dauer der Stressantwort von der Signaldauer bewirkt. Damit stellt diese Arbeit neue Erkenntnisse zur σ^{B}-induzierten allgemeinen Stressantwort vor und vertieft unser Verständnis der Umweltanpassung von *B. subtilis*.

Theses

Ulf W. Liebal, Regulation of the general stress response of *Bacillus subtilis*

Major new insights

1. Different stressors activate the stressosome signalling protein complex identically. Thus, according to the stressosome, a stress of 3% ethanol is as stressfull as 488 mM of NaCl.

2. Structures of truncated icosahedra (vertices as proteins) allow a characteristic collapse of three dimers. This collapse hypothesis of stressosome activation explains the information transfer from the stress sensor to the output protein.

3. Discrimination of differential equation models of the general stress response suggests a protease that degrades the reporter protein. This protease model reproduces the stimulus-independent transient activation of the stress response.

Independent confirmation of knowledge

1. Geometric models show that truncated icosahedra are optimally constructed from dimers. In these models, sixty tetrahedra coincide in their structural arrangement with the arrangements of proteins in the stressosome.

2. A cellular automaton confirms the stimulating effect of phosphorylated RsbR on the kinase activity of RsbT by reproducing different experimental data sets.

3. The fit of the cellular automaton of the stressosome to experimental data is optimal, if the phosphatase RsbX is specific for RsbS-P during low and medium stress, and dephosphorylation of RsbR-P is magnitudes lower.

4. Stress reception of the stressosome leads to structural changes and the activation of a signalling molecule. The slow deactivation of the stressosome repeatedly activates the signalling molecule and decouples the reponse from the signal duration.

Abbreviations

AbrB	ambiactive repressor
AprE	alkaline protease
B. subtilis	*Bacillus subtilis*
Bpr	bacillopeptidase
CCMV	cowpea chlorotic mottle virus
Che(A/B/C/D)	chemotaxis proteins
Clp(C/P)	caseinolytic protease
CodY	control of *dpp*
Com(A/K/P/S/X)	competence proteins
cryo-EM	cryo electro-microscopy
Deg(S/U)	degradation enzyme regulation
E. coli	*Escherichia coli*
EtOH	ethanol
Fli(Y/M)	flagella rotation proteins
Fts(W/Z)	filamentous temperature sensitive
Hpr	histidine containing protein
IPTG	isopropyl β-D-1-thiogalactopyranoside
Kin(A/B/C/D/E)	sensor histidine kinase
lacZ	β-galactosidase mRNA
LOV domain	light-oxygen-voltage
MCP	methyl accepting chemotaxis protein
MecA	medium-independent expression of competence
MgsR	modulator of general stress response
MU	Miller units
NMR	nuclear magentic resonance
OD	optical density
ODE	ordinary differential equation
Opp	oligopeptide permease

Phr(A/C)	phosphatase regulator
Rap(A/C)	receptor aspartyl phosphatase
Rsb(R/S/T/U/V/W/X)	regulator of σ^{B}
ROS	reactive oxygen species
Sda	suppressor of *dnaA*
Sin(I/R)	sporulation inhibition regulation
Spo0/SpoII	sporulation proteins
Spx	suppressor of *clpP* and *clpX*
STAS domain	sulfate transporter and anti-sigma factor antagonist
UV light	ultraviolet light

Contents

Chapter 1

Introduction

Knowledge of bacteria equals knowledge of life. The eminent microbiologist Moselio Schaechter muses in his research blog on the effect of the extermination of multi-cellular life by an asteroid [Schaechter 2012]. The community (presumably microbiologists) agrees that prokaryotes would experience comparably minor effects, and over time, a multi-cellular biosphere, as we witness today, would eventually re-evolve. Life on earth is predominantly prokaryotic (bacteria and archaea) in terms of biomass and environmental distribution [Whitman et al. 1998]. Bacteria are virtually everywhere: they have colonized the hydrothermal vents in the deep sea [Hugenholtz et al. 1998], the dry and frigid valleys in Antarctica [D'Amico et al. 2006], and even the metazoan bodies, where they are pursued by the immune system [Willing et al. 2011]. Indeed, given this wide distribution and environmental tolerance, an asteroid impact would have little effect on the bacterial world. What is the source of the bacterial success? Among the characteristics of bacteria is the ability to survive in harsh environments, as well as the capacity to respawn rapidly in favorable conditions. This thesis focuses on the bacterial stress response, particularly the molecular mechanisms that allow them to adapt to environmental challenges. Of course, the number of bacterial species is innumerable and all are subjected to different challenges so that any choice might appear arbitrary. However, only a few species are accessible to lab experiments and are therefore characterised well enough to provide the requisite knowledge for mathematical modelling.

1.1. The model organism Bacillus subtilis

One of the outstanding bacterial species in terms of knowledge and experimental accessibility is *Bacillus subtilis*. This organism belongs to the Firmicute phylum with positive Gram staining and low G-C, and is a member of the *subtilis-licheniformis* group in the *Bacillus* genus [Barbe et al. 2009; Rey et al. 2004]. Members of this group

are heterotrophic and can be found in diverse environments such as the soil, plant roots, leaves, bird feathers, and the gastro-intestinal tract of animals [Barbe et al. 2009; Earl et al. 2008; Rey et al. 2004]. The ubiquitous presence of this bacterium is due to its ability to form spores, highly resistant dormant cells [Earl et al. 2008]. Another distinguishing phenotype of *B. subtilis* is competence that enables the organism to assimilate and integrate the DNA of closely related Bacillus strains. In addition to enabling the exchange of mutational innovation in a colony during stress, competence has been particularly useful for the genetic manipulation of *B. subtilis*. The ease of cultivation, genetic accessibility, and non-pathogenic nature of *B. subtilis* combined with its agricultural applicability makes it one of the best-studied model organisms, second only to *Escherichia coli*. Indeed, the complete genomes of both these outstanding model organisms were published in 1997 after 10 years of sequencing [Blattner et al. 1997; Kunst et al. 1997]. This wealth of genomic information spurred the identification of transcriptional and regulatory networks [Fadda et al. 2009; Goelzer et al. 2008]. In *Chapter 2*, I provide a review of how mathematical modelling has been used to harvest this knowledge and how computational approaches have contributed to our understanding of signalling.

1.2. Phenotypes for environmental adaptation

***B. subtilis* is equipped with several behavioural strategies, most notably motility, matrix production, competence, sporulation, and the general stress response [López et al. 2008].** This diversity of response strategies reflects the diversity of the environmental changes experienced by the organism. *B. subtilis* is subjected to relatively abrupt temperature variations of up to 20 °C during the day-to-night shifts, and the summer/winter seasons impose an enormous temperature difference of 40 °C. When rain showers flood the surroundings, the osmotic gradient between cell and soil can increase perilously, leading to osmotic-driven water inflow, swelling, and eventually cell disruption. To maximise survival during these challenges, a *B. subtilis* colony becomes phenotypically heterogeneous, with the organism beting on the best response [Dubnau and Losick 2006; Veening et al. 2008a,c]. This phenotypic diversity was visualised for colonies in Petri dish micro-environments, and the illustration in Figure 1.1 summarizes the findings [López and Kolter 2009; Vlamakis et al. 2008]. This illustration represents the locations of the four major phenotypes of growth of *B. subtilis* after about 70 h of incubation.

The motility phenotype is characterised by cells that are loosely integrated into an extracellular matrix. These cells produce flagella and can move to locations with better conditions. Movement is energy intensive and thus sufficient food sources must be available [López et al. 2008; Shioi et al. 1980]. Figure 1.1 simplifies the findings of Vlamakis et al. [2008] who found motility predominantly at locations rich in food, such as the colony-

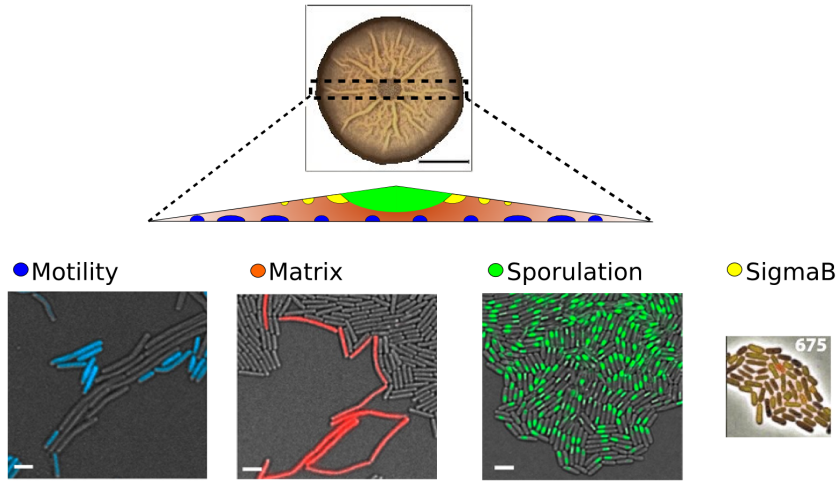

Figure 1.1.: Location-dependent phenotypes of a *B. subtilis* biofilm in a Petri dish. The photo at the top depicts a biofilm after 72 h of incubation (adapted from [Vlamakis et al. 2008]; black scalebar: 1 cm). The spatial location of the phenotypes is taken from López and Kolter [2009] with the exception of the σ^B, which is hypothetical. The microscopic images of motility, matrix, and sporulation are extracted from López et al. [2008], whereas that of σ^B is adapted from Locke et al. [2011].

medium interface. By contrast, matrix producing cells are immobile, they excrete polymers to provide the colony with integrity [Vlamakis et al. 2008]. The illustration in Figure 1.1 indicates that the matrix producers are predominantly distributed in the colony center [Vlamakis et al. 2008]. In the colony, matrix production is a requisite for the development of sporulation [Aguilar et al. 2010]. Sporulation is induced following severe starvation and high cell densities [Sonenshein 2000]. The resulting endospores are small dormant cells surrounded by a mother cell, as shown by the microscopic images from López et al. [2008] in Figure 1.1. The fourth phenotype shown in Figure 1.1 is the general stress response mediated by the transcription factor σ^B. Strictly, it is not a separate phenotype, as cells with activated σ^B are difficult to distinguish from those with silenced σ^B. However, σ^B inhibits other phenotypes like sporulation [Reder et al. 2011] and there are as many genes activated by σ^B as for chemotaxis or matrix producers [Helmann et al. 2001; Nannapaneni et al. 2012; Petersohn et al. 2001; Price et al. 2001]. σ^B is activated by various non-fatal stresses like ethanol, salt, or UV- and infrared light [Hecker et al. 2007; van der Horst et al. 2007]. While there are no studies regarding the localisation of σ^B expression in a colony, I added putative locations based on the available knowledge regarding σ^B activation. The upmost region appears likely, as the light intensity and oxygen concentration is highest there, and the food source is far, but the cells are not as stressed as in the center of the colony where sporulation dominates.

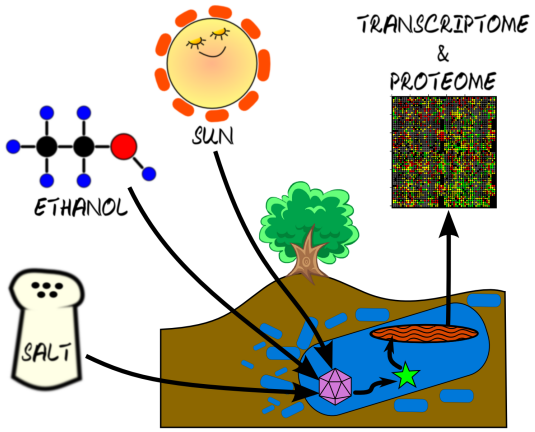

Figure 1.2.: *B. subtilis* (blue rods) is abundant in the soil and needs to adapt to a variety of challenges. The stressosome (pink icosahedron) is sensitive to light, ethanol, and salt stresses, among others, and activates the transcription factor σ^B (green star). σ^B induces expression of stress-protective genes (red, stripe-filled oval) with an eventual adaptation to the challenge.

1.3. The σ^B-induced general stress response

Environmental changes usually trigger alterations in the proteome and changes in the phenotype to ensure the optimal subsistence of an organism (Figure 1.2) [Buescher et al. 2012; Nicolas et al. 2012]. The σ^B response is activated in response to non-life-threatening conditions. Two proteins, RsbU and RsbP, feed either environmental or energy stress signals to the σ^B network [Völker et al. 1995b]. This thesis focuses on σ^B activation by environmental stresses via RsbU. In this context σ^B activation can be summarized by the following four steps [Hecker et al. 2007]:

1. Activation of the stressosome,
2. Release of an enhancement protein,
3. Release of the transcription factor σ^B,
4. Adaptation of the organism.

The stressosome of Step 1 is a signalling hub, targeted by different stimuli [Marles-Wright and Lewis 2007]. However, with the exception of light, the environmental stimuli are believed to activate intermediary sensors, which then transmit the signal to the stressosome [Marles-Wright et al. 2008]. These sensors stimulate phosphorylation reactions on the stressosome [Gaidenko et al. 1999], causing the enhancer protein RsbT to dissociate from the stressosome and become available in the cytoplasm (Figure 1.3) [Marles-Wright and Lewis 2007]. The stressosome is a highly symmetric protein complex with proteins in static

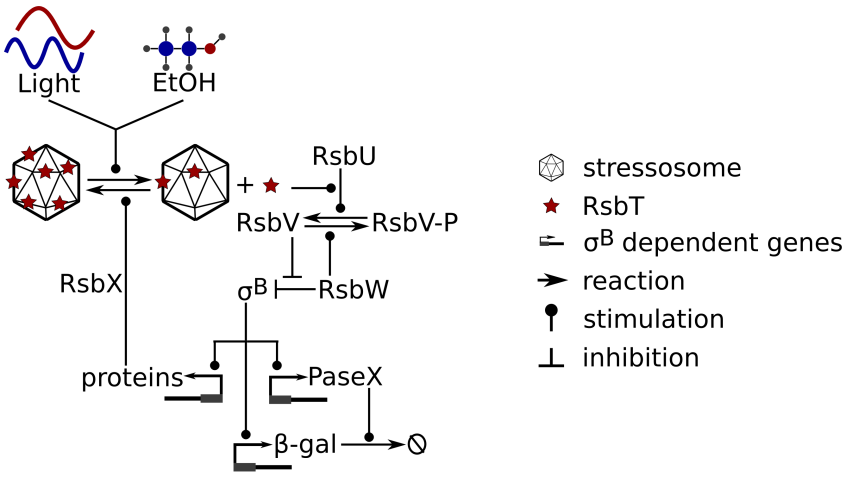

Figure 1.3.: Scheme of the investigated signalling pathway of the σ^B-induced general stress response. Light and ethanol (EtOH) induce the dissociation of the enhancement protein RsbT (star) from the stressosome (icosahedron). Cytoplasmic RsbT activates RsbU which in turn dephosphorylates RsbV. Desphosphorylated RsbV induces the release of the transcription factor σ^B from RsbW. Subsequently, σ^B stimulates the expression of several proteins, among them RsbX, a phosphatase that resets the stressosome to its pre-stimulus level, β-galactosidase, a protein used to monitor σ^B activity, and PaseX, an unidentified protease of β-galactosidase found in the context of this thesis.

positions. Cellular automata are ideal to represent these properties, as they can include the spatial information. Kinetic modelling is inferior for the stressosome, because is requires more complex partial differential equations to represent space, and each protein interacts with a limited number of proteins that may or may not be phosphorylated; therefore, the phosphorylation status cannot be approximated by a real number. Current experimental techniques are ill-suited to characterise the effect of interactions in a given geometric structure. This hinders the process of formulating and testing mechanistic hypotheses. An alternative way is to generate hypotheses via computational modelling and to probe their effects *in silico*. In *Chapter 3*, I introduce a model of stressosome activation that is based on the dynamics of single proteins in the stressosome. Although the proteins form dimers, their treatment as monomers in the simulation allows for a broad reproduction of published experimental data. In a second model, introduced in *Chapter 4*, I assume triangles of dimers as the basic functional unit because this structure appears to be an important geometric property of truncated icosahedra. These models integrate the current knowledge of reactions in the stressosome and allow the testing of new hypotheses.

σ^B, and the related SpoIIA network, are regulated by a characteristic mechanism called 'partner switching' [Hecker and Völker 2001; Hecker et al. 2007; Price 2002]. The partner switching occurs twice during signal transduction in σ^B activation: first, RsbT switches

between its partners RsbS in the stressosome and RsbU; second, RsbW switches between its partners RsbV and σ^B. Indeed, both partner switching modules are related; RsbT is homologous to RsbW, and RsbS is homologous to RsbV [Yang et al. 1996]. Figure 1.3 reflects the reactions of the general stress response in greater detail. During stress-free conditions, the enhancement protein RsbT (star) is inhibited by its partner RsbS in the stressosome (icosahedral icon), and the transcription factor σ^B is inhibited by its partner RsbW. Upon stress stimulation, e.g. by light or ethanol, RsbT dissociates from RsbS into the cytoplasm and associates with its second partner, the phosphatase RsbU. RsbU is activated by RsbT, resulting in the increased dephosphorylation of RsbV. Because non-phosphorylated RsbV binds very efficiently to RsbW, RsbW switches σ^B for RsbV. This partner switch releases σ^B and enables the re-organisation of the proteome.

A change in the environment is usually accompanied by a change in cellular constitution [Gottesman 2003]. New proteins are transcribed and replace previous ones. The transcriptional activity of σ^B is measured using a reporter gene with a promoter containing a σ^B binding sequence. One of the most common reporter genes is *lacZ*, encoding the β-galactosidase protein. However, the *B. subtilis* β-galactosidase is not σ^B dependent. To enable its use, the promoter of the σ^B-dependent gene *ctc* was cloned upstream of a heterologous *lacZ* [Benson et al. 1989]. The antagonistic process to transcription is proteolysis, an essential ingredient to adjust the cellular proteome, especially during stress. Price et al. [2001] detected the up-regulation of five proteases following the stimulation of the general stress response by ethanol and salt. Later, ClpP was added to the list of σ^B affected proteases [Reeves et al. 2007]. Analyses of experimental data become problematic if the reporter protein is subjected to both synthesis and proteolysis.

However, the joint effects of synthesis and proteolysis on σ^B-induced β-galactosidase expression is the ultimate conclusion in a series of experiments described in *Chapter 5*. These experiments were performed in a strain in which the expression of σ^B can be externally controlled by the addition of isopropyl β-D-1-thiogalactopyranoside (IPTG, a non-metabolizable sugar derivative). Because IPTG is a stable chemical compound, a continuous expression of the σ^B-dependent β-galactosidase reporter gene was expected. Strikingly, β-galactosidase activity decreases at a time during which IPTG is still available. The timing and rate of the decline both depend upon the ambient IPTG concentration. After formulating different hypotheses and testing them *in silico*, it was found that only a model representing the degradation of β-galactosidase by a σ^B-dependent protease could conclusively reproduce the data. Subsequent experiments confirmed this σ^B-related instability, though the protease remains unidentified.

B. subtilis is well-studied, and has stimulated the application of mathematical modelling; I discuss the diversity of mathematical studies related to signalling in *Chapter 2*. The intriguing environment-specific phenotypes of *B. subtilis* are difficult to explain by reducing the arguments to only a few molecular players; therefore mathematical modelling and simulation played an important role early on. Sporulation, competence, and also chemotaxis are prominent examples of remarkable developmental and signalling processes apart from which the general stress response appears unspectacular. This moderate phenotype change is probably the reason for the late discovery of the σ^{B}-mediated general stress response in the early 90's of the past century [Benson and Haldenwang 1992; Kalman et al. 1990], with major insights into the mechanism being achieved only in the first years of the 21st century [Hecker and Völker 2001; Price 2002]. Mathematical modelling of σ^{B} began in 2007 [Igoshin et al. 2007], with a second model published in 2011 [Locke et al. 2011]. The stressosome is a fascinating complex; however, details of its construction and function remained vague even longer, until 2008, when its structure was eventually solved [Marles-Wright et al. 2008].

1.4. The truth of numbers

In the opening quote of this thesis the writer Klavki asks: "what is two times two?" His friend replies, "the liar would claim it to be five - the neutral one would say neither two nor five - the cautious esoteric would offer something like the logarithm of 10 000." Klavki then suggests '4', but the friend reacts with a scornful remark. What happened? Imagine that '4' is our observation and we want to explain its origin. We start to prepare a model, for example, '$2 + 3$', and simulate it using the '=' sign. The result for that model is '5', which is false, as also stated in the quote. We improve our model to '$2 + 2$', which gives us '4'. Although this is correct, it does not *truly* explain our data. Presumably, we get new insights, and perhaps we can better predict experimental results, but, just like any model, '$2 + 2$' is a simplification, and an abstraction. We can identify an infinite number of mathematical expressions/models, such as '$log_{10}\,10\,000$', that suit our observation(s), but mathematics is just the tailor to coat reality [Leach 2011]. The quote implies that anyone who is content with a correct result will miss the fantastic part. An opposing but equally esoteric view purports the mathematical universe hypothesis: every piece of reality is math and we are getting increasingly better in approximating it [Tegmark 2008]. Whichever claim approximates reality closer, 'mathematics is biology's next microscope, only better' [Cohen 2004].

Like many interdisciplinary sciences, systems biology was not invented but instead it developed over a long period. Systems biology draws heavily on enzyme kinetics; thus, the mathematical interpretations of enzyme catalysed reactions can be regarded as its

first step. One of the most celebrated enzyme equations is the Henri-Michaelis-Menten equation, formulated in its most general representation by Briggs and Haldane in 1925 [Briggs and Haldane 1925]. The theory of enzyme activity expanded to include inhibition and activation effects and also the description of multi-enzyme complexes and allostery using the Monod-Whyman-Changeaux (Concerted) or the Koshland-Nemethy-Filmer (Sequential) models [Bisswanger 2002; Segel 1993]. The term 'systems biology' was coined in 1968 by Mesarović [1968]. Both enzyme kinetics and systems biology study temporal changes in variables of interest. In contrast to specific enzyme kinetics, systems biology considers a network of interacting variables [Wolkenhauer and Mesarović 2005]. These different interactions can be combined in different motifs and associated with different dynamic effects [Tyson et al. 2003], but they critically depend on the supplied parameter values [Adiwijaya et al. 2006].

Prokaryotes feature some of the most successful applications of systems biology in terms of methodology and experimental reproduction. A prime example is *E. coli*, very likely the best studied organism. Our knowledge of transcriptional regulation dates back to Jacob and Monod [1961] and their study of the *lacZ* operon in *E. coli*. This system is so well known that it is routinely used as a reporter protein to monitor promoter or transcription factor activity [Serebriiskii and Golemis 2000], as in the case of the general stress response used throughout this thesis. The *lacZ* system remains a source of wonder due to, for example, its ability to display bistability [Santillán and Mackey 2008], the effects of noise and its role in population heterogeneity [Roberts et al. 2011], and the unanticipated degradation of β-galactosidase that I report in *Chapter 5*. Knowledge of the metabolism of *E. coli* was central in the development of flux balance- and constraint-based model approaches [Reed and Palsson 2003; Varma and Palsson 1994], culminating in the development of the *E. coli* genome-scale metabolic network [Edwards and Palsson 2000] and eventually that of *B. subtilis* [Oh et al. 2007]. Signalling was investigated early on in bacteria because the topologies appear simpler. A good example is chemotaxis, the directed movement of flagellated bacteria in gradients of substrates or repellents. The signalling for this process is based on sensors arranged as hexamers on the cell membrane, and involves phosphorylation/dephosphorylation cycles and allosteric interactions. Tindall et al. [2008] wrote a thorough review on mathematical approaches to chemotaxis, and in *Chapter 2*, I survey the applications of these approaches to *B. subtilis*. The structural complexity of chemotaxis is similar to that of the stressosome. Both contain hexameric structures, and allosteric interactions are likely to play important roles in both, as I discuss in *Chapters 3* and *4*. The signalling in chemotaxis is based on two-component systems (TCS). TCS are long been known as bacterial signalling mechanisms connecting the environment to gene expression [Mitrophanov and Groisman 2008]. A good amount of knowledge about dynamic properties of the TCS was generated by mathematical analysis

[Alves and Savageau 2003; Igoshin et al. 2008; Kierzek et al. 2010; Mitrophanov et al. 2010]. In this thesis, I focus on the lesser known partner-switching mechanism for gene expression control.

1.5. Aims and outline

A sizeable number of bacteria organise the stress response using σ^B [de Been et al. 2011; Hecker et al. 2007; Pane-Farre et al. 2005]. Among them are human pathogens such as *Listeria monocytogenes*, in which the expression of virulence genes is reported to be controlled by σ^B [Shin et al. 2010; Stavru et al. 2011]. A better understanding of σ^B will also shed light on the activation of sporulation because 1) a central mechanism of sporulation (SpoIIA) functions via a σ^B-like partner switching mechanism [Kalman et al. 1990], and 2) the activation of σ^B inhibits sporulation [Reder et al. 2011]. It is clinically important to control sporulation, as the virulence of many pathogens, e.g. *Bacillus anthracis*, is spore-associated.

Two limitations challenge the full understanding of the σ^B network: 1) the sensitivity of reactions of the stressosome with respect to the structure, and 2) the almost complete reliance on *lacZ* reporter fusions. Relationships between structure and reaction dynamics are hard to elucidate using biochemical, molecular, or microbial experimental techniques; therefore, knowledge is also limited. Systems biology is a suitable way to complement deficiencies in experimental approaches because it enables us to formulate hypotheses about interactions and to predict their measurable differences. The reliance on the β-galactosidase reporter system is understandable, given its experimental ease. If the reporter system used is itself regulated by the transcription factor under study, then care must be taken in the analysis of results. The results presented in this thesis are listed in detail below.

- *Chapter 2*, entitled 'Models for *B. subtilis*', offers a survey of mathematical models dealing with environmental signalling, in order to enable the integration of my research into the field. The overview illustrates the routine use of *B. subtilis* for modelling, but also indicates the low coverage of the σ^B module and the absence of models for the stressosome. This work is adapted from the publication Liebal et al. [2010].

- *Chapter 3*, entitled 'Stressosome simulation I: Monomer interactions', focuses on the impact of the stressosome structure on the initial activation of the general stress response. No reliable information is available about the interactions of monomers in the stressosome. I modelled different hypotheses concerning monomer interactions

computationally, and one of these hypotheses reproduces a large number of published experiments. This work is being published as Liebal et al. [2013].

- *Chapter 4*, entitled 'Stressosome simulation II: Shape transitions', introduces the hypothesis that molecular movements within the structure play key roles in the activation of the signalling events. Different model types (geometric-paper, particle-dynamics, and cellular-automaton) highlight preferred domain-movements and their effects on the activation dynamics of the stressosome.

- *Chapter 5*, entitled 'σ^{B}-induced proteome reorganisation', presents a successful model-experiment-cycle. Three models, based on ordinary differential equations, are compared regarding their consistency with the experimental observations. The conclusions of the simulations were confirmed by subsequent experiments. This work has been published in Liebal et al. [2012], and reproduced by permission of the Royal Society of Chemistry.

- *Chapter 6*, entitled 'Final remarks', briefly summarizes my results and places them in the context of research into the general stress response, and discusses their contribution in our understanding of signalling and environmental responses.

Figures and Matlab files are included in a separate CD, and available for download in the Resource section of `www.sbi.uni-rostock.de`, named 'Liebal_thesis-data.zip'

Chapter 2

Mathematical models for *Bacillus subtilis*

In this chapter, I summarise recent results and trends in the modelling of environmental signalling systems in *B. subtilis*. My objective is to show how mathematical modelling was used to provide a better understanding of cellular responses. *B. subtilis* is a well characterized prokaryote and serves as a model organism for Gram-positive bacteria. Substantial information has been gained from studies with *B. subtilis* regarding the organisation of bacterial life cycles. The knowledge gained in these studies enabled attempts of mathematical modelling of cellular processes. I have summarized this progress recently and this chapter is modified from this publication [Liebal et al. 2010]. Particularly during the last decade, there has been increased interest in systems biology, a discipline at the interface of experimental approaches, mathematical modelling, and computer simulations [Wolkenhauer et al. 2003]. However, Bacilli have been investigated in theoretical biology for a long time. In the 1970s, Sargent compared different models for the control of cell length [Sargent 1975], which have since then been further refined (e.g. Grover et al. [2004]; Koch [1992]). Espinosa et al. [1977] examined the acquisition of competence in cultures, while Jeong et al. [1990] presented a mathematical model for growth processes including sporulation and central metabolism.

2.1. Regulation of chemotaxis

The chemotactic behaviour of various organisms has been studied intensively and Tindall et al. [2008] gave a thorough overview of the mathematical approaches to simulate chemotaxis. Chemotaxis was first studied in *E. coli*, and the proteins involved in this process are conserved in *B. subtilis*, too [Garrity and Ordal 1995]. However, the mechanisms of chemotaxis are fundamentally different between the two organisms [Bischoff and Ordal 1991; Rao and Ordal 2009]. Figure 2.1 outlines a simplified mechanism of chemotactic signalling in *B. subtilis*. Signalling is based on methylation and

phosphorylation reactions and includes the proteins CheR, CheB, CheA, and CheY. Ligand binding to the receptor, the methyl-accepting chemotaxis protein (MCP), stimulates methylation of MCP by CheR. This reaction is antagonised by CheB. Methylation leads to the activation of CheA which in turn phosphorylates CheY (CheY-P). CheY-P binds to the flagellar motor protein FliM and reverses the spin of the flagellum from a clockwise to a counter-clockwise rotation [Garrity and Ordal 1995]. The switching of the flagellar rotation is associated with a transition from an erratic tumbling, to the directed movement along the concentration gradient of the extracellular ligand. *E. coli*, by contrast, performs tumbling for the counter-clockwise flagellar rotation, but smooth runs during clockwise rotation [Garrity and Ordal 1995]. The main phosphatase of CheY-P is FliY, which is located at the base of the flagellum. A competing phosphatase is the CheC subunit of the CheCD heterodimer [Kristich and Ordal 2002]. The CheD subunit in the dimer deaminates a glutamine residue of MCP and thereby increases CheA-MCP affinity [Kristich and Ordal 2002]. An interesting property from the modelling perspective is the adaptivity of the chemotactic response, by which the tumbling frequency will resume its pre-stimulus activity when the ligand level stays constant.

Rao et al. [2004] presented a mathematical model that includes the signalling mechanisms of the sensor based CheY phosphorylation and the motor-based CheY-P dephosphorylation. The authors assumed a mechanism by which CheY-P enhances the transition of an active to an inactive receptor conformation to explain adaptivity in *B. subtilis*. Rao et al. [2004] used published data on *cheBCDR* quadruple mutants to evaluate the model. These mutants display a characteristic but unexpected oscillation of the rotational phenotype. Rao et al. [2004] argue that the oscillation might be caused by a positive feedback between the stimulation of CheA phophorylation by CheV and a negative feedback by the inhibition of CheA by CheY-P. Furthermore, the authors explain the population heterogeneity with the sensitivity of the system to CheV. Variations in the concentration of CheV by just a factor of two can already lead to oscillations. Rao et al. [2004] concluded that the *B. subtilis* system is more robust than the *E. coli* system, since CheY-P steady-state levels and the adaptation time have a higher resilience to concentration changes of CheB and CheR. Although the regulation of the chemotactic systems of *B. subtilis* and *E. coli* differ, the motility of both organisms is similar in effectiveness over five orders of magnitude of stimulus concentration [Rao et al. 2004].

Interestingly, the chemotactic receptors are located at the poles, while the flagella are evenly distributed on the cell surface. The signalling molecule CheY-P has to bridge the distance from the poles to the flagellum motor [Szurmant et al. 2003]. Although the switching decision at a given time is stochastic, the frequency of switching is a crucial parameter in controlling motility and is ultrasensitive to the concentration of CheY-P [Rao et al.

2005]. Potential spatial gradients of CheY-P concentration could interfere with chemotaxis because motors receive conflicting signals. Rao et al. [2005] compared protein localisation in *B. subtilis* and *E. coli* using reaction-diffusion equations. The *E. coli* phosphatase of CheY-P is located at the chemosensing receptor, while the *B. subtilis* phosphatases are located at the receptor (CheC) as well as the flagellum motor (FliY) [Szurmant et al. 2003]. The model showed that *E. coli* establishes a homogeneous CheY-P concentration throughout the cell, because kinase and phosphatase are located close to each other. By contrast, the model predicted a linear decrease of *B. subtilis* CheY-P concentration with increasing distance to the receptor. Moreover, simulations for *B. subtilis* indicated the presence of circular concentration gradients at each motor base. The authors speculated that the phosphatase network of *B. subtilis* optimises signal processing of both membraneous and soluble receptors, similar to what has been shown for aerotaxis [Hou et al. 2000; Rao et al. 2005].

2.2. The Spo0-phosphorelay phenotype hub

The Spo0 phosphorelay is the molecular basis for various phenotypic adaptation reactions such as competence, motility, biofilm formation, and cannibalism or the return to vegetative growth [Fawcett et al. 2000; Fujita et al. 2005; López et al. 2008]. The five histidine kinases, KinA, -B, -C, -D, -E, are the sensor proteins that activate the Spo0 phosphorelay. Various signals, such as nutritional stress, cell density, Krebs cycle (TCC), DNA damage, and presence of extracellular matrix in biofilms [Aguilar et al. 2010; Claverys and Håvarstein 2007] trigger the transfer of a phosphate group from the kinases to the Spo0F protein [Errington 2003; Piggot and Hilbert 2004; Sonenshein 2000]. The phosphate group on Spo0F is then relayed to Spo0B and Spo0A. Phosphorylated Spo0A (Spo0A-P) is the response regulator that directly or indirectly controls the expression of over 500 genes [Fawcett et al. 2000]. The Spo0A-P regulated genes can be classified according to the affinity of their promoter region to Spo0A-P [Fujita et al. 2005]. Promoters with high affinity are activated at early stages of phosphorelay activation, among them genes associated with competence, cannibalism and biofilm formation, while promoters with low affinity are only activated, once sufficiently high levels of Spo0A-P accumulate, among them sporulation genes like the *spoIIA* operon [Fujita et al. 2005].

Various groups attempted to model the processes outlined above because of the well-characterized protein interaction network and the large body of mostly qualitative experimental data. Due to the complexity of the phosphorelay network, a prediction of its behaviour is difficult without the help of computational analysis. While Jabbari et al. [2010] focused on the effects of population size, nutrient availability, and DNA integrity to

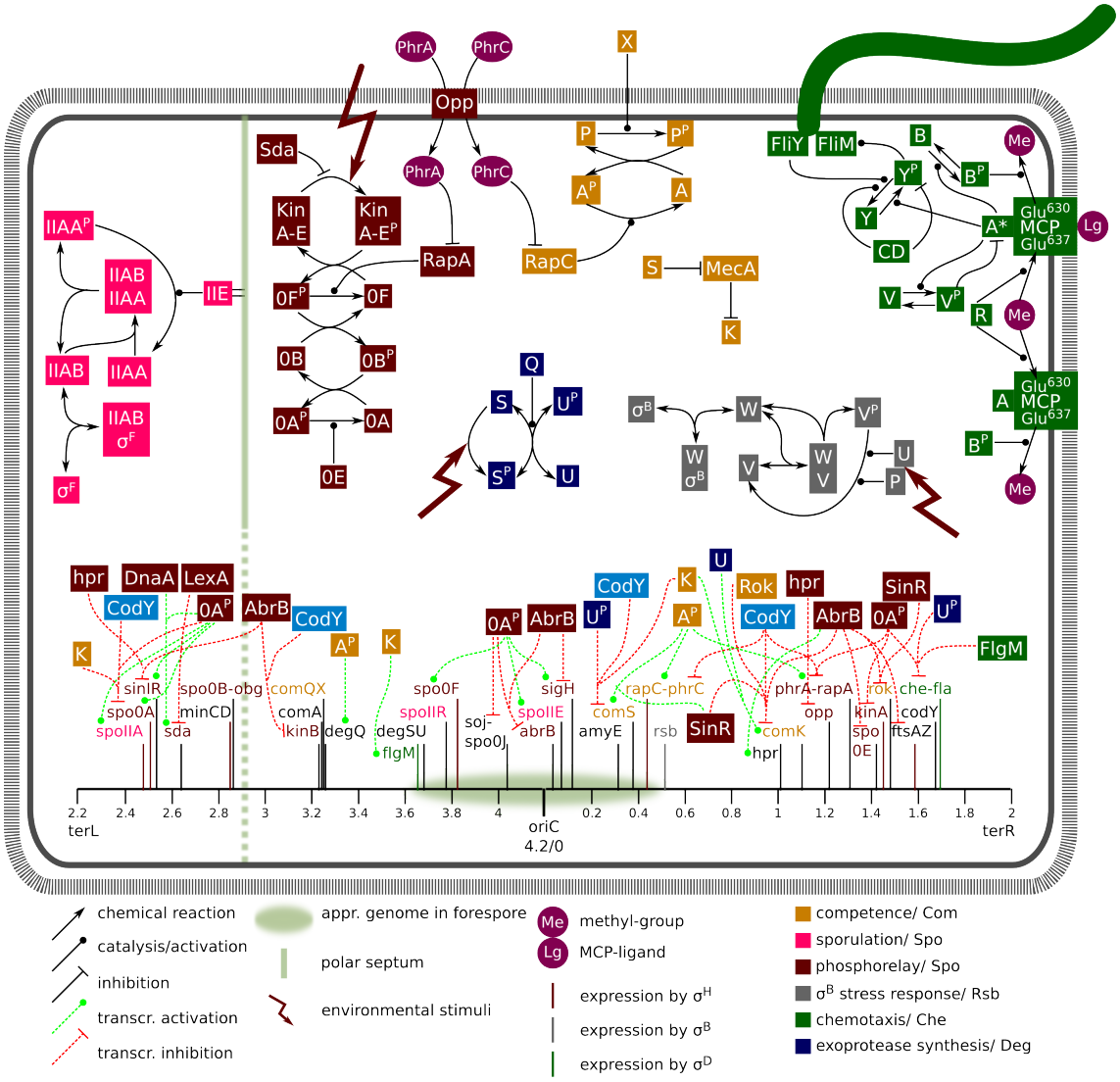

Figure 2.1.: Reaction diagram for the main signalling cascades in *B. subtilis*. The figure shows the signal transduction that leads to switching of flagella rotation after binding of a ligand (Lig) (green) [Rao and Ordal 2009], regulation of competence development (yellow) [Hamoen et al. 2003], the switch of the response regulator DegU to DegU-P (dark blue) [Murray et al. 2009], activation of σ^B-mediated general stress response (grey) [Hecker et al. 2007], phosphorylation of Spo0A via the Spo0 phosphorelay (dark red) [Piggot and Hilbert 2004] and the reactions in the SpoIIA network towards commitment to sporulation (pink) [Errington 2003]. The upper part shows only interactions in the cytoplasm while the lower part indicates the genomic interconnections of the transcription factors (derived from DBTBS at http://dbtbs.hgc.jp). The environmental signals that lead to the activation of KinA-E, DegS and RsbU-P are mostly unknown.

the phosphorelay activity, de Jong et al. [2003] investigated the protein dynamics following Spo0A-P regulation during activation. Morohashi et al. [2007] performed a stability analysis of a simplified phosphorelay model that was extended by Bischofs et al. [2009] to include different environmental signals and phosphatase activities. Within a given population the output of the phosphorelay is highly heterogeneous, enabling the population to follow several distinct phenotypes, a finding of investigations by de Jong et al. [2010] and Chastanet et al. [2010]. Schultz et al. [2009] also took competence into consideration, which is connected to the phosphorelay reactions [López and Kolter 2009]. As an alternative to the phosphorelay dynamics for their studies on extracytoplasmic protease dynamics, Veening et al. [2008b] used the Spo0A regulated AbrB repressor as the input signal.

The work by Jabbari et al. [2010] concentrated on modelling the environmental and cellular conditions that accumulate Spo0A-P and thereby allow activation of sporulation. Their model consists of several modules, which are the regulations of KinAB activity, the phosphorelay, the expression of SinIR proteins, and the activity of RapA by PhrA. Environmental factors stimulate KinA/B and increase the phosphorylation of Spo0A by the phosphorelay [Sonenshein 2000]. Spo0A-P inhibits the transcription factor *abrB*, resulting in 1) an elevated expression of σ^{H}, and a subsequent increase in Spo0F and Spo0A concentrations, 2) higher concentrations of KinB, 3) lower levels of AbrB with the subsequent reduction in the concentration of the transcription factor Hpr and increased SinIR expression, and 4) a reduced level of Hpr and subsequent de-repression of *opp*-genes thus increasing the role of quorum sensing by Phr proteins. The environmental signals and cellular states that Jabbari et al. [2010] investigated are:

- population density sensed via PhrA,
- cellular nutrient and energy availability sensed via CodY-GTP,
- competence decision sensed via the level of ComA,
- condition of the DNA sensed via Sda.

The authors transformed these four cellular states into yes/no decisions and assigned a priori whether sporulation is desirable or not. While reproducing biological knowledge at large, the simulations contradicted with the expected response for a cell with a combination of conditions of a large population (high PhrA level), no nutrients available (no CodY-GTP), no competence (no ComA), and damaged DNA (high Sda level). The model predicted a delayed sporulation in the presence of damaged DNA. This delay is caused in the model by the PhrA sporulation signal that neighbouring cells emitted. The increasing PhrA signal and the nutrient limitation grew stronger in the model than inhibition

of KinA by Sda, eventually activating sporulation. Thus, PhrA does not only act as a quorum-sensing molecule [Bischofs et al. 2009], but also as a timer for sporulation. Jabbari et al. [2010] conclude that *phrA* and *rapA* transcription activation by ComA serves to heighten the sensitivity of the phosphorelay for the input signals. Presumably, this increase in phosphorelay sensitivity may cause the heterogeneity in the phosphorelay output [Chastanet et al. 2010; de Jong et al. 2010].

Jabbari et al. [2010] tested their sporulation model for the efficiency of various environmental factors to stimulate sporulation. By contrast, de Jong et al. [2003] tested their model with the experimental data obtained from a dozen sporulation mutants. This allowed the validation of the current understanding of the internal structure of the initial sporulation network. Furthermore, the model of de Jong et al. [2003] is based on a different modelling framework as it uses discrete time and protein concentration steps that allows predictions about relative steady-state concentrations. The differences in simulation between de Jong et al. [2003] and Jabbari et al. [2010] make the two models incomparable. One outcome of the simulations by de Jong et al. [2003] is that phosphorelay activation may result in two steady-state solutions independently of the Spo0A-P levels because of a competition of activating KinA and inhibiting Spo0E activity in the sporulation network. The system is extremely sensitive with respect to environmental variation and noise in gene transcription, providing an explanation for the observed phenotypic variations in experiments. These findings were further corroborated by Morohashi et al. [2007] with a stability analysis of a simple model of the phosphorelay. This model only considers phosphorylation of Spo0A-P by the phosphorelay and its dephosphorylation by Spo0E. They conclude that the feedback of Spo0E influences the distribution of sporulating to nonsporulating cells.

A more detailed model of the phosphorelay mechanism is examined by Bischofs et al. [2009]. The authors focused particularly on the integration of quorum-sensing related starvation signals involving Rap and Phr proteins. They examined the steady-state levels of Spo0A-P in response to varying ratios of kinase activity (the environmental signal) to phosphatase activity by the Raps (the population signal). Four different phenotypes are possible: 1) Spo0A-P is not affected by changes in kinase and phosphatase activity; Spo0A-P is either sensitive to changes in 2) kinase-, or 3) phosphatase activity; 4) Spo0A-P is sensitive to changes of both kinase and phosphatase activity. Only mechanisms underlying the fourth phenotype can properly integrate the different signals termed by the authors 'signal integration regime'. Interestingly, Spo0B, the second phosphotransferase of the phosphorelay, is devoid of feedback regulations by Spo0A-P. Bischofs et al. [2009] showed that if a positive feedback from Spo0A-P to Spo0B would be present, the cell would not be able to properly integrate nutrient level and population density and it would thus be

unable to measure the 'food per cell'.

Most models discussed in this review focused on supposedly separate and simplified functional modules of signal transduction. However, we can only understand *B. subtilis* in greater detail if we gain more insight in the interplay and cross-talk of the different environmental response strategies. A step towards dealing with this challenge is made by Schultz et al. [2009]. Schultz et al. [2009] investigate interactions between the processes of sporulation, competence and quorum sensing and find that small noise levels in the input are amplified into different phenotypes in an otherwise isogenic population. The examined signals are environmental and community related. They are transmitted by Phrs and Raps and the key for variability is the concentration of Spo0A-P. The authors related the mutual inhibition of Spo0A-P by AbrB and Spo0E to the 'repressilator', a synthetic genetic regulatory network with an oscillation phenotype designed by Elowitz and Leibler [2000]. It leaves us with the intriguing question of whether the early phase of sporulation should be composed of a regulatory network that could generate oscillations and how those detrimental oscillations could be suppressed.

Variability in the Spo0A-P output is an overarching conclusion of most of the articles investigating the phosphorelay and discussed here. Jabbari et al. [2010] as well as Schultz et al. [2009] observed that Phr and Rap proteins sensitize the output to the input. de Jong et al. [2003] and Morohashi et al. [2007] detected the competition between Spo0E and KinA as a source for variability and bistability. Further information comes from studies by de Jong et al. [2010] and Chastanet et al. [2010] who examined the heterogeneity in gene expression after activation of Spo0A. Because of the experimental classification of cells in sporulators and non-sporulators as well as the positive and negative feedback regulations with respect to phosphorylation and dephosphorylation of Spo0A it was tempting to view the phosphorelay as a bistable switch. Bistability is a property that describes the switching of the system between an activated and de-activated state [Millat et al. 2008]. Under such a regime, the system can be sensitive to a signal, leading to a switch-like transition into a new steady state. Once it is activated, the system can resist deactivation, see Figure 2.2. Bistability is particularly interesting for biological systems as it provides the cell a way for fast yes/no decisions as well as enabling a heterogeneous population with only some cells being activated [Veening et al. 2008c].

Bistability is implicated with several of the *B. subtilis* signalling networks, including competence (ComK) [Maamar and Dubnau 2005], production of exoproteases (DegU) [Veening et al. 2008b] or biofilm formation (SinR) [Chai et al. 2007]. However, the data by de Jong et al. [2010] and Chastanet et al. [2010] show that there is no bistability in Spo0A-P, instead Spo0A-P induced expression is highly heterogeneous. Neither is σ^{H}, pro-

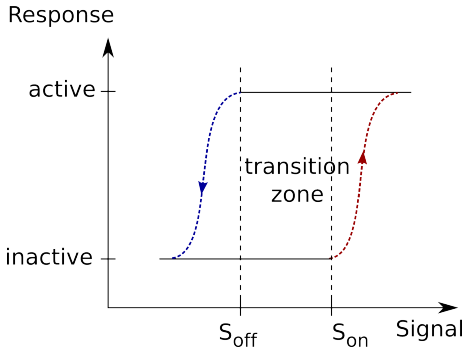

Figure 2.2.: Hysteretic signal-response curve that can give rise to bistability. In the study of Igoshin et al. [2006], the authors tested dynamical properties of the availability of σ^F (response) as a function of the dephosphorylation rate of AAP (signal). For particular parameter region of the dephosphorylation, the system becomes bistable. Under such conditions, the inactive state can easily switch to the active state characterized by a high σ^F availability, at latest at a signal strength S_{on} (AAP dephosphorylation rate threshold). However, the active state is robust against deactivation (decrease in AAP dephosphorylation), since the signal strength S_{off} is reached at lower value compared with S_{on}. In the transition zone, the response is highly sensitive to changes in the signal, with a sufficient perturbation the system can switch easily from the inactive to the active state.

viding the positive feedback via KinA, necessary for establishing a heterogeneous Spo0A-P signal. To reproduce a sufficient accumulation in Spo0A-P using a computational model Chastanet et al. [2010] had to increase the concentration of all Spo0-phophorelay proteins. This modelling outcome is surprising since Spo0B concentration remains constant during stationary phase [de Jong et al. 2010] and since the modelling of Bischofs et al. [2009] showed that Spo0A-P driven *spo0B* expression violates the signal integration of nutrients and community density. Sporulation is an all-or-nothing process and surely has to be controlled with switch-like dynamics. However, the phosphorelay is not the sporulation switch but prepares the cell for a variety of phenotypic responses [López et al. 2008].

2.3. Signalling mechanisms in sporulation

One of the most conspicuous phenotypes of *B. subtilis* is sporulation. The final commitment to this developmental process is established by σ^F dependent gene expression [Dworkin and Losick 2005]. Spo0A-P mediated expression of *sigF* is crucial for establishing compartment-specific gene expression during sporulation. Two studies thoroughly investigated the regulation of σ^F activity using ordinary differential equation models. One study focused on molecular processes that lead to asymmetrical differentiation [Iber 2006] while the other primarily aimed to uncover the principles of irreversibility of the σ^F activation [Igoshin et al. 2006]. A simplified graphical description of the regulation of σ^F activity is

shown in Figure 2.1. Its activity is negatively regulated by the formation of a heterodimer with SpoIIAB (AB), upon which the binding of the sigma factor to its target DNA is prevented. SpoIIAA (AA) is able to competitively bind to AB and release σ^F. However, in non-sporulating conditions AA is predominantly phosphorylated by the kinase activity of AB. Thus, the steady-state ratio of phosphorylated to non-phosphorylated AA determines the level of free σ^F. This level is additionally regulated by the rate of dephosphorylation via the phosphatase SpoIIE (IIE).

Iber [2006] modelled in detail the different states which exist for AB: i) its basic form of a homodimer, ii) bound with σ^F, and iii) bound with one or two molecules of AA (phosphorylated or non-phosphorylated). Each of these configurations harbours combinations of ATP and ADP in the nucleotide binding pockets of the dimer. Finally, the number of states doubles since a central aspect of the model is the allosteric functionality of AB. In any configuration AB is either in a relaxed or in a tense conformation that affects its enzymatic activity [Iber 2006]. Ultimately, the authors determined 50 states connected by 150 reactions and 25 rate constants. The model was successful in approximating qualitative results of a number of published experiments. A quantitative demand of the model regarding the reaction rate constant of IIE phosphatase was that it is 75 to 150 times lower compared with *in vitro* rates. In order to resolve this paradox, IIE activity was measured by the authors in an assay with supposedly more *in vivo* like conditions (switching from manganese to magnesium dominated solutions) and indeed the phosphatase activity matched the model predictions. Iber [2006] modelled the higher activity of σ^F in the forespore by assuming that the IIE phosphatase associates with FtsZ homogeneously over the septum. The forespore volume is about four times smaller than that of the mother cell, thus the concentration of phosphatase facing the forespore is four times larger compared to the mother cell [Iber 2006]. This concentration difference leads to an effective increase in the ratio of IIE to the substrate AA in the forespore and is the primary developmental trigger. The model did not include alternative triggers for the activation of σ^F like effectors with a compartment specific expression due to the genetic asymmetry [Feucht et al. 2002] and thus cannot judge these effects. The allostery of the AB kinase activity further amplifies the different AA-P dephosphorylation dynamics in the two compartments. Furthermore, the result implies that the allosteric system is optimised to reduce the need of ATP [Iber 2006].

A similar study is published by Igoshin et al. [2006], who examined the same regulation system with more or less the same intermediate complexes. However, instead of the allosteric nature of AB their model focused on the so-called 'dead-end complex' of AA-P/AB-ADP. The dead-end complex serves to buffer the concentration of AB such that AB is unable to titrate σ^F. Igoshin et al. [2006] constructed a model with 27 states, 55

reactions and 12 independent parameters. Analyses of the steady-state concentrations of σ^F under various conditions revealed that for certain physiologically feasible circumstances the system shows a hysteretic response, i.e. activation of the system is more easily achieved than deactivation. The hysteretic behaviour necessitates a higher concentration of AA over AB (considering monomers) in the model, a situation that could arguably take place in the forespore since AB is much more unstable than AA [Dworkin 2003]. Igoshin et al. [2006] suggest that the dead-end complex of AA-P/AB-ADP is effectively causing increased σ^F activity in the forespore and that the stability of the complex serves to conserve ATP. A saving of ATP was also implicated by Iber [2006] with respect to the allosteric forms of AB. However, how the submicromolar concentrations of the AB/AA complex may contribute to the conservation of ATP present in millimolar concentrations is not discussed. Whereas the two studies by Iber [2006] and Igoshin et al. [2006] both explain the compartment specific developments during sporulation, they assume different mechanisms: Iber [2006] focuses on AB allostery while Igoshin et al. [2006] focus on the AB-AA dead-end complex.

2.4. The consequences of excitability in competence

Besides sporulation, the development of competence is one of the best studied phenotypic adaptations of *B. subtilis* and is a widely used example for stochasticity in survival strategies [Leisner et al. 2008; Raj and van Oudenaarden 2008]. During late exponential growth when nutrient availability decreases and the population density increases, about 10% of the individuals in a *B. subtilis* population become competent [Hamoen et al. 2003]. Competence development is governed by ComK, a transcriptional factor that regulates the expression of more than 100 genes including those required for DNA binding and uptake [Berka et al. 2002; Hamoen et al. 2002; Ogura et al. 2002]. As shown in Figure 2.1, *comK* expression is controlled by a positive feedback loop, since ComK binds to its own promoter, and by a negative feedback loop via ComS. ComS protects ComK from degradation by the MecA/ClpC/ClpP proteolytic complex. Nevertheless, ComK inhibits expression of *comS* [Maamar and Dubnau 2005; Süel et al. 2006]. Development of competence is tightly connected with the activation of the phosphorelay [López et al. 2008]. The expression of *comK* is inhibited by AbrB and thus *comK* expression can only be effectively activated if the concentration level of AbrB is sufficiently reduced by inhibition via Spo0A-P [Hamoen et al. 2003]. However, further increase in the concentration of Spo0A-P induce *rok*, an inhibitor of *comK* expression, and thus again development of competence is blocked [Hamoen et al. 2003]. Development of competence is additionally regulated via pheromones and quorum sensing [López et al. 2008]. The pheromone ComX activates autophosphorylation of ComP which activates the transcription factor ComA by transfer of the phosphate group [Hamoen et al. 2003]. A second

pheromone PhrC (also: competence stimulating factor, CSF) promotes competence by inhibition of RapC, the ComA-P phosphatase [López and Kolter 2009]. ComA-P induces the expression of *comS*, thus stabilizing ComK, and also induces expression of *phrA-rapA* [López et al. 2008]. ComA-P as an input to the phosphorelay was examined by Jabbari et al. [2010] while Schultz et al. [2009] simulated the dynamic sequential activation of competence and sporulation respectively.

The competence system is an example for excitability: a small perturbation induces a significant developmental response which however is only transient and the cell eventually returns to vegetative growth [Lindner et al. 2004; Süel et al. 2007]. Positive autoregulation of ComK was found to be the most important factor for the transition to competence [Maamar and Dubnau 2005; Smits et al. 2005]. Süel et al. [2006] developed a model to investigate the importance of ComS for switching to competence. They added a noise term to the equation of ComS generation and simulated the concentrations of ComK and ComS. Their model predicted that if ComK positively affects the transcription of *comS* then the competence state becomes much more stable without affecting the probability to enter this stress pathway. Experiments with mutants, in which ComS is positively regulated by ComK, revealed that 4.2% of the mutant cells entered competence, similar to wild type cells with a percentage of 3.6%. In accordance to the simulations, 88% of the mutant cells were locked in the competent state compared to 39% of wild type cells. Next, Süel et al. [2007] have examined the factors controlling entry to competence and the duration of that state. They found that the higher the *comK* expression rate, the higher the probability to enter competence. These findings apply until an oscillation-like regime with successive enter and exit cycles is reached. ComS in turn determines the duration of competence that finally leads to a bimodal distribution of competent cells. Additionally, they showed that after sensitisation of the cell by environmental signals, it is noise that stimulates activation of competence. They used an *ftsW* mutant which develops long filamentous cells that are connected via a common cytoplasm. In this mutant noise is reduced due to the averaging affect implied by diffusion while the physiological mean concentrations are not affected. Indeed it turned out that the probability to develop competence becomes lower with decreasing noise.

Maamar et al. [2007] employed a stochastic simulation approach, using the Gillespie algorithm [Gillespie 1977], to address the question whether the noise is of transcriptional or translational origin. They performed experiments in which transcription is improved and translation of *comK* is reduced, resulting in conditions with relatively constant ComK levels. The analysis revealed that fewer cells became competent in the engineered strains, showing that increased levels of transcription result in less competence. The authors argue that the initiation of competence is determined by noise, and that the source of

the noise can be attributed to irregularities in transcription. An interesting condition of competence is that the phenotype can only be developed within a certain time window in culture conditions [Leisner et al. 2007; Maamar et al. 2007]. This idea requires that the system is robust most of the time and becomes sensitive and excitable to gene expression noise only for specific conditions.

Leisner et al. [2009] examined the system from a different perspective by addressing the question under which condition bistability arises. They excluded the negative feedback loop of *comS* transcriptional regulation by ComK and used ComS as an external parameter that represents quorum sensing signals. Their results imply that during exponential growth, when ComS levels are low and ComK degradation is high, the system is monostable which indicates that variation in the protein concentrations are not sufficient to activate competence. Only if ComK levels increase due to the reduced degradation the system can enter the transition state leading to bistability as result of gene expression noise [Leisner et al. 2009].

2.5. Production of extracytoplasmic proteases

One of the alternative responses following Spo0A activation is the increase in expression of the extracellular protease AprE (subtilisin) and Bpr (bacillopeptidase) [López and Kolter 2009; López et al. 2008; Murray et al. 2009]. Initiation of sporulation can be delayed by the production of extracellular proteases, which break down proteins in the environment to supply the cells with additional nutrients. The pivotal regulator is DegU. In its phosphorylated form as DegU-P the expression of exoproteases, among them AprE, is stimulated while competence is suppressed [Murray et al. 2009]. DegS-P phosphorylates DegU, and activation of DegS via autophosphorylation is regulated by as yet unknown environmental signals. The kinase activity of DegS-P is further stimulated by DegQ [Kobayashi 2007]. DegQ is itself connected to ComA-P and thus activated at high cell densities via ComX [Murray et al. 2009]. In Veening et al. [2008b], the authors conduct several experiments and used mathematical modelling to detect the original signals and the mechanisms that regulate the dynamics of AprE expression. Transcription of the proteases is additionally inhibited by AbrB. This inhibition is compensated upon phosphorylation of Spo0A at early stages in the preparation of sporulation [Veening et al. 2008b]. Veening et al. [2008b] built a mechanistic model of the DegSU two-component system which calculates protease expression based on experimentally measured sporulation-related AbrB levels. Deterministic analysis uncoveres bistability of DegU depending on the ratio of phosphorylated/non-phosphorylated protein. The model predicts an increase in AprE levels until 20 hours of growth. Indeed, this prediction was subsequently verified by the authors in microculture experiments [Veening

et al. 2008b].

2.6. Operon organisation of stress responses

Operon organization can improve the performance of stress response strategies. This was examined by Iber [2006] for the *spoIIA* network and by Voigt et al. [2005] for the phosphorelay with respect to the SinI/R dynamics. The implications of the co-regulation hypothesis of the operon theory by Jacob and Monod [1961] were tested by Iber [2006] based on her model of the dynamics of the *spoIIA* network during sporulation. The central question addressed with the existing and validated model was how sporulation efficiency is affected if noise in protein expression is either coupled or uncoupled among the proteins of the *spoIIA* operon (compare Figure 2.1). This coupling can, to a certain degree, be justified by the assumption that ribosomes can continue protein synthesis on one mRNA to a following protein coding region without dissociation and re-association rounds. These conditions are met for the mRNA of *spoIIAA* and *spoIIAB*, which have an overlap of four bases. Simulations of sporulation efficiency showed that the detrimental effects of expression noise are more pronounced if protein expression is uncoupled. An operon organisation therefore reduces noise by means of co-expression [Iber 2006; Tabor et al. 2008]. This implies that operon organisation would be disadvantageous for regulation of competence, in which noise plays a purposeful role [Süel et al. 2006].

Voigt et al. [2005] published a conceptually related study by investigating possible dynamics regarding the co-regulation of *sinI* and *sinR* with a special focus on evolutionary implications. As described earlier and shown in Figure 2.1, SinR is a sporulation inhibitor and controls biofilm formation, and SinI is the antagonist that deactivates SinR [Bai et al. 1993]. A σ^{A}-dependent internal promoter upstream of *sinR* (P3) establishes an excess of SinR over SinI during vegetative growth. In the model SinR represses activation of the promoter upstream of sinI (P1/2) that transcribes the whole operon (*sinI+sinR*). These mutual negative feedback relations can generate a variety of dynamics in SinI, ranging from a graded response to bistability, oscillation, and pulse response. The dynamics are most sensitive to the production rate of SinR and indeed a sequence comparison of several *Bacillus* genera shows a pronounced conservation of the P3 promoter region. The sporulation probability is determined by the efficiency of the P1 promoter as well as the SinI-R protein-protein interaction. Since different *Bacilli* are adapted to distinct environments it seems likely that their tendency to enter sporulation evolve differently. Sequence comparison reflects this drift since the P1 promoter is very diverse and SinI accumulated mutations that could potentially affect the dimerisation rate of SinI and SinR while still allowing for dimerization [Voigt et al. 2005]. However, new experimental findings challenge two model assumptions, namely that SinR inhibits *sinI* [Chu et al. 2005] and the

spo0A promoter [Kearns et al. 2004]. These inhibitions are necessary for the development of bistability, thus, either the SinIR network is not intrinsically bistable or there are as of yet unknown negative feedbacks. Nonetheless, the article by Voigt et al. [2005] expands our understanding of sigma-factor anti-sigma-factor interactions and depicts the potential to understand evolutionary tendencies that take place over years based on the dynamic events of protein concentrations occuring within minutes at most.

2.7. Partner switching mechanism and general stress response

The partner switching mechanism, including proteins on the *spoIIA* operon, is based on exclusive mutual interactions of an anti-sigma factor with both a sigma factor and an anti-anti-sigma factor [Hecker and Völker 2001; Hecker et al. 2007; Price 2002]. In addition to the irreversible initiation of sporulation, the principle of partner switching mechanism observed for σ^{F} is also seen in other adaptation responses. One of them is the general stress response, which is mediated by σ^{B} and activated by a whole collection of environmental challenges including the transition from exponential to stationary phase [Hecker et al. 2007; Price 2002]. Although both share a similar regulation scheme, they display critical mechanistic differences which reflect the different physiological needs [Price 2002]. The anti-anti-sigma factor RsbV (V) is homologous to SpoIIAA and the anti-sigma factor RsbW (W) is related to SpoIIAB. Comparable to the *spoIIA* interaction network the phosphorylation status of V regulates the available pool of free σ^{B}. However, while there is only one phosphatase of SpoIIAA, namely SpoIIE, two phosphatases dephosphorylate V-P (phosphorylated RsbV) in a stress dependent manner [Hecker et al. 2007]. RsbU (U) reacts largely to physical stress while RsbP reacts to nutritional stress [Hecker et al. 2007; Price 2002]. The main difference in the structures of the sporulation and general stress response is the dead-end complex of AA-P/AB-ADP, which does not exist for V-P/W-ADP because the latter complex can quickly exchange nucleotides [Price 2002]. Since the dead-end complex is missing, the general stress response is readily reversible. This reversibility is necessary since the physiological task of σ^{B} is to respond to temporary cues from the environment. The second difference is the transcriptional feedback loop since the three proteins V, W, σ^{B} are arranged in an autoregulated operon [Price 2002]. Following σ^{B} activation by energy stress, the increased expression of σ^{B} and V provides the potential for further amplification of σ^{B} activity. By contrast, σ^{B} driven W expression on the operon counteracts the positive feedback loop since W deactivates σ^{B} by dimerisation.

Based on the analysis of the *spoIIA* operon, Igoshin et al. [2007] compared the differences of σ^{F} and σ^{B}. Simulations showed that this negative feedback by W results in a two stage response, i.e. the full activity of σ^{B} is delayed whereas in the absence of W σ^{B} is

immediately fully active. The positive transcriptional feedback increases the capacity for regulation, i.e. it maximises the differences in free σ^B before and after stress activation [Igoshin et al. 2007]. While Igoshin et al. [2007] included RsbX, which is involved in negative regulation in response to environmental challenges [Hecker et al. 2007], they did not include the partner switch that controls the activity of the phospatase RsbU which is responsible for environmental stress response activation of σ^B.

The modelling approach of Igoshin et al. [2007] focused on the activation of σ^B because in contrast to experimental findings simulated long term σ^B activities are too high. A representative study to elucidate the σ^B network uses a culture of *B. subtilis* with β-galactosidase as the reporter for σ^B activity. The stress is measured either by the transition of the culture from exponential to stationary phase, caused by starvation, or by the addition of ethanol during exponential phase (reference is any publication between 1995 and 2010 by the major σ^B groups headed by e.g. Völker, Price or Haldenwang). The timescale of sampling is typical until σ^B response reaches pre-stimulus level. By contrast, Locke et al. [2011] examined the expression of σ^B-dependent yellow fluorescent protein (YFP) in single cells using time-lapse microscopy. Surprisingly, even stress-free cells with abundant resources activated σ^B with the same intensity although lower frequency than stressed cells [Locke et al. 2011]. These stochastic bursts of σ^B activation strikingly resemble the activation of competence and were discussed before in the context of a study by Süel et al. [2007]. In both cases the question arises whether the pulses are either 'truly' stochastic, meaning there is a stochastic availability of σ^B, or originating from a perturbed limit cycle oscillator, i.e. the pulsing is a system inherent property with randomised appearance. Just like in the competence study Locke et al. [2011] used an *ftsW* mutant and found reduced σ^B activation burst. Therefore, a random release of σ^B causes the pulse like behaviour, just like in competence.

Whereas the network organisation of σ^B response and competence is completely different, the functional outcome is highly similar. In competence the transcription factor ComK induces its own expression, just like the positive feedback of σ^B, though σ^B has an additional positive feedback by expression of the anti-anti-sigma factor RsbV (repression of a repressor). On the other hand there is a negative feedback by which ComK inhibits ComS, and this results in increased proteolysis of ComK. The negative feedback in σ^B is the expression of the anti-sigma factor RsbW. Amplification of noise is realised in σ^B by ultrasensitivity towards phosphatase levels (RsbP, RsbU) [Locke et al. 2011], whereas competence initiation is highly sensitive to the expression of ComK [Süel et al. 2007]. Like competence, σ^B is excitable. Small perturbations can trigger large excursions of the phase space, beginning with a positive feedback that is overwhelmed eventually by a negative feedback, and finally the system reverts back to prestimulus. Competence is costly and

the time spent in this state must be reduced. General stress response is regarded as a preparation for future stresses [Hecker et al. 2007; Price 2002], a short σ^B activity burst might be sufficient to produce enough protective proteins for a given time.

2.8. Conclusions

The complexity of signalling in *B. subtilis* has motivated numerous studies that used mathematical modelling to elucidate principles and mechanisms of the cellular response to changing environmental conditions. Despite the apparent gap between the complexity of cell signalling networks and the simplicity of their models, many positive examples exist in which mathematical modelling has offered additional insights and in which the models provided guidance for the design of experiments. For example, analysis of the phosphorelay by Bischofs et al. [2009] convincingly shows how the regulation is organised to optimise the information of available nutrient per cell. The combination of model and experiments by Maamar et al. [2007] could elegantly explain that temporal regulation of transcription controls the frequency of transition to the competent state.

The partner switch mechanism of the σ^B mediated general stress response has, so far, stimulated two mathematical models [Igoshin et al. 2007; Locke et al. 2011]. These studies confirmed that our current knowledge is sufficient enough for a detailed understanding of the dynamics of the general stress response. The given network design of the σ^B partner switching maximises the differences of inhibited σ^B during stress-free and activated σ^B during stressed conditions, as the mathematical analysis explains [Igoshin et al. 2007]. Locke et al. [2011] additionally showed that the combination of positive genetic feedback and negative feedback by anti-sigma factor RsbW causes a pulse like behaviour, reminiscent of the competence system. These two studies of the general stress response focused on the energy stress activation of σ^B, and ignored the stressosome mediated environmental activation of the stressosome. In the following two chapters, I fill this gap by introducing two different computational approaches of the dynamics of the stressosome. *Chapter 5* then introduces an alternative mechanism of pulse-generation via the expression of proteases that are at work in the general stress response.

Chapter 3

Stressosome simulation I: Monomer interactions

The stressosome signalling complex of *B. subtilis* is activated in response to diverse environmental stresses, including ethanol, temperature, UV light and osmolarity [Hecker and Völker 2001; Hecker et al. 2007; Price 2002]. The stressosome initiates a protein partner switching cascade that leads to the release of the alternative transcription factor σ^{B} [Hecker and Völker 2001; Hecker et al. 2007; Price 2002]. The complex is the most upstream component so far characterised of the environmental arm of the general stress response in *B. subtilis* [Hecker and Völker 2001; Marles-Wright and Lewis 2007]. Its activation results in the upregulation of nearly 200 genes, including proteins which provide protective adaption to environmental change [Helmann et al. 2001; Nannapaneni et al. 2012; Petersohn et al. 2001; Price et al. 2001].

The stressosome has a supra-molecular structure of a truncated icosahedron [Delumeau et al. 2006; Marles-Wright et al. 2008] and consists of the presumed sensor protein, RsbR, and the scaffold protein, RsbS [Akbar et al. 1997, 2001; Yang et al. 1996]. The cryo electro-microscopy (cryo-EM) of the stressosome revealed its molecular organisation with 40 copies of RsbR associated with 20 RsbS molecules (arranged in homodimers) (Figure 3.1) [Marles-Wright et al. 2008]. In the stress-free state, 20 RsbT molecules are bound by 20 molecules of RsbS [Marles-Wright et al. 2008]; RsbT dissociates from the stressosome following activation by environmental stress [Yang et al. 1996]. Five paralogues of RsbR are present in *B. subtilis*: RsbRA, -B, -C and -D (formerly RsbR, YkoB, YojH, YqhA) [Akbar et al. 2001; Kim et al. 2004b] all of which retain the ability to form functional stressosomes with RsbS [Delumeau et al. 2006; Kim et al. 2004b; Reeves et al. 2010]. The fifth paralogue, YtvA, mediates the stress response to UV light [Avila-Perez et al. 2006; Gaidenko et al. 2006] and is also capable of forming stressosome complexes, at

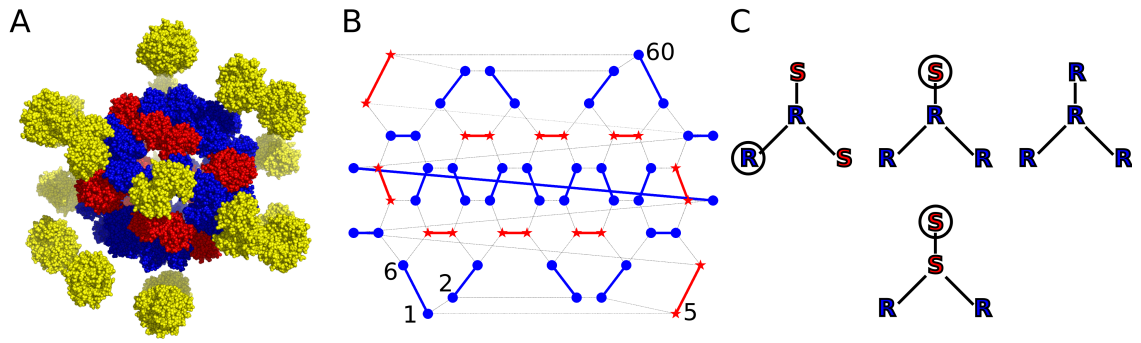

Figure 3.1.: Molecular composition of the stressosome. (A) The atomic model of the stressosome [Marles-Wright et al. 2008] is coloured by domain; C-terminal, RsbR-STAS domain is blue, N-terminal RsbR domain is yellow, RsbS is red, and RsbT is not shown for clarity. (B) The stressosome as a two-dimensional network, with RsbR monomers (blue circles) connected by blue lines to display the distribution of RsbR dimers. Similarly, RsbS monomers (red stars) are connected by red lines to form dimers. Close contact between neighbouring proteins is represented by thin-black lines. The numbers indicate the scheme I used to identify individual proteins in the structure. (C) The four different neighbourhoods will experience different protein cooperativity effects on the phosphorylation reaction and thus different phosphorylation rates of the central protein. In the description of the neighbourhood composition, I always start by naming the unpaired protein, these are circled in the figure.

least *in vitro* (Marles-Wright and Lewis, personal communication). This ability to form complexes appears to stem from the high sequence conservation of the common C-terminal, STAS domains possessed by these proteins [Pane-Farre et al. 2005]. By contrast, the N-terminal domains of the paralogues are highly variable, suggesting differences in either stress perception, or the interactions with RsbT [Delumeau et al. 2006; Reeves et al. 2010].

3.1. Known facts of stressosome activation

The role of the stressosome is the binding and the controlled release of RsbT in response to stress signals. Both RsbR and RsbS are necessary for the association of RsbT in the stressosome [Chen et al. 2003; Kim et al. 2004b]. In stress-free conditions, a significant proportion of RsbR molecules are phosphorylated, whereas RsbS remains non-phosphorylated [Eymann et al. 2011; Kim et al. 2004a]. The imposition of stress leads to an increase in the phosphorylation levels of RsbR (Figure 3.2) [Chen et al. 2003; Eymann et al. 2011; Kim et al. 2004a,b], which is a requirement for the subsequent phosphorylation of RsbS by RsbT [Chen et al. 2003, 2004; Gaidenko et al. 1999]. As the level of phosphorylated RsbS increases, the affinity of RsbT for the stressosome decreases (Figure 3.2) [Kang et al. 1996; Kim et al. 2004a], resulting in the dissociation of RsbT.

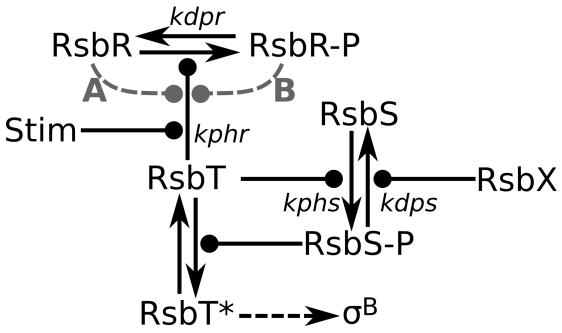

Figure 3.2.: Schematic of the reactions of the stressosome. The reactions take place on the icosahedral stressosome structure, except for RsbT*, which is cytoplasmic RsbT. RsbT* initiates the general stress response by binding to RsbU and releasing σ^B by the partner switching mechanism. Stim represents stimulation of the stressosome by a stressor. I tested three models of interactions between RsbR and RsbT: no interactions; RsbR as an activator of RsbT (A); RsbR-P as an activator of RsbT (B). The reaction parameters correspond to those of Table 3.2. Arrows represent reactions and lines with circles denote activation.

The released RsbT activates the protein phosphatase RsbU [Kang et al. 1996] and the activation of the partner switching cascade which ultimately leads to the release of σ^B from its quiescent complex with anti-sigma factor, RsbW [Hecker and Völker 2001; Hecker et al. 2007; Price 2002]. Once released, σ^B directs RNA polymerase to the promoters of genes of the general stress regulon to stimulate their expression [Yang et al. 1996]. To reset this switch, the phosphorylation statuses of both RsbS and RsbR must be returned to pre-stress levels to allow RsbT to re-associate with the stressosome. The dephosphorylation of RsbS and/or RsbR appears to be catalysed by the phosphatase, RsbX [Völker et al. 1997; Yang et al. 1996]. The properties of the stimuli that activate the general stress response can be summarised in two categories, 1) environmental stress, and 2) energy stress [Boylan et al. 1993; Völker et al. 1995b], both of which activate a phosphatase for RsbV-P [Völker et al. 1997; Yang et al. 1996]. The environmental stress (ethanol, UV light) is transmitted via the stressosome and the activation of phosphatase RsbU whereas energy stress (glucose limitation) leads to the stressosme-independent activation of phosphatase RsbP [Vijay et al. 2000]. However, there is insufficient knowledge of the phosphorylation dynamics of the stressosome because of the limitations of the experimental methods applied thus far. For instance, it is not known how the perception of an environmental signal causes the increase in RsbR and RsbS phosphorylation levels. Functional explanations for the existence and the mechanisms of the four RsbR paralogues are also missing; the paralogues have broad and overlapping sensitivities regarding stress stimuli [Reeves et al. 2010].

Microbiological, molecular, and biochemical techniques have provided general knowledge of protein interactions and chemical reactions of the stressosome, but they are insufficient to understand the molecular events taking place in the complex. Here, I use computational modelling of the cryo-EM stressosome structure to test three hypotheses about protein interactions within it, to gain insight on the spatial events associated with RsbR phosphorylation and their regulatory capacities, published in Liebal et al. [2013]. I compared three models: 1) 'no cooperativity', where the phosphorylation reactions in the stressosome are independent of neighbouring proteins; 2) 'substrate activation', in which non-phosphorylated protein neighbours stimulate phosphorylation; and 3) 'product activation', where phosphorylation is increased by the presence of phosphorylated neighbours. I evaluated the simulation results by comparing them with published data and found the 'product activation' model provided the best fit to the experimental data. A comparison of the simulation results with the signal-response data of Marles-Wright et al. [2008] revealed identical sigmoidal stressosome activation patterns for salt and ethanol treatment; indicating that the activation dynamics of the stressosome are independent of any specific stressor.

3.2. A geometric model of the stressosome

The experimental information used to construct the models, including a description of the geometric properties that may affect allosteric behaviour, is summarised by the following. The basic units of the stressosome are twenty dimers of RsbR and ten dimers of RsbS. Each protein interacts with a homodimer partner, but the icosahedral structure requires two additional interaction partners for each protein. The stressosome structure is constructed in such a way that while RsbR homodimers can interact with each other, RsbS homodimers never directly interact with each other. These rules, along with the observed stoichiometry of the complex, yield a single, unique assembly (Figure 3.1(A)). The truncated icosahedron of the stressosome core can be visualized as a two-dimensional network, as in Figure 3.1(B). Each protein is in the centre of a triangle whose corners are defined by its neighbouring proteins (Figure 3.1(C)). Because the edges in a geometric icosahedron are all equidistant, I adopted the simplifying assumption that all positions in the neighbourhood have the same interaction strength with the central protein. The identification of single proteins is based on a numbering scheme of the elements in the icosahedral network representation, starting from '1' in the lower left and finishing with '60' at the top-right (Figure 3.1(B)). A second list associated each protein with its interaction partners, e.g. protein '1' (RsbR) is neighboured by ('5', '2', '6'), (RsbS, RsbR, RsbR; listing starts with the solitary protein type, the circled protein neighbour in Figure 3.1(C)). If a protein is phosphorylated then a '1' is assigned to it, otherwise its

Table 3.1.: Allosteric parameters, p_a, for the different models. The first column represents the neighbourhood composition (compare to Figure 3.2(C)) and columns two to six represent different phosphorylation states of the models and their allosteric parameter. The table labelled 'General' contains the model independent allosteric parameters, whereas the three tables below show the parameters for 'No cooperation', 'Substrate activation', and 'Product activation'.

Triangle	000	010	011	100	110	111
General						
R3	0.7	0.7	0.7	= {010}	= {011}	0.7
S1	0	0	1	0	0	0
No cooperation						
R1	1	1	1	1	1	1
R2	1	1	1	1	1	1
Substrate activation						
R1	0.7	0.7	0	0.5	0.5	0
R2	1	0.7	0.5	0	0	0
Product activation						
R1	0	1	0	1	1	0
R2	0	1	1	0	0	0

state is '0'.

There is no experimental evidence about the effect of the stressosome phosphorylation status on the dephosphorylation rate and consequently I assumed that the dephosphorylation rates are constant and are not affected by the state of neighbouring proteins. Therefore, the transition from state '1' to '0' (equivalent to RsbR-P/RsbS-P dephosphorylation) in the model takes place with a predefined probability identical for each of the three models and which is independent of any neighbours. By contrast, I modelled the transition from state '0' to '1' (RsbR/RsbS phosphorylation by RsbT) to be dependent upon the phosphorylation status of neighbouring proteins (Table 3.1), consistent with the biochemical data [Chen et al. 2003]. The phosphorylation probability is determined based on a pre-defined maximum phosphorylation probability, *kphr*. The value is chosen to best reproduce the phosphorylation magnitude and time-scale for experimentally measured data on the stress response (Table 3.2) [Eymann et al. 2011; Kim et al. 2004a].

In the stressosome, four different neighbourhood configurations (triangles) exist, which are summarised in Figure 3.1(C). Of the four combinations, three place RsbR in the centre, and one places RsbS in the middle. Each neighbourhood has a different number of RsbT molecules associated with it and thus the activation of RsbT by RsbR and RsbS within these regions is presumed to differ. To account for this triangle-specific activation,

I have introduced the 'allosteric parameter', p_a, which represents the ability of a triangle to stimulate RsbT to maximum activity. The allosteric parameter can take any value between 0 and 1, and is multiplied by the maximum phosphorylation probability. In addition, the phosphorylation state of the three neighbours affects RsbT activity in each triangle. By permutation, there are thus 22 possible phosphorylation states for the four triangles: three triangles have six phosphorylation states (see R1, R2, and S1 in Table 3.1) and one triangle has four phosphorylation states (see R3 in Table 3.1). The resulting 22 free allosteric parameters represent a challenge for reasonable quantification, but by using biological insight it is possible to reduce their number.

An increase in RsbS phosphorylation has been measured as a function of increased levels of RsbR phosphorylation [Chen et al. 2003, 2004]. Therefore, the kinase activity for the triangle with RsbS in its centre (S1) is at maximum if all RsbR neighbours are phosphorylated. Moreover, neighbouring RsbS molecules must be non-phosphorylated because otherwise the kinase dissociates. Hence, only S1 with neighbourhood (0, 1, 1) has an allosteric parameter of 1, all other five states are inactive ($p_a = 0$).

RsbR with three RsbR neighbours (R3) lacks a nearby RsbT kinase, because in the structure of the stressosome RsbT is always immediately adjacent to RsbS [Marles-Wright et al. 2008]. A value for the allosteric parameter of 0.7 for all models allowed the optimal reproduction of the data of Kim et al. [2004a] and of Marles-Wright et al. [2008]. The phosphorylation of RsbR in R3 is independent of the status of the neighbours because it is isolated from direct phosphorylation by RsbT due to its neighbourhood composition, and the influence of its neighbours on its phosphorylation is therefore minimal. Two triangle combinations with a central RsbR remain: R1 with arrangement (RsbR, RsbS, RsbS) and R2, arranged (RsbS, RsbR, RsbR) (Figure 3.1(C)). The neighbourhood R2 has six different phosphorylation combinations: either none, one, or both of the RsbR molecules in the triangle are phosphorylated. These three states can occur in combination with phosphorylated and non-phosphorylated RsbS. The central RsbR cannot be phosphorylated if the neighbouring RsbS is already phosphorylated, because the cognate RsbT would have dissociated. Similarly, R1 has six phosphorylation combinations and the next section shows how I use the phosphorylation combinations to model different hypotheses of protein interactions in the stressosome.

I developed three computational models to test their capacity to reproduce experimental data, and they differ in the way that RsbR activates the RsbT. The possible circumstances are that RsbR 1) activates, 2) inhibits, or 3) has no effect on RsbT. Instead of assuming an inhibition of RsbT by RsbR, I investigate the activation of RsbR by RsbR-P, the two processes being indistinguishable within the modelling setup. The interactions of

RsbR and RsbT are reflected in different allosteric parameter values for phosphorylation in the triangles R1 and R2. In the no cooperation model, I assumed that RsbT activation is independent of its neighbours, which corresponds in the presented framework to setting to 1 (constant maximum kinase activity) all the allosteric parameters in the triangle configurations (Table 3.1). In the substrate activation model, non-phosphorylated RsbR stimulated RsbT and the allosteric parameter values increased from 0 to 1 with a decrease in the phosphorylation of RsbR. By contrast, the allosteric parameter increased from 0 to 1 along with an increase in the number of phosphorylated RsbR neighbours for the product activation model. The specific values for the allosteric parameters were optimized empirically for the best reproduction of experimental data (Table 3.1).

The stressosome reactions were split into regular steps for the following rationale. Consider the two time periods, the time between two reactions of a given protein, referred to as the 'waiting-time', and the time during which all proteins in the stressosome react once, referred to as the 'process-time'. If the process-time is smaller than the waiting-time, then a step-wise update rule is appropriate to approximate stressosome dynamics because the system appears step-wise regarding waiting times. Long waiting-times are a central assumption of the stochastic simulation algorithm used to simulate stochastic systems with low copy numbers comparable to the 60 proteins of a stressosome [Gillespie 1977]. Second, a longer waiting-time than process-time for the stressosome is valid because after phosphorylation, the kinase has to exchange ADP for ATP in its active site and the phosphatase has to diffuse to the stressosome complex to catalyse its dephosphorylation.

In the simulation the initial phosphorylation state of RsbR and RsbS was randomly assigned with a probability of 50% for each to allow rapid equilibration of the system. The equilibrium was independent of the exact initial state which affects the relaxation time only. During a simulation step, the occurence of a phosphorylation reaction was determined for all 60 proteins in random order. For instance, the triangle R2 has neighbours (RsbS, RsbR, RsbR) with a phosphorylation status (0, 1, 1) and the central RsbR is non-phosphorylated. From Table 3.1, it follows that the allosteric parameter for the 'no-cooperation' model is $p_a = 1$, for 'substrate activation' $p_a = 0.5$, and 'product activation' $p_a = 1$. To calculate the reaction probability, the allosteric parameter was multiplied by the maximum phosphorylation probability, $kphr$, which is 0.1 for stress-free and 1 for stressful conditions. Whether a reaction actually occurs was determined using a Monte-Carlo approach: the reaction probability was compared with a number drawn from a uniform distribution in the interval [0,1]. Only if the phosphorylation probability was smaller than the random number was phosphorylation deemed to have occurred. Dephosphorylation was determined similarly using the dephosphorylation parameter. Simulations were repeated 50 times while assuring that statistical properties did not change significantly. The

Table 3.2.: Parameter values for the probabilities of reactions in the stressosome. The parameter *kphr*, the phosphorylation probability, has two values, the first for stress-free, the second for stress-response conditions. To consider the effects of neighbours, *kphr* is multiplied by the allosteric parameters of Table 3.1.

Parameter	Meaning	Value
kphr	Phosphorylation of RsbR	0.1/1
kdpr	Dephosphorylation of RsbR-P	0.06
kphs	Phosphorylation of RsbS	0.4
kdps	Dephosphorylation of RsbS-P	1

model was implemented in Matlab® (7.11.0) and is included in the attached CD in folder '3rd-Chapter_monomer-interactions', and available for download in the Resource section of `www.sbi.uni-rostock.de`, named 'Liebal_thesis-data.zip'.

3.3. Normalisation of signal-response data

The experimental data by Marles-Wright et al. [2008] and the simulation results differ in their input and read-out variables and therefore, for comparison, they were normalised. The experimental data followed a sigmoidal shape and I used a hyperbolic tangent to characterise it,

$$f(x) = \frac{a}{2}\left(\tanh\Big(b\big(x-c\big)\Big)+1\right). \tag{3.1}$$

In this formula, a represents the maximum response, the β-galactosidase activity in the experiments ($a = 85$ Miller units for ethanol stress, and $a = 60$ Miller units for NaCl stress) and RsbS phosphorylation in the simulation ($a = 0.2$ for product activation). Parameter b encodes the sigmoidality, i.e. how fast the system switches between on and off ($b = 8 \cdot 10^{-1}$ and $b = 6 \cdot 10^{-3}$ for ethanol/NaCl and $b = 12$ for product activation). Parameter c encodes the inflection point; in the experiments this is the concentration of stressor producing half maximal β-galactosidase activity ($c = 3\%$ for ethanol, and $c = 488\,\mathrm{mM}$ for NaCl), in the simulation this is the RsbR phosphorylation probability resulting in half maximal RsbS level ($c = 0.14$ for product activation). The response (β-galactosidase and RsbS fractional phosphorylation) were divided by their associated estimated a-parameter in the hyperbolic tangent formula. For the experiment both signals, i.e. NaCl and ethanol concentrations, were divided by their respective c parameter. For the simulation the signal parameter, *kphr* (equivalent to RsbR phosphorylation), was divided by its associated c parameter. Thus, all data in the response range from zero to approximately one, and the response of 0.5, correlates to a signal strength of 1.

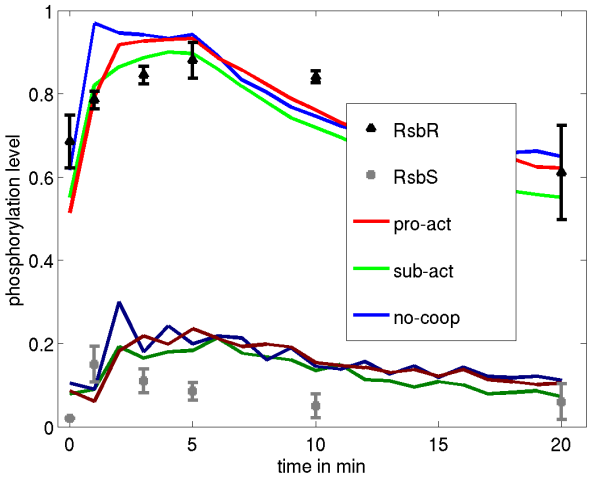

Figure 3.3.: Fractional phosphorylation of RsbR and RsbS during stress. Comparison of mean and variance of RsbR (triangles) and RsbS (squares) phosphorylation level during NaCl or ethanol induction of stress response. The experimental data were extracted from Kim et al. [2004a]. The three different models for simulation are: the product activation model (red line), the substrate activation model (green line), and the no cooperativity model (blue line). Stress is simulated assuming an increase in the phosphatase probability of RsbR, *kphr*, to 1. In the simulation stress is stopped at 5 min by reversion of *kphr* to the according stress-free value of 0.1.

3.4. Experimental reproduction of stressosome simulations

I compared the simulation results with the experimental data from Kim et al. [2004a] (similar results were obtained by Eymann et al. [2011]). Kim et al. [2004a] measured the fractional phosphorylation of stressosome components RsbR and RsbS during exposure to NaCl and ethanol. The parameter settings used for fitting the observations are given in Table 3.2 and observations (markers) and simulations (lines) are shown in Figure 3.3. Activation of the stressosome is simulated with an increase in RsbR phosphorylation probability, *kphr*, from 0.1 to 1. In the experiment, the fractional phosphorylation of RsbR decreased after 5 min, while levels for RsbS decreased after only 1 min. To simulate this apparent stress adaptation, I reset *kphr* from 1 to 0.1 after 5 min and therefore the stress is only active in the simulation between 0 and 5 min.

In the Kim et al. [2004a] study, the fractional phosphorylation of RsbR pre-stress is around 0.7, and is thus similar to the simulation results of 0.6. The peak phosphorylation levels are also comparable, although shifted to later times for RsbS in the simulation. In the experiments of Kim et al. [2004a], the RsbS fractional phosphorylation level increased rapidly following stress induction, whereas in the model RsbS phosphorylation increased only after the phosphorylation of RsbR. The RsbR fractional phosphorylation

decayed faster in the simulation in comparison to the experiment, but both experiment and simulation arrived at comparable values of 0.6 towards their respective conclusions.

I did not attempt to model the long-term regulation of stressosome activation because that requires the additional consideration of gene expression. Therefore, while the ranges of RsbS and RsbR phosphorylation are captured, the dynamics of the RsbS deactivation process are not reproducible in the presented framework. A notable difference between the models was the faster activation of RsbR and RsbS in the 'No-cooperation' model in Figure 3.2. This faster response is caused by an increase in the phosphorylation probability for all RsbR molecules, because, unlike in the other models, the phosphorylation probability is not restricted to neighbouring molecules. All three models perform comparably in relation to the activation profiles in Kim et al. [2004a], indicating that another parameter must determine the biological significance of one model over the others.

To determine the crucial parameter that separates the three models, and to understand the phosphorylation dynamics of the structure of the stressosome, stress activation was modelled as a function of the increase in RsbR phosphorylation probability. Marles-Wright et al. [2008] measured σ^B dependent β-galactosidase activity in response to different concentrations of the stressors NaCl and ethanol. A sigmoidal signal-response curve for both these environmental stressors was observed [Marles-Wright et al. 2008]. The sigmoidal signal-response was not observed during the stressosome-independent activation of σ^B by energy stress, suggesting strongly that the sigmoidal environmental stress response is stressosome-specific. I evaluated the simulation using these data because the direct outcome of the simulation is the RsbS fractional phosphorylation, which correlates directly to the release of RsbT from the stressosome and to the activation of σ^B. To compare experiments and simulations, the experimental data were normalised as described in Section 3.3. Strikingly, the experimental data for the stressosome response generated for ethanol (triangles) and NaCl (squares) coincide almost perfectly after normalisation (Figure 3.4). Consequently, the stressosome response is identical for these two different signals. Among the three models generated, only the product-activation model resulted in a signal-response curve with a comparable sigmoidal character (pro-act curve in Figure 3.4), where the deviations from the experimental data are probably rooted in the model simplifications.

I also evaluated the product activation model using experimental data from Völker et al. [1997]. Here, the cellular concentration of the phosphatase RsbX was controlled by cloning it downstream of an IPTG inducible promoter. The ethanol stress response was tested by titrating the cellular levels of RsbX with IPTG. Yet again, the experimental outputs were measured using a σ^B dependent β-galactosidase reporter gene fusion, whereas the

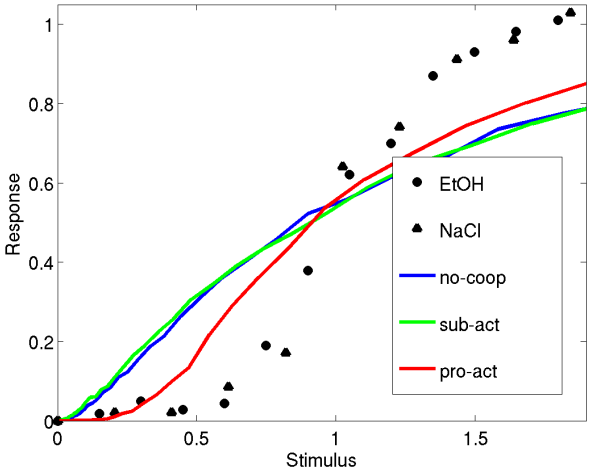

Figure 3.4.: Stimulus-response characteristics of the stressosome. The different stimuli used in experiments by Marles-Wright et al. [2008] are ethanol (EtOH, triangles) and NaCl (circles). The simulations according to the three models tested are: product activation (red line), substrate activation (green line), and no cooperation (blue line). As experiment and simulation use different stimuli (NaCl, ethanol and *kphr*, respectively), and response definitions (β-galactosidase and RsbS phosphorylation) the stimuli and responses were normalised according to Equation 3.1. Ethanol and NaCl activate the stressosome in an identical manner, leading to identical stimulus-response characteristics. Only the product activation model approximates the experimentally observed sigmoidal character of this response. The parameters are identical to the reproduction of the Kim et al. [2004a] data and are shown in Tables 3.1 and 3.2.

simulations produced fractional phosphorylation levels of RsbS. As described above, these two measures correlate directly because RsbS phosphorylation leads directly to σ^B activation. I normalised the two data sets internally with their highest unperturbed output, i.e. wild type β-galactosidase activity and RsbS phosphorylation. Stress was applied at 20 min by the addition of ethanol in the experiment and by increasing the phosphorylation parameter of RsbR, *kphr*, from 0.1 to 1 in the simulation. Since RsbX is a phosphatase, the probability of dephosphorylation of RsbS (*kdps*) and RsbR (*kdpr*) need to be adapted in the model. In conclusion, modification of only *kdps* reproduced the data by Völker et al. [1997]: $kdps = 1$ (wild type, red line), $kdps = 0.6$ (RsbX reduced, green line), and $kdps = 0.3$ (RsbX low, blue line). In the simulation, a reduction in the dephosphorylation of RsbR failed to reproduce the experimental data, because the response after activation remained constant at the level of the wild type response (not shown). The response in the simulations was faster than the experimental data, because the additional time delay caused by the expression of the reporter gene is omitted when examining directly the RsbS phosphorylation as output. The time delay between maximum RsbS phosphorylation and maximum reporter protein signal is about 15 to 25 min [Kim et al. 2004a], which is only

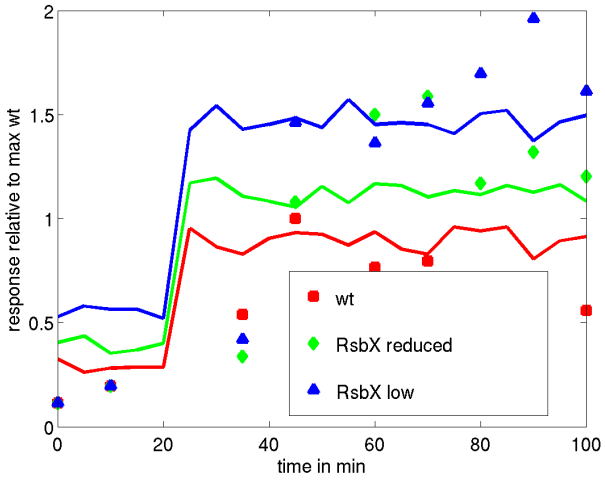

Figure 3.5.: Effect of reduced levels of RsbX on stress activation of σ^B. Three data-sets from Völker et al. [1997] were digitized in which the level of RsbX is controlled by the addition of IPTG (BSA46, [wild type], squares, BSA337+1 mM IPTG [RsbX reduced], diamonds; BSA337+0.1 mM IPTG [RsbX low], triangles). The simulation was performed with the product activation model. The responses of experiment and simulation are normalised to the maximum response of the wild type. The lines represent simulations with parameters as listed in Table 3.1 and 3.2 but with appropriately adapted dephosphorylation probabilities (*kdps*), wt with $kdps = 1$ (red line); reduced RsbX with $kdps = 0.6$ (green line); low RsbX with $kdps = 0.1$ (blue line). The activation of the stressosome by ethanol (experiment) or by increase in *kphr* (simulation) both took place at 20 min.

slightly smaller compared to the approximate 30 min delay of simulation and measurements in Figure 3.5. The experimental results of Völker et al. [1997] are explained in the model by assuming that the stressosome and thus the environmental stress response is reset by the unique dephosphorylating of RsbS-P by RsbX.

By relating experimentally measured σ^B activities to the fractional phosphorylation of RsbS (the model output), it is possible to compare the simulations with a number of published experiments (see Table 3.3). First, Akbar et al. [2001] measured stress responses for strains with mutations in both RsbRA and RsbRB, and in either RsbRC or RsbRD or both (see Table 3.3). The major outcome is that RsbRC and RsbRD increase the pre- and post-stimulus β-galactosidase levels. In the experiment of Martinez et al. [2010], stress was induced by the transition to stationary phase (energy stress), and it was thus reported by these authors that RsbRC and RsbRD can sense energy stress. The unbiased simulations support this notion and provide clues about the kinetic implications of these findings. The most direct way to replicate this finding in the simulation is to increase the phosphorylation likelihood for RsbS, *kphs*. Thus, RsbRC and RsbRD are more efficient than RsbRA

and RsbRB in inducing the RsbT kinase activity towards RsbS during energy stress stimulation. The mixture of RsbRC and RsbRD, with stress-insensitive RsbRA and RsbRB, lowers the apparent activation of RsbS (Appendix A) [Martinez et al. 2010]. Second, Kim et al. [2004b] detected a hyperbolic β-galactosidase stress response for RsbRD instead of the sigmoidal response seen for RsbRA and RsbRB. As shown in Figure 3.4, the models of 'Substrate activation' and 'No cooperation' produce hyperbolic responses while the sigmoidal response generated by the 'Product activation' model is caused by the allosteric behaviour of RsbR interactions (see Table 3.1). Although the data of Kim et al. [2004a] are in form of a time course and the sigmoidal property is derived from a dose-response curve, a time course can be controlled by the dose-response if the stressosome adapts faster to the stimulus than the stimulus changes itself. On the basis of this assumption, the model predicts that RsbRD is less allosteric than RsbRA. Finally, the cellular automaton enables qualitative analysis of RsbR mutations. Amino-acid substitutions on certain positions of RsbRA result either in elevated or reduced pre-stress output while maintaining a wild type stress response (Table 3.3) [Gaidenko et al. 2011, 2012]. Since the stress response is unaffected, the protein interactions of the stressosome are not involved and thus table 3.1 remains unchanged. Based on the assumption that stress stimulation increases RsbR phosphorylation by RsbT, the substitutions either activate or inhibit RsbT without stress stimulation if the mutations increase or decrease the pre-stimulus response, respectively. However, the stimulation of RsbT after stress perception is undisturbed.

3.5. Consequences of the assumptions and limits of prediction

I presented the first computational model of the stressosome based on a Boolean representation of phosphorylation. The consequences of the unique neighbourhood compositions in a truncated icosahedron were simulated in a cellular automaton-like computational environment wherein the future state of a protein is based upon the phosphorylation status of its neighbouring proteins. I analysed simulated time course data of RsbR and RsbS phosphorylation, as well as steady state phosphorylations at different stress inputs and compared them to data from the literature. For simplicity, I disregarded any effects that may originate from the interactions between dimers of RsbR and RsbS as there are no experimental data available about such effects. Moreover, I also ignored the potential for the RsbR paralogues to display a localisation bias within the stressosome (e.g. the R3 neighbourhood). This is, because, to date, there is no information available on the localisation patterns of RsbR and its paralogues within the stressosome. Although four RsbR paralogues contain two threonine residues as potential phosphorylation sites [Gaidenko et al. 1999], the model considers only single phosphorylations of RsbR. The double phosphorylation of RsbR occurs only in response to the imposition

Table 3.3.: Comparison of experimental observations with simulation. The phosphorylation of RsbS is correlated to the β-galactosidase response because phosphorylated RsbS releases RsbT, the activator of σ^B.

Experiment	Phenotype	Reference	Model adaptation	Simulation
Reduced RsbX	increase in β-galactosidase response	Völker et al. [1997]	decrease in *kdps*	increase in post-stress RsbS-P
ΔRsbR(AB), ΔRsbR(ABC), ΔRsbR(ABD)	alteration in pre- and post-stress β-galactosidase response	Akbar et al. [2001]	increase in *kphs*	increase in RsbS-P
ΔRsbR(ABC), RsbRD stressosome	hyperbolic response	Kim et al. [2004b]	increase in background phosphorylation (Table 3.1), decrease of cooperativity	hyperbolic response
RsbR, RsbS phosphorylation after stimulus	transient increase in phosphorylation	Kim et al. [2004a]	increase in *kphr*	increase of RsbR-P
Stimulation with different stress level	sigmoidal dose-response curve	Marles-Wright et al. [2008]	adaptation of the allosteric parameter for R1 and R2 neighbours	allosteric activation of RsbT by RsbR-P
RsbRA T86A, N129A, Q142A	elevated basal β-galactosidase level but wild type stress response	Gaidenko et al. [2011] and Gaidenko et al. [2012]	increase of pre-stress *kphr*	increase of pre-stress RsbR-P
RsbRA L141A, Q147A, L149R	reduced basal β-galactosidase level but wild type stress response	Gaidenko et al. [2012]	decrease of pre-stress *kphr*	decrease of pre-stress RsbR-P

of strong stresses and the double phosphorylation actually limits stressosome activation [Eymann et al. 2011]. I have avoided the double phosphorylation phenomenon in order to keep the model simple, whilst maintaining a model that is applicable for all but the most extreme of stressful incidents. The fitting of the model to the experimental data required a high phosphorylation status for RsbR molecules in a neighbourhood with only RsbR neighbours (R3-neighbourhood).

Whereas the majority of bacterial sensory systems consist of monomers or dimers, some systems, including the stressosome and chemotaxis arrays, form large complexes. Amongst the possible reasons for this phenomenon is an increase of the regulatory space; a sensor that interacts with its neighbours expands its input signal range. An adaptation of the interactions can thus affect the response. In terms of cellular automata, these interactions correspond to the update tables. What is the knowledge we can expect from such an abstraction? A cellular automaton is first and foremost a spatial model; it reproduces patterns like the distribution of black and white squares on a lattice. A different update table yields a different pattern, fitting an observation better, or worse. The best test of the cellular automaton of the stressosome is the direct observation of phosphorylation patterns. For example, the model predicts hyper-phosphorylation of RsbR in the neighbourhood of R3. This, however, is technically impossible to measure and probably biologically irrelevant. The purpose of the stressosome is the release of RsbT from phosphorylated RsbS, and thus no particular pattern but the total phosphorylation matters. The cellular automaton of the stressosome allows the examination of different interactions by adapting Table 3.1, and the effect of external inputs, as represented by the parameters of phosphorylation and dephosphorylation of Table 3.2. In this context, predictions are hard to formulate because the output of an altered RsbS phosphorylation can be reproduced by a number of patterns generated by different update tables and input parameters. Consequently, I evaluated the model on existing data that enables association of model parameters with biological functions.

3.6. Integration of the results to current knowledge

The phosphorylation of RsbR is a requirement for the activation of the stressosome, because inhibition of the threonine residue targeted for phosphorylation in RsbRA (T171A) blocks stress response [Kim et al. 2004b]. Furthermore, the phosphorylated form of RsbR was found to stimulate the kinase activity of RsbT [Chen et al. 2003]. The simulations in this chapter reproduce these findings. Only the model of RsbT stimulation by RsbR-P simultaneously fitted the two experiments of 1) RsbR and RsbS phosphorylation frequencies, and 2) stress signal-transcriptional response data. This RsbR phosphorylation requirement also explains why RsbR is phosphorylated

to high levels in stress-free conditions [Eymann et al. 2011; Kim et al. 2004a].

Environmental stresses lead to an increase in RsbT kinase activity against RsbR and RsbS, either by direct interactions of RsbT with RsbR paralogues, or through some, as yet, undetermined secondary interactions [Gaidenko et al. 1999]. Reanalysis of the data presented in Marles-Wright et al. [2008] shows that the levels of the activation of RsbT in response to stress is independent of the nature of the stress (Figure 3.4). How is this achieved? The N-terminal domains of RsbR, presumed sensors (in part because this domain of YtvA is blue light sensitive), may interact with a secondary messenger molecule, or with a protein that integrates the initial stress signal. A candidate for this possibility is Obg, a ribosome-interacting protein with unclear roles in sporulation and σ^{B} activation [Kuo 2007]. Ethanol and NaCl have similar physiological effects by inducing secondary oxidative stress (reactive oxygen species) in the electron transport chain [Mols and Abee 2011], potentially linking these stressors with the stressosome. Whether RsbT activation requires the involvement of a small molecule, or a protein integrator, are aspects of the stress response that remain to be determined experimentally.

In vitro, RsbX can dephosphorylate RsbS-P and RsbR-P, but the latter only at residue T205 [Chen et al. 2004]. The dephosphorylation reactions have also been studied *in vivo* [Eymann et al. 2011], and the two approaches provide broadly consistent results. The inefficient dephosphorylation of RsbR T171-P by RsbX probably explains the slow decrease in RsbR phosphorylation observed by Kim et al. [2004a] (summarised in Figure 3.3), whereas RsbS was dephosphorylated rapidly. In the simulations, the dephosphorylation probability for RsbR is nearly two orders of magnitude lower than that for the dephosphorylation of RsbS-P (0.06 and 1, respectively, see Table 3.2). The stress response of strains expressing different levels of RsbX following a challenge with 4% ethanol has been tested [Völker et al. 1997] and such a challenge should lead to only a single phosphorylation in RsbRA at residue T171 [Eymann et al. 2011]. Indeed, the data of Völker et al. [1997] could be reproduced in the model by assuming that RsbX was active as a phosphatase only towards RsbS-P. A functional stressosome also requires a balanced phosphorylation status of RsbR. Experiments and simulation do not support the prior assumption that RsbX mediated the dephosphorylation of RsbR-P, though it is still formally possible at a low, but significant level.

3.7. Conclusions

In reproducing numerous published experiments, the stressosome simulations add weight to a model in which RsbT is activated allosterically by phosphorylated RsbR. The simulation results also suggest that RsbX is only required to

dephosphorylate RsbS to reset the stressosome to a pre-stress state. Furthermore, the normalization of the data of Marles-Wright et al. [2008] shows that stressosome activation and thus phosphorylation dynamics are identical for different stressors. This model approach forms the foundation for future computational experiments to explore the effects of phenomena for which the mechanism of their action is currently unknown. These experiments could explore the impact of RsbR T205 phosphorylation on stressosome activation, the impact on localisation constraints of RsbR paralogues in the stressosome, or the negative feedback exerted on the system via σ^{B} mediated control of RsbX expression. The model I introduced in the passing chapter provides a proof of the utility of using Boolean network simulations to model stressosome activation, as demonstrated by the modelling of the activation dynamics of the stressosome for moderate stresses. For a complex and fascinating molecule like the stressosome, many questions remain to be answered despite two decades of intensive research on the regulation of σ^{B}. The limitations of biological experimentations in this system can be overcome by computational modelling, which is proving to be a valuable tool to shed light on the function of not only this system [Igoshin et al. 2007; Liebal et al. 2012; Locke et al. 2011], but other signalling networks too [Liebal et al. 2010]. Consequently, the application of Boolean network simulations is likely to provide insight to other, highly symmetric molecules that are poorly understood, for instance, the co-ordinated assembly and disassembly of bacteriophage, viruses, and bacterial micro-compartments and the communication of enzymatic active centres in pyruvate dehydrogenase complex [Milne et al. 2002] and the dynamic effects of pore opening and closing on iron uptake in ferritins [Liu et al. 2003; Weeratunga et al. 2010].

In the passing chapter, I modeled the stressosome based on the view of protein monomers with identical interactions among all their nearest neighbours. However, these identical interactions are only a simplification, although apparently efficient, because the stressosome is composed of dimers of RsbR and RsbS. This simplification is appropriate because the nature of the interaction of proteins and the transmission of information among the proteins of the stressosome is still a matter of debate. In the following chapter, I abandon the simplification of identical interactions and assume that dimers form the basic units of the stressosome. It is also a contribution to the debate of information transfer among the proteins because a geometric model examined in the next chapter makes strict predictions about structural motions within the stressosme for the purpose of information transfer.

Chapter 4

Stressosome simulation II: Shape transitions

The stressosome has been introduced in the previous chapters as an environmental sensor responsible for the activation of the general stress response. The stimulation of the stressosome induces structural and functional modifications that cause the release of the protein kinase, RsbT, and converts the original signal into a concentration of free RsbT. Since the regulation of the stressosome has already been covered in the previous chapter, in this chapter, I focus on the stressosome's structural properties. In *B. subtilis*, RsbT activates a 'partner switching' signalling cascade that involves RsbV, RsbW and the alternative sigma factor σ^{B}, and ultimately leads to the induction of the general stress response [Hecker and Völker 2001; Hecker et al. 2007; Price 2002]. Marles-Wright et al. [2008] used cryo electro-microscopy (cryo-EM) to determine the atomic structure of the stressosome, which adopts a truncated icosahedral geometry and is composed of 20 dimers of RsbR and 10 dimers of RsbS. A simplified illustration of the stressosome is visualised in Figure 4.1, together with a trimer of dimers of RsbR and RsbS and their domains, that jointly form a triangle. RsbS belongs to the STAS-domain superfamily, with other STAS members in *B. subtilis* including RsbR, RsbV and SpoIIAA [Aravind and Koonin 2000; Mittenhuber 2002; Pane-Farre et al. 2005]. The multiple RsbR paralogues of *B. subtilis* possess a conserved C-terminal STAS domain [Murray et al. 2005], but they differ in their N-terminal, globin-like domains [Akbar et al. 2001; Pane-Farre et al. 2005]. The STAS domain of RsbR paralogues and RsbS are jointly responsible for the construction of the icosahedron [Marles-Wright et al. 2008]. The variable N-terminal domain is proposed to act as a sensor, or enables interactions with RsbT [Delumeau et al. 2006; Reeves et al. 2010]. One of the RsbR paralogues, YtvA, carries a UV light sensitive, N-terminal LOV domain (light-oxygen-voltage) instead of a globin-like fold [Akbar et al. 2001; Losi et al. 2002]. UV light induces the formation of a covalent bond between

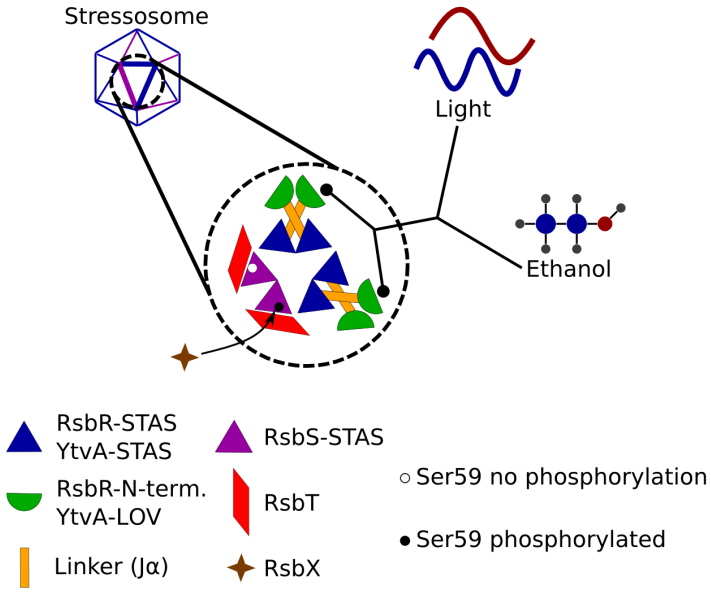

Figure 4.1.: Interaction and domain structure of stressosome proteins and their organisation as trimer of dimers, a triangle structure. A triangle of dimers in the stressosome contains two RsbR dimer and one RsbS dimer with an associated RsbT. The STAS domains are structural elements, whereas the RsbR-N terminus is implicated in the sensing of the signal. RsbX is the phosphatase for the RsbT mediated phosphorylation of RsbS.

Cys62 and a flavin nucleotide cofactor of the YtvA LOV domain [Losi et al. 2002]. By contrast, the molecular details of signal transduction in the other RsbR paralogues remain unknown.

The next step in the signal processing cascade involves transmitting the signal from the N-terminal domain to the C-terminal STAS domain of the RsbR paralogues (Figure 4.1). Both RsbR and YtvA possess a flexible linker region between their two domains, the so-called Jα linker [Buttani et al. 2007], which undergoes conformational changes upon signal perception [Möglich and Moffat 2007]. The structural changes are presumably transmitted to the STAS domain [Herrou and Crosson 2011], and stimulate the kinase activity of RsbT [Avila-Perez et al. 2009; Chen et al. 2003]. The ensuing increase in RsbS phosphorylation releases RsbT, and thus activates the general stress response [Kang et al. 1996; Yang et al. 1996]. On the other hand, the dephosphorylation of RsbS-P is performed by the phosphatase, RsbX (Figure 4.1), thereby resetting the system to the resting state [Chen et al. 2004; Völker et al. 1995a].

The STAS domains are implicated in both the signal transmission and the construction of the icosahedron. Thus, it is possible that changes in the conformation of the STAS

domains change the global structure of the stressosome in order to facilitate the information transfer. The stressosome is an icosahedron, and this structure alone allows us to derive rules for the motions of the stressosome's domains. This approach is possible because geometric constraints remain valid over different orders of magnitude [Whitesides and Boncheva 2002]. Cuccia et al. [1994] studied the structure of carbon allotropes by using paper-folding techniques that reproduce the sp2-carbon bond properties. Combining the carbon-bond models in different ways allowed Cuccia et al. [1994] to construct the allotropes of carbon, like ring molecules, fullerenes, etc. Geometric models can not only represent static protein structures, but also the processes of protein folding and self-assembly. Burnley and Cox [2004] constructed chains of paper to study folding processes related to protein folding which were agitated and folded spontaneously into defined shapes. This approach can also be applied to the assembly of viral capsids [Burnley and Cox 2005; Gracias et al. 2002]. Caspar and Klug [1962] studied properties arising from the geometry of icosahedral viral capsids. From paper models they learned that arrangements of structure units consisting of pentamers and hexamers are a geometric necessity. The particular organisation of pentamers and hexamers maximises the contacts between the units [Caspar and Klug 1962]. It is a frequent approach to simplify the structure of proteins using spherical or elliptical bodies to study geometric and thermodynamic constraints [Bruinsma et al. 2003; Feng et al. 2008; Zandi et al. 2004]. Similarly, I devised a particle-dynamics simulation where the RsbR and RsbS proteins are approximated by tetrahedral constructs. This procedure allowed us to generalise results obtained by the geometric model. These results inspired the construction of a cellular automaton. This cellular automaton is based on the automaton-model of *Chapter 3* with appropriate modifications. While the geometric models have a very limited capacity to study stressosome dynamics, a cellular automaton enables an analysis of the effect of different parameters on the activation profile.

Though much is known about the consequences of stressosome activation, several questions remain unanswered: 1) What is the stressor activation mode for RsbR? 2) How does RsbR activate RsbT by phosphorylation? 3) How is the activation signal transferred from the stressosome-integral STAS domain to the RsbS associated RsbT? 4) What are the advantages of an icosahedral structure in this system? Here, I have combined independent modelling approaches for the stressosome, including a geometric model, particle dynamics simulation, and a cellular-automaton model to answer these questions. The resulting model of the stressosome activation suggests a method of communication between RsbR and RsbT, the basis of which is an orchestrated collapse of three dimers in a triangle. This collapse is caused directly by the environmental conditions that affect the RsbR and YtvA N-terminal domains; no intermediary signal transducers are necessary, explaining why none have been found thus far. The structural interactions between RsbR and

RsbT after the collapse stimulate RsbT. Finally, the ability of the icosahedral geometry to support the collapse is an inherent property of this type of geometry. I expand my original 'Collapse Hypothesis' by the assumption that one collapse stimulates the collapse of nearby structures. Simulations using cellular automata lead to the conclusion that the cooperative collapse propagation expands the regulatory power of the stressosome. Furthermore, a single signal event of the RsbR paralogues is amplified by multiple phosphorylation/dephosphorylation events on RsbS, as revealed by the rigorous sequencing of intramolecular events in the stressosome.

4.1. Construction of geometric models for the stressosome

The stressosome is a truncated icosahedron and these geometric structures are popular origami folding models. I constructed a paper-based, geometric model of the stressosome based on a folding sequence visualised in Figure 4.2. For this construction, 90 quadratic paper units were folded and assembled as indicated by steps 1-7 in Figure 4.2(A).

In collaboration with Peter Raasch, a particle-dynamics simulation of the stressosome was developed to experimentally verify the observations obtained from the geometric paper model. In the simulation, the proteins of the stressosome were represented by particles with a three dimensional position and velocity. Interactions and connections between proteins were modelled by two types of forces, connective and interactive, acting between those particles. The particles are distributed in space like the vertices of an icosahedron and a connective force acts between the particles. The force is similar to a the the force produced by a linear spring, flexible within a certain range but stiff beyond it. The interaction force was used to model repulsion and attraction between proteins at the tips of the structure, which have a certain degree of freedom to move. It acts in repulsion when two proteins are too close to one another and in attraction when the proteins are within a certain distance. Phosphorylation of proteins resulting in either stronger or weaker attraction was modelled per protein by changing the interaction force. External disturbance by proteins in the cytoplasm was simulated by a short random impulse on all proteins in the structure. The code is written with Visual Basic® and available on the attached CD in the folder '4th-Chapter_shape-transitions' and subfolder 'Particle-Dynamics'.

The stressosome is assembled from dimers of RsbR and RsbS (Figure 4.2(B)) [Chen et al. 2003]. Three dimers form a triangle at the molecular 3-fold axis, equivalent to a hexamer in terms of monomers (Figure 4.2(B)). Overall, the structure is composed of twenty triangles and these form the basic agents in the cellular automaton. The neighbours were organised such that an icosahedral geometry is generated comparable to the icosahedral cellular

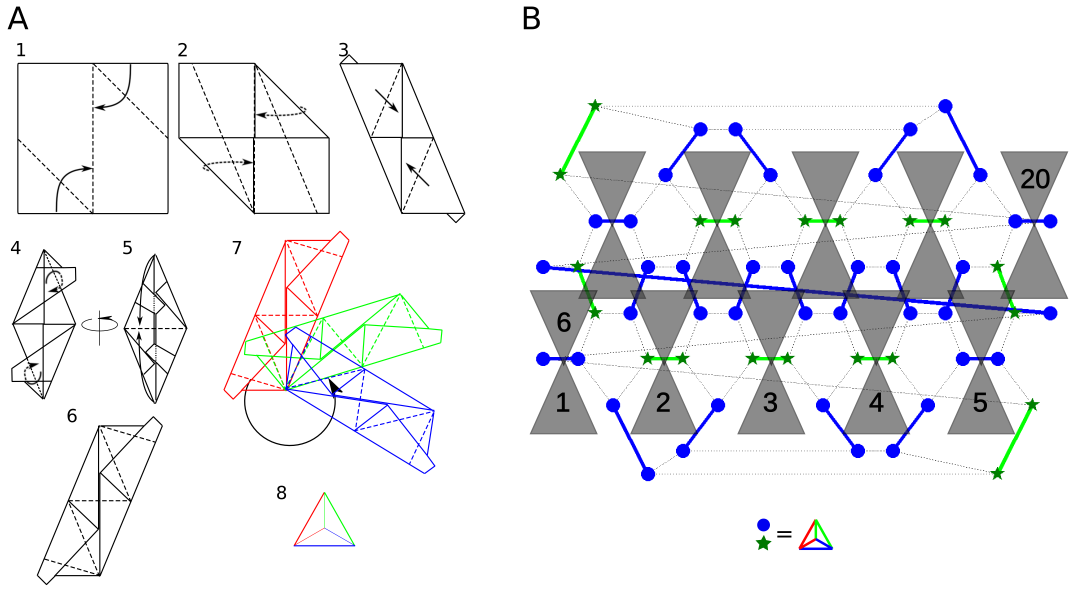

Figure 4.2.: Modular origami approach (A) and network diagram of the stressosome (B). Six steps to fold a single square paper unit, sketch 7 indicates how three monomers are connected to form a three-dimensional construction unit of which the view from above is shown in sketch 8 (A). Icosahedral surface organization that guides the assembly of the paper model (B). Each protein is formed by three paper monomers that form one construction unit. Dimers in the stressosome are connected with continuous bars. The simulation of the cellular automaton is based on trimers of dimers in the form of triangles. Each triangle is identifiable according to the numbering scheme. RsbR is depicted with blue circles, RsbS as green stars. Each protein is represented by one tetrahedron of sketch 8 in (A).

automaton of Kiester and Sahr [2008]. In the cellular automaton of the stressosome, three states were deemed possible for each triangle: 1) 'relaxed condition', where all dimers protrude out of the stressosome; 2) 'collapsed condition', where all dimers in a triangle are physically close to each other, or 3) 'inhibited triangle', this is a partially collapsed triangle, some dimers have collapsed onto a neighbouring triangle, thus an inhibited triangle cannot be in the collapsed state. Physiologically a triangle collapse corresponds to the reception of a stress signal by the stressosome, and a relaxation of a triangle corresponds to the reversion to a pre-stimulus stressosome. Each triangle was numbered from the lower left to upper right (Figure 4.2(B)) and its state was stored in a list, the 'Position-list'. Thus, the Position-list represents the output of the model. A second list, the 'neighbour-list', associated each triangle to its three neighbouring triangles and documents their state. This neighbour-list was essential for determining collapse probability in the collapse cooperativity model.

Table 4.1.: The three parameters used for simulation of the stressosome cellular-automaton model. The numerical values are empirically chosen to establish a low collapse frequency of the stressosome in stress-free conditions. An increase of the co-operation of collapse to a value of 0.5 leads to a nearly 2.5-fold increase in the collapse fraction.

Parameter	Meaning	Value
r_{col}	Probability of collapse	$1 \cdot 10^{-3}$
r_{rlx}	Probability of relaxation	0.25
coop	Cooperation of collapse	$1 \cdot 10^{-2}$ (0.5 stress-induced)

In the following section, I introduce the different components and processes specific to the simulation and give an example of how the simulation was implemented. At the beginning of each simulation with the cellular automaton all triangles in the stressosome were relaxed. The dynamics of the stressosome were independent of the initial stressosome state because a simulation can, in principle, realise every possible stressosome configuration in a limited number of update steps. During a simulation the stressosome adopts many different possible configurations and each can be regarded as an initial start. Furthermore, it is not possible to assign completely random initial conditions; there are more forbidden configurations than allowed ones because each collapsed triangle must have all neighbours inhibited. The simulations reached a steady state typically before 140 update steps, using the parameter values in Table 4.1. For optimal reproducibility the simulations were repeated 50 times; more simulations did not reduce the standard deviation further. The code is written with Matlab® and available on the attached CD in folder '4th-Chapter_shape-transitions', and available for download in the Resource section of `www.sbi.uni-rostock.de`, named 'Liebal_thesis-data.zip'.

In one simulation step each triangle was evaluated once in a random order. Only relaxed triangles (no direct triangle neighbour is collapsed) can collapse, i.e. the Position-list is 1 for the triangle. A collapse at position A took place if the following condition held:

$$N_{\mathrm{rand}} < r_{\mathrm{col}} + {}^{A}F. \tag{4.1}$$

This is a standard Monte-Carlo evaluation of chemical reactions as used for example in the Gillespie-algorithm [Gillespie 1977]. In Equation 4.1, N_{rand} is a random number in the interval [0,1], and r_{col} is the probability parameter for the collapse (Table 4.1). The parameter ${}^{A}F$ quantifies the effect of neighbours on the collapse according to the equation:

$${}^{A}F = coop(1 - r_{\mathrm{col}})\frac{\sum_{i=1}^{3} {}^{A}I_i}{3}. \tag{4.2}$$

The middle term $(1 - r_{\mathrm{col}})$ ensures that the sum of r_{col} and ${}^{A}F$ in equation (4.1) has a maximum value of one. This term corresponds to the potential by which collapse efficiency can be increased. The cooperation parameter *coop* quantifies how effective the neighbours can use this potential and ranges from zero (neighbours cannot increase collapse, no collapse cooperation) to one (neighbours can make collapse a certainty, collapse cooperation). The results of the particle-swarm simulations implied that triangles inhibited for collapse (triangles with collapsed neighbours) stimulated collapse reactions of their neighbours. In equation (4.2), the parameter ${}^{A}I_i$ represents inhibited neighbours and is derived from the neighbour-list; ${}^{A}I_i$ is one if the i-th neighbour of A was inhibited, the neighbour-list is '3', and zero otherwise. Each triangle has three neighbours (Figure 4.2(B)), and an increase in the number of inhibited neighbours increases the probability of collapse of triangle A. The relaxation reactions are determined similar to equation (4.1), by exchanging the collapse probability with the relaxation probability (r_{rlx}) and without the neighbour effect, ${}^{A}F$.

The parameter *coop* allows the testing of different levels of cooperation for collapse as observed during the particle-dynamics simulations. Here, cooperation describes a spatial activation process, in which collapsed second order neighbours (the neighbours of neighbours) activated the collapse of triangles. This second order neighbour interaction was observed in the particles-dynamics simulation and is coded in the cellular-automaton formulation by using collapse inhibited triangles. A collapse inhibited neighbour informs a triangle that the neighbour of this neighbour is collapsed.

For example, the collapse of triangle no. 1 in Figure 4.2(B) is evaluated. Triangle 1 is relaxed (represented in a state table by '0'), therefore it is not collapsed (state table value of '1'), and it is also not inhibited for collapse (state table value '2'). First, we examine the neighbours of triangle 1, these are the triangles 2, 5 and 6. None of these can be collapsed, because otherwise triangle 1 would be inhibited. But if the triangles 2, 5 and 6 are inhibited themselves, then these triangles can stimulate the phosphorylation of triangle 1. For example, triangle 2 has neighbours 1, 3 and 7, and of those triangle 3 is collapsed. Consequently, triangle 2 is inhibited and stimulates collapse of triangle 1, via the parameter ${}^{1}I_2 = 1$ in equation (4.2). Similarly, triangles 5 and 6 might exert positive effects. If a collapse of triangle 1 occurs, then the state table of triangle 1 is changed to '1' and the states of triangles 2, 5 and 6 are changed to '2', representing the inhibited state. The effect of different combinations of parameter values was studied using an orthogonal sampling method. For two parameters under investigation the sampling space in the interval of [0,1] was divided into 15 squares. For each parameter two random numbers were generated in each square, resulting in 450 samples. Each sample of parameter combinations was simulated independently 50 times for statistical confidence. Every simulation was performed for 300 update steps, to ensure the steady state was achieved. The mean fraction

of collapsed triangles was calculated for steps 200 to 300 for each triangle position to get statistics only for the steady state. Note that the maximum number of simultaneously collapsed triangles is 0.4 (8/20), because collapsed triangles inhibit neighbour collapse.

4.2. Structure and motions of icosahedra

Modular origami techniques are able to reproduce the truncated icosahedron structure of the stressosome; a paper based geometric model of the stressosome is illustrated in Figure 4.3(B). By comparison, the molecular structure of the stressosome, solved by cryo-EM by Marles-Wright et al. [2008], is illustrated in Figure 4.3(A). In the geometric model, RsbR and RsbS proteins were represented by tetrahedra, and each tetrahedron had three nearest neighbours. However, the distances between the neighbours were unequal; each tetrahedron was closer to one neighbour than to the other two, thus forming a tetrahedron-dimer. The tetrahedron-dimers of the geometric model have the same distribution as the RsbR and RsbS dimers in the stressosome. A particle-dynamics simulation was employed to assess whether the structure of the modular origami model was independent of the construction method used and ensure that the origami model obeyed general geometric principles. Indeed, the minimum energy configuration of the particle-dynamics simulation was identical to that of the geometric model, and both were similar to the cryo-EM-reconstruction of the stressosome (Figure 4.3). The surface of the stressosome comprises trimers of dimers (two RsbR dimers and one RsbS dimer) and pentamers formed at the intersection of these; in Figure 4.3(B) a trimer of dimers points toward the observer, and three pentamers are adjacent to it.

The geometric model is flexible in the movements of the tetrahedral protrusions. Two dimers can approach one another when pressed together, indeed the force needed for the dimers to approach one another appears lower if all the dimers in a triangle are pushed together, a process here designated as triangle collapse. The triangle collapse was visualized for the three stressosome representations in Figure 4.3(D-F). If each dimer was a member of two triangle structures, it could only collapse into one of these triangles. If a dimer was collapsed into the first triangle, then the second triangle could not collapse (inhibited), and *vice versa*. A physical separation of the dimers was also possible in the geometric model when the pentamers were pushed together. This, however, required substantially more force in comparison to a triangle collapse. Given the strong interaction between dimers of RsbR and RsbS seen *in vivo* [Marles-Wright et al. 2008; Murray et al. 2005] this collapse is excluded on a molecular level.

In collaboration with Peter Raasch, a particle-dynamics simulation was constructed to verify the generality of the geometric model results. In the simulation, tetrahedral struc-

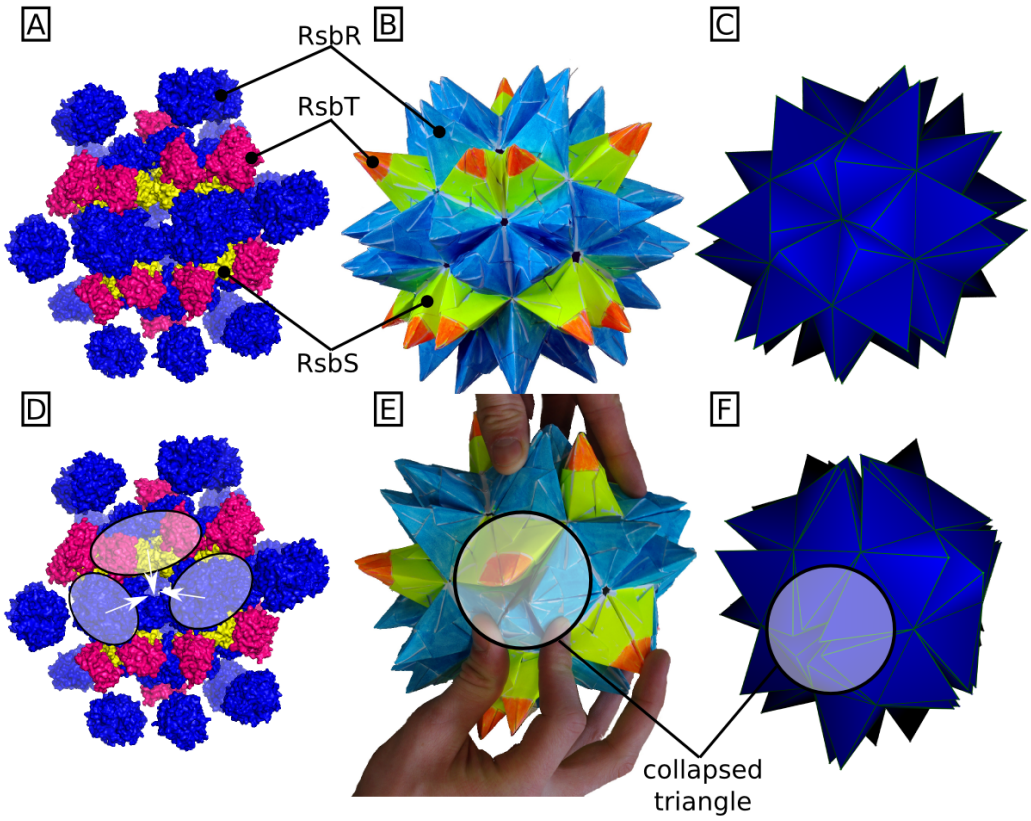

Figure 4.3.: Summary of the structural models of the stressosome. Subfigure (A) shows the surface model of the stressosome at atomic resolution determined by Marles-Wright et al. [2008], with RsbR coloured in blue; RsbS, yellow; and RsbT, red. Subfigure (B) shows the result of a modular origami geometric paper approach, and (C) shows a particle dynamics simulation of a truncated icosahedron model in which the tetrahedra are only attached by the edges of their triangular base. A-C show the stress-free, relaxed condition, whereas D-F shows the stress-induced, collapsed state. Triangles of dimers (hexamers) lead to a 'triangle collapse'. Isolated dimers are dimers that are not collapsed but for which all their neighbouring dimers collapsed, thus inhibiting the further collapse of isolated dimers. Both the geometric model and particle dynamics reproduce the dimer construction of the stressosome.

tures were used to represent the proteins (Figure 4.3(C)). The connections between the vertices were spring-like, with a restricted capacity for shrinking and elongation. In the non-excited state, no force acted between the tips of the tetrahedra, whereas the excited state was simulated by an increase in the attractive force between the tips. Excitation rendered the relaxed dimer configuration meta-stable. Slight imbalances in the force distribution resulted in the triangle collapse (Figure 4.3(F)), thus reproducing the findings of the paper-based geometric model.

4.3. Efficient stressosome activation via cooperation

Triangle collapse was the common result obtained for both the geometric model and the particle-dynamics simulation. Furthermore, the particle-dynamics simulation indicated that the collapse of one triangle redistributed the forces within the icosahedron such that the collapse of neighbouring triangles became more likely. Could the cooperation of triangle collapse be used in the regulation of stressosome activation? To answer this question, a cellular-automaton model was developed that combined the icosahedral structural [Liebal et al. 2013] with the dynamic information of triangle collapse and cooperation. Simulation results of cellular automata are inherently spatial and a graphical representation of two different simulation results of the cellular automaton of the stressosome is illustrated in Figure 4.4. The evolving patterns of collapse are unique for every simulation, but some general properties can be observed. Figure 4.5(A) represents a typical outcome regarding the frequency of collapse. In this simulation, many triangles collapsed with a frequency between 0.2 and 0.5, while there are a few triangles with a high (> 0.5) and low activity (< 0.1). Figure 4.4(B) shows a simulation with exactly 8 frequently and 12 rarely collapsing triangles. Only a minority of simulations follow this pattern, because the collapse of one triangle inhibits the collapse in the neighbouring triangles and this requires an optimal positioning of collapse to maximise collapse. The spatial representations of the cellular automaton simulations of the stressosome are included to exemplify direct simulation results. The patterns produced as direct outcome of the cellular automaton are, just like those of *Chapter 3*, of no practical use because they are experimentally inaccessible. Instead of examining the activity of each and every triangle we have to focus on all triangles of the stressosome over time.

Figure 4.5 shows the collapse activity over 600 update steps (corresponding to time) for a single stressosome (A) and for an ensemble of 50 simulations (B) using the parameter values of Table 4.1. At steady state about 15% (3 of 20) of the triangles were collapsed. However, it should be noted that a maximum of 40% (=8) of the possible triangles can collapse simultaneously because of steric collapse inhibition. Figure 4.5(A) shows the trajectory for a single simulation, and which also reveals the high noise level: the system

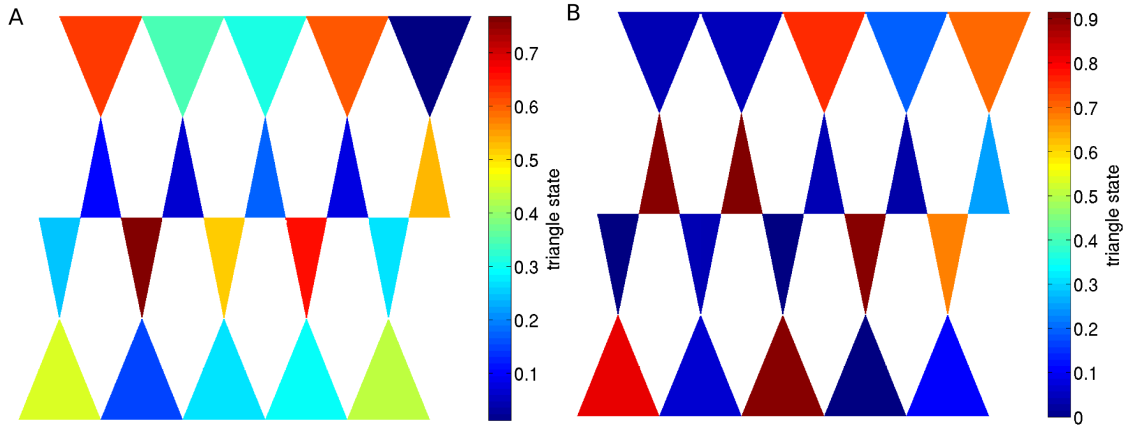

Figure 4.4.: Triangle specific collapse average over time. A simulation was performed for 200 update steps with the parameters listed in Table 4.1 with the high *coop* parameter and the average number of collapse events was calculated for each triangle. The visualization of triangles corresponds to the stressosome net of Figure 4.2(B). (A) shows a representative result with a majority of triangles activated with a frequency between 0.2 and 0.5 and a few high and low active triangles. (B) Represents a rare result for which the triangles have assumed a particular arrangement that allows for the maximal number of 8 simultaneous collapses. Highly collapsed triangles always have low active neighbours, because a collapsed triangle inhibits its neighbours.

varies between no collapsed triangles and 25% (=5) of collapsed triangles. Therefore, the standard deviation of 7% was high. After 400 update steps (dashed line), the parameter for the cooperativity of collapse (*coop*) was increased from 0.1 to 0.5 according to the hypothesis that stressosome activation is based on an increase of cooperation of collapse. The fraction of collapsed triangles immediately increased to 33% (=6.6). This is concomitant with a decrease in the standard deviation to 5%. Overall, the results show that stressosome activation can be regulated by an activation of the cooperation of collapse, but the outcomes in Figure 4.5 are limited to a particular combination of parameters. To justify the validity of our results, and to compare the response sensitivity if the stressosome is activated either by probability of collapse or by cooperation of collapse, I analysed a wide range of parameter values.

4.4. Parameter scan for stressosome activation

With the cellular-automaton modelling approach it is possible to study how different collapse probabilities (r_{col}) and an altered cooperation of collapse (*coop*) affect the fraction of collapsed triangles in the stressosome. An efficient stress response requires a strong increase in the amount of collapsed triangles. This can either take place by increasing the (i) collapse probability, (ii) collapse cooperation, or (iii)

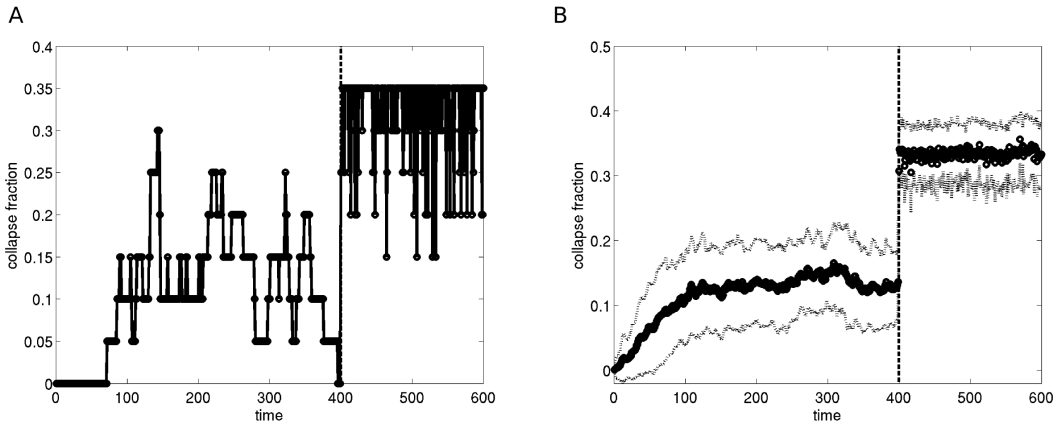

Figure 4.5.: Dynamics of triangle collapse of the cellular automaton (time). The data are collected from a single simulation (A) and the mean (circles) and standard deviation (dotted line) of 50 simulations (B). From simulation steps 0-400 (thick line) collapse cooperation was low, at $coop = 0.01$, whereas from 400-600 was increased to $coop = 0.5$. During stress-free condition on average 14% of triangles are collapsed whereas during stress the collapsed fraction increases by nearly 2.5-fold to 33%.

by decreasing the collapse relaxation (r_{rlx}). Figure 4.6 shows the change of the collapse fraction for parameter changes in the pairs $r_{\mathrm{col}} - r_{\mathrm{rlx}}$ (A) and $r_{\mathrm{rlx}} - coop$ (B). By evaluating Figure 4.6, I derived parameter combinations with a high collapse ratio between an active/non-active stressosome. The collapse probability needed to be below $r_{\mathrm{col}} < 0.05$ to result in a high activation ratio. By contrast, the value of the relaxation probability had limited effect on the activation ratio (Table 4.1). Strikingly, the relaxation reaction became more effective for the collapse cooperation mechanism (Figure 4.6(B)). In this condition the fraction of collapsed triangles decreased with increasing relaxation probability. Moreover, the relaxation probability had a larger effect on the collapse fraction, particularly at high r_{rlx} values. This capacity of the cooperation of collapse to enable regulation via a relaxation pathway allows for more regulatory control. The collapse is closely related to phosphorylations of the RsbR and RsbS proteins and thus dephosphorylation is necessary for relaxation to occur. Stressosome activation leads to the expression of RsbX, a phosphatase, and conceivably to an increase in the relaxation. The increase of collapse by the way of increasing cooperativity thus enables negative feedback regulation.

4.5. A new review of events during stressosome activation

The model of the stressosome activation proposed here is a variation of the stressosome model introduced in *Chapter 3*. Although the previous model also considered the stressosome structure and related the future state of a protein with its closest

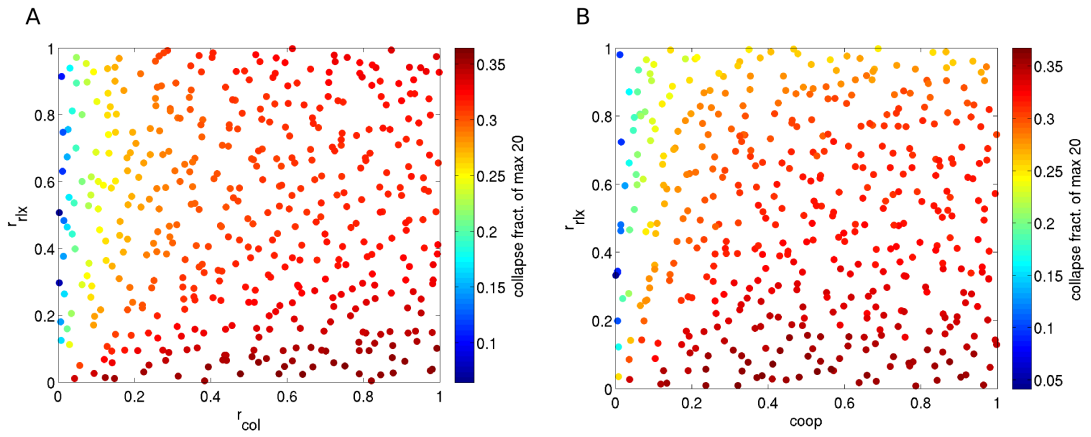

Figure 4.6.: Parameter scan of collapse frequency for collapse (r_{col}), relaxation (r_{rlx}), and cooperation (*coop*). (A) Probability distribution if partially collapsed triangles do not stimulate collapse of neighbouring triangles (*coop* = 0). (B) The average collapse fraction for different values of *coop*. If no cooperation exists then the collapse fraction is independent of the relaxation reaction and increases rapidly with the collapse probability. By contrast, if collapse becomes cooperative (increase in *coop*) then the relaxation reaction becomes influential. The parameter combination of cooperation and collapse probability shows an increase in collapse for both parameters but contains no new information and is given in *Appendix B*.

Table 4.2.: Comparison of two cellular-automaton models for stressosome activation. The model of the previous chapter focuses on phosphorylation reactions on protein monomers, whereas the model of the current chapter has explanatory power for structural events.

Property	Monomer model	Triangle model
Model basis	cellular automaton	cellular automaton
Simulated structure	trunctated icosahedron	regular icosahedron
Agent interpretation	protein monomers	triangles (3 dimers)
Number of agents	60	20
Different agent states	2 (phosphorylation)	3 (conformation)
Truth table size	22 (4 neighbourhoods with $3 \cdot 6 + 1 \cdot 4$ combinations)	4[1]
Number of parameters	4	3
Simulation output	fractional phosphorylation	fractional collapse

[1]The truth table is not explicitely modelled, but can be interpreted as such

neighbours, there are noteworthy differences (listed in Table 4.2). The model proposed here is tailored to investigate the observed structural rearrangements of icosahedra; it has been developed specifically with the stressosome in mind, but the model could be adapted to suit other icosahedra that undergo conformational change, such as the disassembly of many viruses on infecting their host's cells. In this study I have shown that the dimers in an icosahedron can physically approach each other, and this movement additionally induces the approach of two neighbouring dimers, ultimately leading to a collapse of a triangle of dimers (Figure 4.3(D-F)). The collapse of one triangle also induced the collapse of neighbouring triangles in a particle-dynamics simulation. This process was named co-operativity of collapse and it increases the influence of the parameter for the relaxation of triangles (the inverse of collapse) on the collapse occurrence. Whilst it is convenient to describe the conformational changes that occur during stressosome activation as the collapse of a triangle composed of protein dimers, this does not imply that the stressosome components undergo drastic collapse or structural rearrangement. Rather, any conformational change that occurs on activation in one protomer is transmitted through its neighbours within a triangle and propagated throughout the entire structure. Whether this conformational change takes place coincident with a stressosome intramolecular symmetry axis, or orthogonally to the axis, is irrelevant, the geometric principles surrounding neighbouring triangle collapse remain constant.

Overall, the modelling process suggests the following sequence of events for stressosome activation (Figure 4.7):

1. Stressors activate the sensory domain causing a conformational change [Jurk et al. 2011; Möglich and Moffat 2007];
2. The Jα linker transmits the signal to the STAS domain [Gaidenko et al. 2012; Möglich and Moffat 2007; Tang et al. 2010];
3. The Collapse Hypothesis explains the communication between RsbR and RsbS;
4. Phosphorylation of RsbR (catalysed by RsbT) [Chen et al. 2003; Gaidenko et al. 1999], and/or FMN-induced conformational changes in YtvA [Avila-Perez et al. 2009] stimulate phosphorylation of RsbS by RsbT;
5. Phosphorylation of RsbS triggers dissociation of RsbT [Chen et al. 2003];
6. RsbX dephosphorylates RsbS-P [Yang et al. 1996],
7. RsbT re-association and phosphorylation of RsbS;
8. RsbT re-association and slow recovery of pre-stimulus conformation of the sensors [Losi et al. 2003].

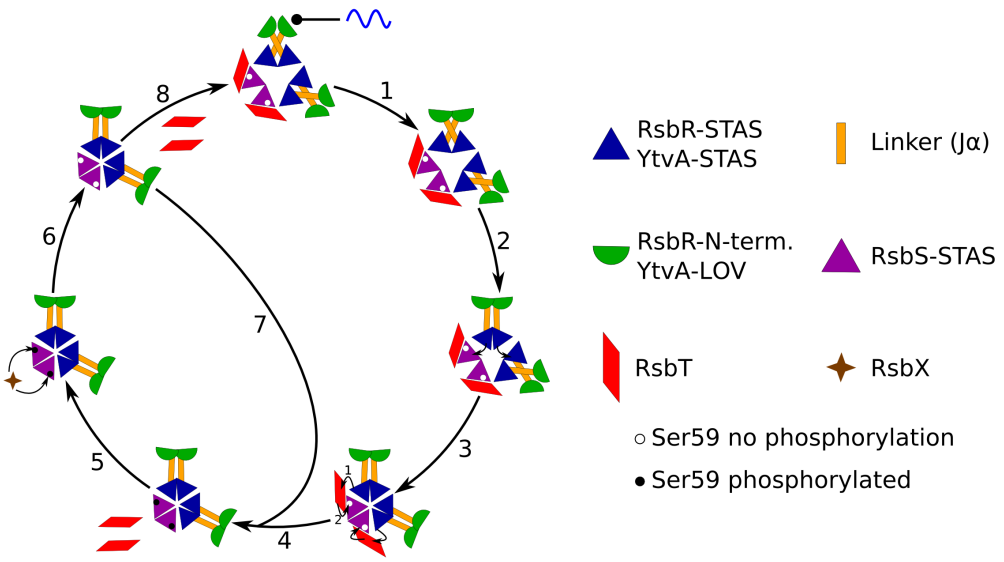

Figure 4.7.: Process diagram for the environmental stimulation of a triangle. An activation/deactivation process proceeds as follows: (1) signal perception; (2) conformational change transmitted to the STAS domain of RsbR/YtvA; (3) triangle collapse; (4) stimulation RsbT kinase activity; (5) RsbT dissociation; (6) RsbX mediated RsbS dephosphorylation; (7) RsbT re-association and stimulation; (8) RsbT re-association and recovery of pre-stimulus state.

This general stressosome activation model embodies the Collapse Hypothesis to explain the intermolecular communication between RsbR and RsbS. The graphical representation of the events leading to the stressosome activation in Figure 4.7 emphasizes an important regulatory function of the stressosome, generated by an auto-activation loop. After dephosphorylation of RsbS-P, the activated and collapsed triangle can participate in two reactions: 1) conformational change to re-activate the sensor and cessation of RsbT stimulation; or 2) re-association of cytoplasmic RsbT to the activated triangle, including the repeated phosphorylation of RsbS. The conformational changes associated with the reactivation of the sensor are in the order of 1 h for the LOV domain of YtvA [Losi et al. 2003], and also the dephosphorylation of the RsbR-P paralogues is considerably slower than RsbS-P dephosphorylation (*Chapter 3* and Chen et al. [2004]). Since reaction (7) is faster than reaction (8), the stressosome activation cycle is more likely closed via reaction (7), which decouples the stressosome response duration from the activation by the stimulus duration of reaction (1) (Figure 4.7). The rate of reaction (8) controls the length of the response and an adaptation of this reaction rate enables modification of stress response duration, independently of the stimulus duration. This feature is not associated with the Collapse Hypothesis, and thus is generic to the stressosome.

4.6. Relation of the results to experimental observations

RsbR and RsbS are the minimal combination of proteins required to form a stressosome *in vitro*, but as many as five paralogues of RsbR are also component parts of the stressosome *in vivo* [Akbar et al. 2001]. RsbS appears to act as a scaffold for the assembly of the stressosome, but it also plays a central role in the recruitment and regulated dissociation of the signalling protein, RsbT [Chen et al. 2003]. Of the RsbR paralogues involved in the environmental signalling pathway, the stimulus, UV light, is known only for one of the paralogues, YtvA [Avila-Perez et al. 2006; Gaidenko et al. 2006; Losi et al. 2002]. Moreover, the structure of YtvA before and after light reception has been determined. The LOV domain of YtvA appears to perform a scissor-like rearrangement following stimulation, with a distinct movement of the Jα helix linking the signalling and STAS domains [Möglich and Moffat 2007]. Solution studies of full length YtvA suggest that its overall shape is maintained in response to stimulus, but that rearrangements within the YtvA dimer, and particularly within the stressosome-anchored C-terminal STAS domain, may change the way YtvA interacts with its partners in the stressosome [Jurk et al. 2011]. To involve the stressosome-anchored STAS domain in the signalling pathway requires information transduction from the N-terminal LOV sensor. The two domains are connected by a flexible linker, called the (Jα) helix. Whereas Jurk et al. [2011] did not find that the Jα is involved in intramolecular interactions, Möglich and Moffat [2007] did detect molecular motions of Jα between dark and light state. The importance of the Jα linker has also been confirmed for RsbR [Gaidenko et al. 2012]; substitution of conserved residues increased stressosome activation, whereas substitution of non-conserved residues reduced it. These results fit the Collapse Hypothesis by allowing the linker to modulate the probability of a collapse of dimers, and subsequently triangles.

The observations of the geometric model, and the results of the particle-dynamics simulation, suggest a global structural reorganisation of the icosahedral structure of the stressosome. van Vlijmen and Karplus [2001] used normal mode analysis to study the motions of an icosahedron composed of 60 dialanine peptides *in silico*. The peptides can perform several motions, but the most prominent is 'breathing', a process during which the peptides depart from each other. The capsids of icosahedral viruses are well studied: a pH-dependent global shape transition has been observed for the cowpea chlorotic mottle virus (CCMV) [Bancroft et al. 1967; Speir et al. 1995]. Tama and Brooks III [2002] described a mechanism for the swelling of the CCMV particles using normal mode analysis. Strikingly, the motions of hexamers during swelling-induced expansion are more prominent compared to those of pentamers, and furthermore, dimers in the capsid stay close to one another. Hexamer expansion is the inverse of the triangle collapse proposed here. Computational investigations by normal mode analysis have also been applied to other icosahedral [Tama

and Brooks 2005], and non-icosahedral viruses [Nguyen et al. 2005]. Thus, shape transitions in icosahedral structures are common and well studied phenomena in the discipline of mathematical virology [Indelicato et al. 2011; Twarock 2006].

4.7. Model predictions and tests

Shape transitions of viral capsids are environment sensitive, an increase in pH, or a decrease in metal ion concentration leads to swelling of CCMV [Bancroft et al. 1967; Speir et al. 1995]. Probably, the triangle collapse is environmental sensitive, too. This enables the stressosome to monitor directly the constitution of the cytoplasm. For example, there is no knowledge how osmotic stress activates the stressosome. The suspicious absence of an osmotic signalling pathway could be elegantly explained by an induction of triangle collapse in response to the ionic strength.

In Figure 4.6(A) the increase in the probability of collapse (r_{col}) dominated over the probability of relaxation (r_{rlx}). The probability of collapse may correspond to the phosphorylation rate, and relaxation may correlate with RsbX mediated dephosphorylation. During stress response RsbX is expressed so as to reduce stressosome activation by increasing the relaxation rate, as shown in Figure 4.6(B). If also the probability of collapse would be increased, for example by a higher RsbT kinase activity, then the RsbX mediated negative feedback would fail to limit stressosome activation.

The release of RsbT from the stressosome allows the transmission of the perception of a stress signal to the downstream σ^{B} partner switching cascade [Kang et al. 1996]. Motions of the stressosome components following its excitation with specific stress signals have been found previously in several studies [Jurk et al. 2011; Marles-Wright et al. 2008; Möglich and Moffat 2007], and here we propose a radical structural hypothesis that links the release of RsbT with a shape transition in the stressosome. The hypothesis can be tested by computational elastic network models or normal mode analysis of the stressosome. Experimentally, cryo-EM or NMR studies of the activated stressosome could shed light on the magnitude of motions.

4.8. Conclusions

If icosahedra enable triangle collapse, then the stressosome can *in principle* use this mechanism for regulation. The chain of arguments is deductive and a direct proof needs to be established. It is impossible to estimate the magnitude of the collapse in the stressosome, though by keeping close to the results from the icosahedra, they can be substantial. The scientific achievements of this analysis includes a close association of

the structure and the function of the stressosome. The communication of the N-terminal RsbR/YtvA residues to the RsbT molecules is facilitated via a purely icosahedral and mechanical property. Cellular automata are idealy suited to deal with two dimensional system with spatial inhomogeneities. These conditions apply to chemotaxis. A chemotaxis array is located at the poles [Briegel et al. 2009] composed of two trimers of Tar-sensor dimers, a CheA dimer and two CheW monomers as basic unit (*Chapter 2* for details on chemotaxis) [Li and Hazelbauer 2011]. Cellular automata have already been applied to chemotaxis [Bornhorst and Falke 2003; Shimizu et al. 2003]. Lattice models have also been used to study signalling of Ras nanoclusters in the membrane of eukaryotes [Gurry et al. 2009]. The study of spatial implications of signalling is still developing [Kholodenko et al. 2010], and advancing technologies have only recently provided glimpses into the structure of signalling complexes [Cebecauer et al. 2010]. Geometric organised structures are increasingly observed, like the inflammasome [Davis et al. 2011], or the apoptosome [Acehan et al. 2002], and the principles I determined in this study will find utility in virology and other aspects of the systems biology of symmetrical macromolecular assemblies.

The previous two chapters focused on computational models for signalling events in the stressosome. The subsequent step in the general stress response signalling cascade is the partner switch of RsbW between RsbV and σ^{B}, modelled by Igoshin et al. [2007] and Locke et al. [2011]. Among the outstanding results of these computational models is their explanation for the positive feedback regulation of the σ^{B} operon. The positive activation provides a high activation capacity [Igoshin et al. 2007], whereas the negative feedback including RsbW equips the system with pulse-like dynamics [Locke et al. 2011]. In the next chapter, mathematical modelling of the dynamics of a β-galactosidase reporter of the general stress response unveils a protease activity that can also participate to generate pulse like dynamics of σ^{B}-dependent β-galactosidase expression.

Chapter 5

σ^{B} induced proteome reorganisation

[1]**Bacteria adapt to environmental challenges by altering their gene expression program.** These gene expression adjustments involve sensory networks, signal integrators of the environmental and cellular states, eventually regulating the activity of transcription factors. An important transcription factor of *B. subtilis* is σ^{B}, which is activated by a variety of environmental factors including acids, ethanol, heat, and salt, as well as oxidative stress, low temperature growth, desiccation, energy depletion, and light [Hecker et al. 2007; Price 2002; van der Horst et al. 2007]. σ^{B} regulates about 200 genes [Helmann et al. 2001; Petersohn et al. 2001; Price et al. 2001], encoding proteins involved in functions like multidrug efflux, non-specific oxidative stress resistance, acid stress resistance, membrane integrity, and transport [Hecker and Völker 2001; Price 2002].

The processes activating the σ^{B}-dependent general stress response have been studied in great detail [Haldenwang 1995; Hecker et al. 2007; Price 2002]. σ^{B} is activated via the 'partner switching' mechanism [Yang et al. 1996], illustrated in Figure 5.1. The anti-sigma factor RsbW binds and hence reduces the free sigma-factor concentration [Benson and Haldenwang 1993a]. Release of σ^{B} from RsbW, and thus activation of general stress response, is initiated if RsbW binds the anti-anti-sigma factor RsbV. RsbV and σ^{B} have overlapping binding sites on RsbW resulting in binding competition. Since RsbV has a higher affinity to RsbW, an increase in RsbV leads to a release of σ^{B} constituting the partner switch [Dufour and Haldenwang 1994]. During non-stress conditions, phosphorylation of RsbV results in a reduced affinity to RsbW, and most RsbW is associated with σ^{B} [Benson and Haldenwang 1993b; Dufour and Haldenwang 1994; Völker et al. 1996]. Energy limitation and environmental stress induce the activation of the two phosphatases of RsbV: RsbP and RsbU, respectively, thus initiating the partner switch [Vijay et al. 2000; Völker et al. 1995b, 1996; Yang et al. 1996]. Homologous mechanisms of σ^{B} activation can

[1]The original work of Liebal et al. (2012) is reproduced by permission of the Royal Society of Chemistry.

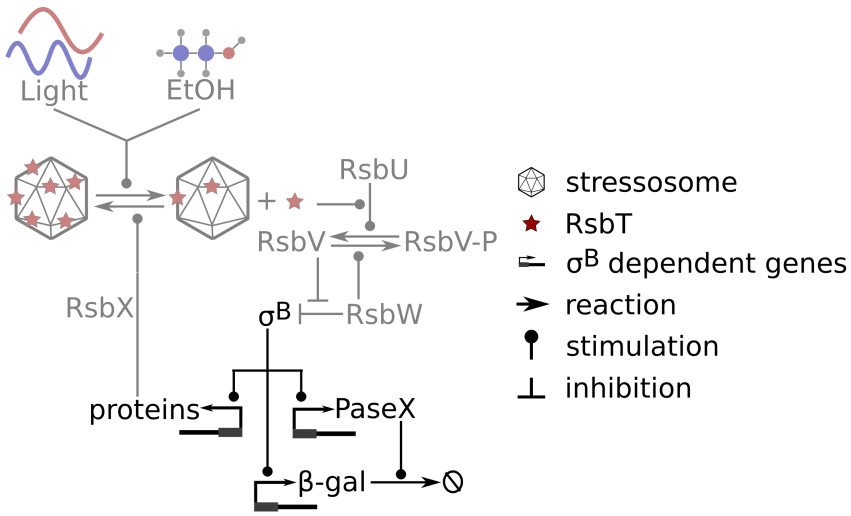

Figure 5.1.: Graphical thesis context of *Chapter 5*. The network shows the investigated signalling effect of σ^B to the expression of β-galactosidase and the hypothetical protease PaseX. In BSA115 upstream regulation of σ^B is disabled due to the absence of RsbW.

also be found in related bacteria although RsbP is confined to *B. subtilis* [Hecker et al. 2007; Pane-Farre et al. 2005; Price 2002]. Moreover, this control mechanism seems to have been analogously developed for general stress response in *Methylobacterium extorquens* [Francez-Charlot et al. 2009] and is used during activation of sporulation [Igoshin et al. 2007; Liebal et al. 2010].

5.1. Open questions in the general stress response

Despite the long years of research is our picture of σ^B activation via partner switching still incomplete. For example *B. subtilis* mutants lacking the anti-anti-sigma factor RsbV should normally be insensitive to stress activation, yet if *B. subtilis* grows continuously at low temperature strong induction of σ^B-dependent transcription was still observed in a *rsbV* mutant [Brigulla et al. 2003]. Also the mechanisms restricting σ^B activity and accomplishing the transient nature of the σ^B response are not fully understood.

σ^B-activity tests commonly rely on the use of *ctc::lacZ* reporter gene fusions which use the activity of β-galactosidase as an approximation of σ^B activity. β-galactosidase has a long history as a reporter enzyme and provides valuable insights into many cellular processes [Serebriiskii and Golemis 2000; Silhavy and Beckwith 1985]. *E. coli* and many other organisms tolerate extremely high protein levels of β-galactosidase, up to 20 % of total protein while still displaying robust and reliable activities [Santillán and Mackey 2008; Serebriiskii and Golemis 2000]. However, amount of protein and enzymatic activity do

not strictly correlate, e.g. after cessation of protein synthesis the enzyme-specific activity might still increase [Cazorla et al. 2001]. In *B. subtilis* heat-shock results in a quick drop in β-galactosidase activity, most probably caused by proteases like Lon and ClpCP that recognize the *E. coli* β-galactosidase as foreign [Mogk et al. 1996; Zuber and Schumann 1994].

In the following, I present a collaborative effort with the Functional Genomics Lab at the Ernst-Moritz-Arndt University in Greifswald and published as Liebal et al. [2012]. In this study an *rsbW* mutant (BSA115), in which expression of σ^B is solely controlled by the IPTG inducible promoter P_{SPAC} was used to learn more about the function of the autoregulatory loop of wild-type *B. subtilis* strains. The wild-type regulation is based on the σ^B driven expression of *rsbV*, *rsbW*, *sigB*, and *rsbX* (Figure 5.1). In strain BSA115, due to the lack of RsbW, all σ^B produced from P_{SPAC} in the presence of IPTG should be active and allow constitutive expression of a *ctc::lacZ* fusion. To render the *rsbW* mutant viable, the autoregulatory loop of σ^B expression upstream of *rsbV* was disrupted by deletion of the σ^B-dependent promoter. This strain is well suited to test the consistency of a σ^B model that I constructed based on a model by Igoshin et al. [2007]. Surprisingly, the BSA115 mutant displays similar transient induction patterns of β-galactosidase activity compared to a wild-type strain with an intact autoregulatory loop. Mathematical modelling suggested increased protease or RNase activities as the most likely explanation for the observations. Subsequent Northern- and Western-blot experiments then proved that β-galactosidase protein degradation was responsible for the transient σ^B response pattern observed in BSA115.

5.2. The reporter protein has transient activity in BSA115

The experiments were performed with three IPTG concentrations (low: 0.1 mM, medium: 0.2 mM, and high: 1 mM). Addition of IPTG activates *de novo* expression of σ^B, which then induces the transcription of *lacZ* of the σ^B-dependent *ctc::lacZ* fusion. Employing a *ctc::lacZ* fusion as a reporter, the induction of σ^B activity with high IPTG levels was approximately six times stronger compared with an induction in the wild type following the addition of ethanol (Praveen K. Sappa, personal communication). This course of events implies that different IPTG concentrations will cause different maximum β-galactosidase activities. Maximal β-galactosidase activity should be maintained depending on the stimulus level. However, a transient pattern of β-galactosidase activity is apparent (Figure 5.2(B)). Activity increased to reach a maximum, with higher IPTG concentrations causing a faster accumulation of β-galactosidase. After the peak, β-galactosidase activity declined rapidly and all experiments displayed a similar low activity 275 min after addition of IPTG.

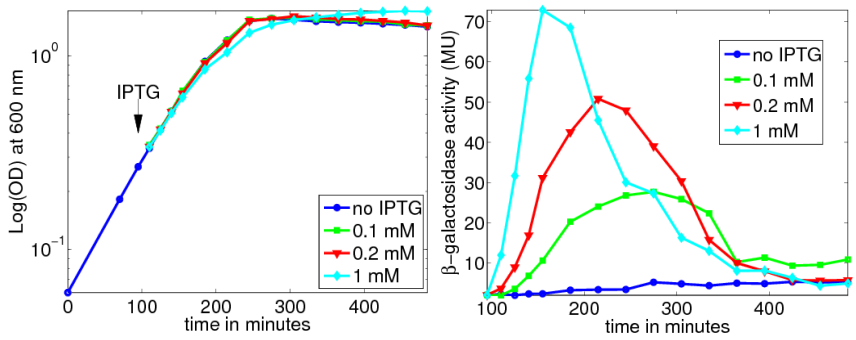

Figure 5.2.: Shake flask culture experiments of BSA115. Shown are the OD600 (a) and the activity of β-galactosidase per cell (b). Induction of expression of σ^B occurs at the time indicated when cells reached an OD600 of approximately 0.3.

5.3. Modelling of transient responses

Since the *a priori* assumption about the dynamics of the β-galactosidase activity differed with the observations, I hypothesized three mechanisms to explain the data. All hypotheses assume the expression of a σ^B-dependent regulatory protein. The decrease in the observed β-galactosidase activity seems to be independent of the growth phase because two cultures with identical growth characteristics (Figure 5.2(a)) had distinct β-galactosidase peaks (0.1 and 0.2 mM IPTG) (Figure 5.2(b)). Addition of high IPTG levels (1 mM) slightly retarded growth and transition to stationary phase but maximum β-galactosidase activity occurred still within the exponential phase of growth. These observations indicate that the decrease in β-galactosidase activity is not concurrent with the transition to stationary phase and is therefore not caused by the changing availability of RNA-polymerase or ribosomes during stationary phase. Additionally, I generated a model for proteolytic β-galactosidase degradation independent of σ^B but dependent on the optical density. In this model, the time of protease synthesis was chosen to correlate with the transition to stationary phase. The σ^B-independent model is not consistent with the experimental data (Appendix C). The stability of the IPTG induction system was tested by adding IPTG at regular intervals (Appendix C). These results indicate that the transient induction of β-galactosidase activity relies on a member of the *sigB* regulon. Three different mechanisms and the respective models that might account for the observations are shown in Figure 5.3, and can be biologically interpreted as follows:

1. **Transcription inhibition model**: The expression of a hypothetical protein, denoted with X, is induced by σ^B. X can be interpreted as a hypothetical transcription factor that inhibits the activity of σ^B. Therefore, following induction of σ^B activity

with IPTG, higher levels of X are generated and protein synthesis is subsequently inhibited. In this scenario, I assume X to be an unspecific protein expression inhibitor, but I also tested specific inhibition of *lacZ* expression which gives comparable results (not shown). This hypothesis resembles findings related to Spx, a protein involved in the regulation of disulfide stress response. Spx binds to the α-subunit of RNA-polymerase, thereby regulating expression rates for genes related to disulfide stress [Nakano et al. 2003; Newberry et al. 2005]. MgsR (YqgZ) is a Spx paralogue in *B. subtilis* implicated in the regulation of general stress response [Reder et al. 2008].

2. **σ^{B} proteolysis model**: In this model the hypothetical protein X is assumed to be a protease involved in σ^{B} degradation. This mechanism is biologically inspired by the regulation of the general stress response sigma factor σ^{S} in *E. coli* by RssB (SprE). RssB binds to σ^{S} and delivers it to the ClpXP proteolytic complex for degradation [Mitrophanov and Groisman 2008].

3. **Post-transcriptional instability model**: The decrease in the β-galactosidase activity can also be caused by degradation events acting directly on β-galactosidase either at the mRNA or protein level. The hypothetical protein X then represents an RNase or a protease. Within our modelling framework, I cannot distinguish between RNase and protease because I combine mRNA and protein production into a single step, assuming a quasi-steady-state approximation for mRNA. Thus, the corresponding variable in the equations can either represent mRNA or protein. However, I focus on protein instability as recombinant β-galactosidase has been indicated to be subjected to degradation in response to heat shock [Krüger et al. 1994; Mogk et al. 1996; Schrögel and Allmansberger 1997].

Although I assume in our models a direct control of σ^{B} regarding the regulator, this control might as well be indirect. There may be one or more intermediary σ^{B}-dependent factors activating the regulator. Direct versus indirect regulation are indistinguishable within our modelling framework.

5.4. Model setup and parameter estimation

Model details of the applied ODE-systems and the respective network diagrams are given in Figure 5.3. The parameter values that represent the best fit to the experiments and that are used to generate the time courses are given in Table 5.1. For the construction and the analysis of the models, the Systems Biology Toolbox2 for Matlab® was used [Schmidt and Jirstrand 2006]. SBML files of the model are uploaded to the JWS-model database and accessible with the following accession numbers: transcription inhibition (bsa_trscrinhib20122131995), SigmaB proteolysis (bsa_sigbprlysis201221319839), and

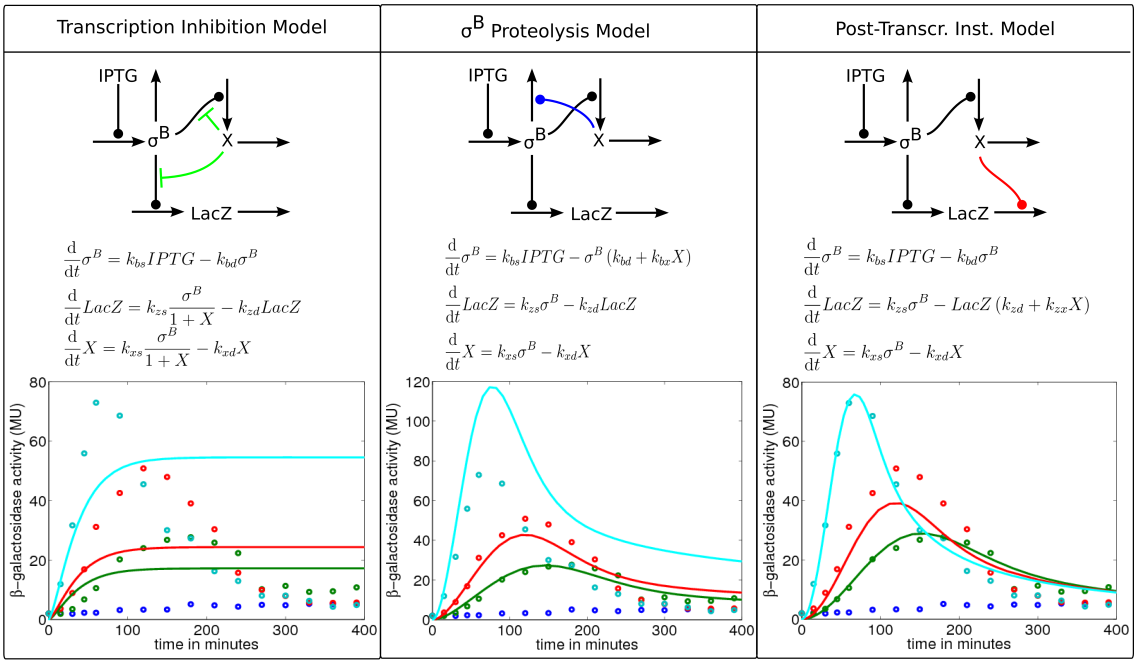

Figure 5.3.: Comparison of the tested models showing their process diagrams, their mathematical representation and their experimental fit. Only the 'post-transcriptional instability' model can reproduce the observations sufficiently. Northern-blot experiments of *lacZ*-mRNA and Western-blot experiments with β-galactosidase (Figure 5.4) narrow the instability down to proteolytic degradation of the β-galactosidase protein. Lines finishing with a bar denote inhibition of the associated reaction. Induction by IPTG is assigned to time 0 in the concentration-time plots.

post-transcriptional instability (bsa_ptinst201221319512). The model and the experimental data is available on CD in folder '5th-Chapter_protease-expression', and available for download in the Resource section of `www.sbi.uni-rostock.de`, named 'Liebal_thesis-data.zip'.

The parameters of σ^B synthesis (k_{bs}) and σ^B degradation/dilution (k_{bd}) are highly correlated, because they describe the dynamics of a variable for which no experimental information is available. To be able to estimate k_{bd}, I constrained k_{bs} arbitrarily to $100\,\mathrm{min}^{-1}$. This procedure is possible since only the ratio of synthesis and degradation determines the β-galactosidase dynamics. Parameter estimation was performed in the SBToolbox2 with the particle swarm algorithm that was applied to the model until no fitness improvement could be achieved [Schmidt and Jirstrand 2006; Vaz and Vicente 2007]. Measurements took place with three different experimental conditions. Different levels of σ^B were induced via three different medium concentrations of IPTG, namely low, medium and high (0.1, 0.2 and 1 mM). The data obtained with low and medium IPTG concentration were used as training set for parameter estimation, while the data for high IPTG addition served as test

Table 5.1.: Parameter values for the three competing models used to fit the experiments as shown in Figure 5.3. The dimension for IPTG concentration is μM and reaction rate constants are in Miller units per minute (MU min^{-1}). The adapted parameter values for fitting the post-transcriptional instability model to experimental data in BSG56 in Figure 5.6 are shown in brackets. Parameter fitting analyses indicate that the parameters can be estimated independently and have in general a low cross-correlation (Appendix C).

Parameter	Meaning	Transcription Inhibition	σ^B Proteolysis	Post-transcriptional Instability
IPTG	IPTG conc. for σ^B activation	100, 200, 1000 (28.9)		
k_{bs}	σ^B synthesis	100	100	100
k_{bd}	σ^B degradation	$4.4 \cdot 10^{-2}$	$5.8 \cdot 10^{-9}$	$1.7 \cdot 10^{-2}$
k_{bx}	regulator mediated σ^B degr.	–	$8.4 \cdot 10^{-5}$	–
k_{zs}	*lacZ*/β-galactosidase synth.	$4 \cdot 10^{-4}$	$1.7 \cdot 10^{-6}$	$9 \cdot 10^{-7}$ ($8.2 \cdot 10^{-6}$)
k_{zd}	*lacZ*/β-galactosidase degr.	$4.1 \cdot 10^{-2}$	$5.2 \cdot 10^{-2}$	$1.3 \cdot 10^{-7}$
k_{zx}	regulator mediated β-galactosidase degr.	–	–	$3.2 \cdot 10^{-3}$
k_{xs}	regulator synth.	$7.6 \cdot 10^{-1}$	$2 \cdot 10^{-6}$	$9.3 \cdot 10^{-8}$
k_{xd}	regulator degr.	9	$1.2 \cdot 10^{-13}$	$1.1 \cdot 10^{-9}$

set to evaluate how well the parameters can predict this experiment. I adapted the model of σ^B by Igoshin et al. [2007] to reproduce the σ^B dependent expression of β-galactosidase during the transition from exponential to stationary growth phase in BSG56, Table 5.1. The parameter estimation was conducted as explained above. Parameter estimation of the 'Post-transcriptional Instability' model with this data took place using only the measurements after 5 hours of cultivation since only then σ^B expression was induced. That time therefore represents the addition of IPTG in the BSA115 strain experiments. Only the two parameters $IPTG$ and k_{zs} were allowed to vary during estimation with particle swarm algorithm. The numerical results of the parameter estimation are shown in brackets in Table 5.1 and the fit is shown in Figure 5.6. In the following section the three models are compared and verified with the experimental observations.

5.5. Simulation and experiment cycles prove proteolysis

The process diagrams (Figure 5.3, top) were used to formulate systems of coupled ordinary differential equations. I then estimated parameter values of the

models to reproduce our experimental results. The resulting fits are shown in Figure 5.3. The 'transcription inhibition' model fails to explain the observed β-galactosidase dynamics, because the model prediction differs qualitatively from the observations (Figure 5.3). I also tested a model for inhibition of translation. Its results are similar to the 'transcription inhibition' model (not shown). The 'σ^B proteolysis' model is able to capture some characteristics of the measured dynamics, notably the transient, adaptive nature of the response. However, this model fails to reproduce the observation at 275 minutes after induction, where the different IPTG additions approaching a comparable low β-galactosidase activity. High IPTG stimulation results in a disproportional high β-galactosidase activity in the 'σ^B proteolysis' model. Therefore, also the 'σ^B proteolysis' model does not provide a plausible explanation for our experimental observations. By contrast, the 'post-transcriptional instability' model successfully reproduces all aspects of the experimental observations, i.e. transience of the dynamics and comparable β-galactosidase activity at the end of the experiment. The model is even able to reproduce the inverted activity results for the three IPTG concentrations at 245 min. At that time, low IPTG addition causes highest activity while high IPTG addition results in the lowest signal. The following sections provide a more detailed analysis of the 'post-transcriptional instability' model.

Model simulations and their analysis allowed us to identify instability of either mRNA or β-galactosidase protein as an explanation for the observed transient dynamics of β-galactosidase activity in BSA115. However, mRNA and protein instability is indistinguishable within the model because I assumed a rapid and direct correlation between mRNA and protein level to limit the number of unknown parameters. In effect, we arrive at a variable that combines information about mRNA and protein. To distinguish between mRNA and protein level, my collaboration partners at the University of Greifwald performed Northern- and Western-blot experiments to measure *lacZ*-mRNA and β-galactosidase-protein levels. mRNA levels during IPTG activation are shown in Figure 5.4A and display persistent high *lacZ*-mRNA levels. The smear besides the detected main transcript is explained by specific hybridization of the probe to exo- and endonucleolytically truncated degradation intermediates of the full-length mRNA as well as still nascent *lacZ*-mRNA molecules. The Western-Blot experiments mimicked the transient nature of the β-galactosidase activity. Remarkably, in the absence of IPTG, and hence at low basal level of σ^B activity, β-galactosidase remained stable (Figure 5.4(B) lower panel). The faint bands of β-galactosidase detected in the absense of IPTG induction are likely a reflection of low basal level expression from the leaky P_{SPAC} promoter.

One of the primary suspects responsible for degradation of β-galactosidase was the ClpCP protease [Krüger et al. 1994]. This complex is activated by stress and is also σ^B sensitive. In the collaboration with Uwe Völker at the University of Greifswald, we used

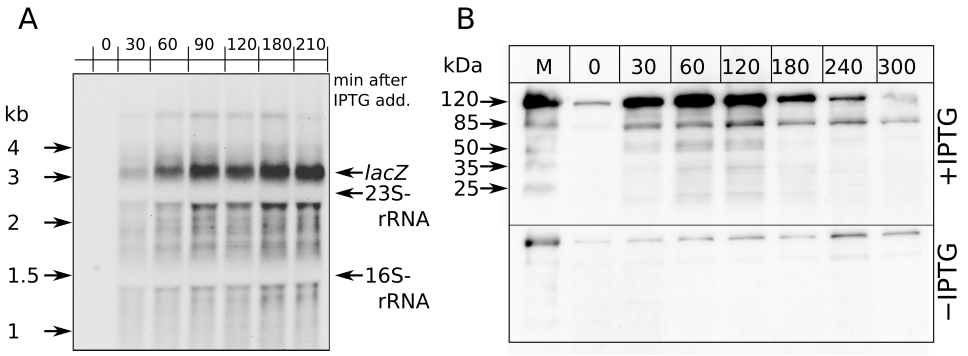

Figure 5.4.: (A) Northern-blot results for *lacZ* mRNA. Induction of σ^B expression and activity of BSA115 with 1 mM IPTG started at 0 min. Induction took place in early exponential phase as indicated in Figure 5.2(a). The blot was exposed for 30 min. (B) Western-blot results for the β-galactosidase protein which was detected at 120 kDa with respect to the marker (lane-M) used in this experiment. The upper panel reflects β-galactosidase levels after induction of σ^B by the addition of IPTG to a final concentration of 1 mM at 0 min. After 120 min the protein level declines, while the negative control without IPTG induction (lower panel) displays a continued low β-galactosidase. The blot was exposed for 30 s. The experiment was performed by P. K. Sappa at the Ernst-Moritz-Arndt Unversität Greifswald.

the *clpP*-deletion strain BSG115 and followed the stability of β-galactosidase. The reporter protein signal was still transient, comparable to the signals in the *clpCP* wild-type strain indicating that the ClpCP protease is not responsible for the observed β-galactosidase instability (Figure 5.5).

5.6. Proteolysis as part of transient wild-type responses

In experiments with BSG56, a wild-type strain with respect to σ^B regulation, σ^B-dependent gene expression first increases during transition into stationary phase, subsequently followed by a decrease in the level of the σ^B-dependent reporter protein, often a β-galactosidase-reporter system, close to pre-stimulus activity (compare β-galactosidase measurements in for example Brigulla et al. [2003]; Delumeau et al. [2004]; Kim et al. [2004b]; Scott et al. [2000]; Zhang et al. [2005]). Our presumption for the *rsbW* mutant strain BSA115 was to observe an initial increase in the β-galactosidase activity, with a sustained high and IPTG specific β-galactosidase activity. Negative feedback control mechanisms can explain transient responses and Igoshin et al. [2007] and Locke et al. [2011] proposed an RsbW-mediated negative feedback. Indeed, the model of σ^B regulation presented there can reproduce the adaptive β-galactosidase response shown in Figure 5.6, where I fitted

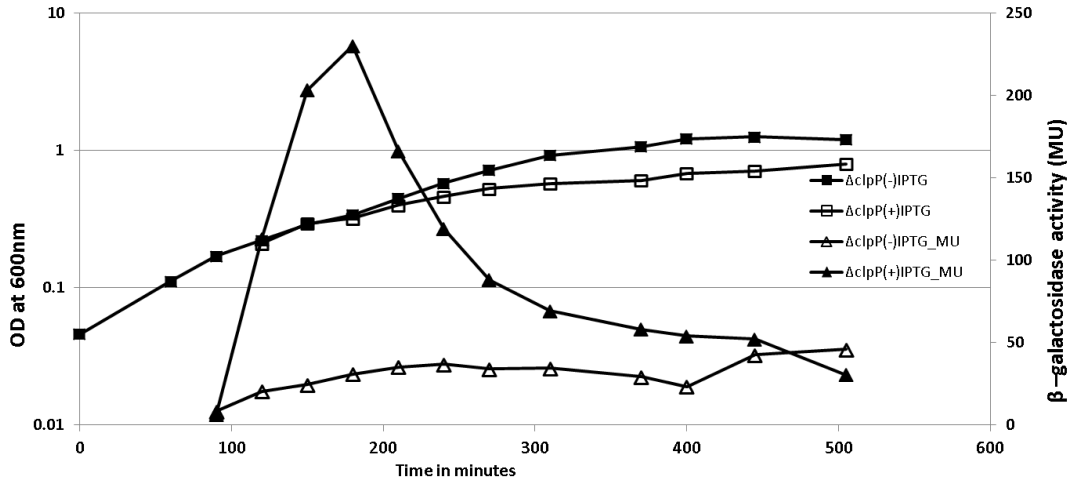

Figure 5.5.: β-galactosidase expression in a *clpP* knock-out strain. The filled triangles show the β-galactosidase activity following addition of IPTG at 100 min to a final concentration of 1 mM. Similarly to the dynamics in the wild type, the reporter activity increases and drops in the isogenic *clpP* deletion mutant approximately 80 min after induction with IPTG. The negative control without addition of IPTG is shown with open triangles. Optical densities are represented as filled squares for IPTG and open squares for +IPTG. The experiment was performed by P. K. Sappa at the Ernst-Moritz-Arndt Unversität Greifswald.

the model σ^B-feedback ('sigB fbck.' model) to an experimental course of general stress induction in a culture experiment with strain BSG56 (blue-dashed line). There is no ongoing β-galactosidase expression in our experiments with BSA115 (Figure 5.2), instead the response was similar to the transient response known from an *rsbW* wild type. The σ^B-dependent proteolytic activity that explains our observations in BSA115 was probably also present in previous experiments using BSG56. Thus, I sought to test how much of the transient nature of σ^B activation in BSG56 could be attributed to proteolytic degradation of β-galactosidase. The continuous red line in Figure 5.6 represents a fit of the proteolysis model ('post-translational instability' model in Figure 5.3) using experimental data from BSG56. Only two parameters, IPTG and k_{zs}, both not associated with the properties of the hypothetical protease, were used for parameter estimation. For the reproduction of the wild type, IPTG corresponds to the cellular energy level (approximated by medium glucose concentration). The synthesis rate of β-galactosidasek_{zs} was estimated to allow for fitting of the different absolute Miller unit maxima in the two experiments. While not necessarily being the only explanation for the transient dynamics, the mathematical proteolysis model (prot. model) in Figure 5.6 suggests an involvement of proteolytic degradation of β-galactosidase.

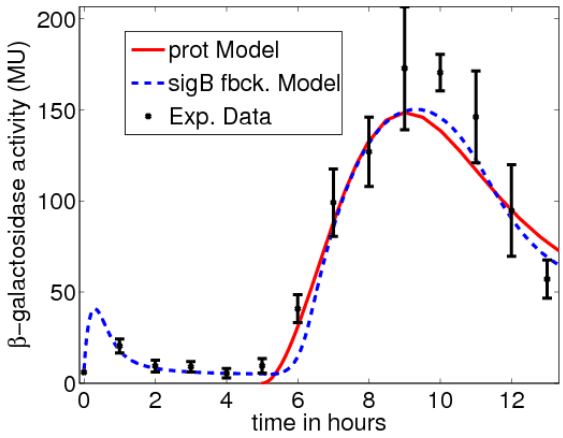

Figure 5.6.: Reproduction of general stress response during starvation in BSG56. The activity of the general stress response transcription factor σ^B was measured with a *ctc::lacZ* fusion. Black points represent experimental data. The blue-dashed line represents a fit of a σ^B model that includes the regulation of σ^B activity by the Rsb-proteins. The red-continuous line represents the fit of the 'post-translational instability' model for the transient activation of the general stress response.

5.7. Implications of reporter protein instability

The results show an activation of proteolytic degradation of β-galactosidase following IPTG induction of σ^B. I adapted the model of σ^B response by Igoshin et al. [2007] by including glucose starvation as a trigger for activation and fitting it to existing experiments. This model can reproduce experimental observations of σ^B activation and deactivation as represented by the blue-dashed line in Figure 5.6. In the collaboration with Uwe Völker at the University in Greifswald, we then performed an experiment in which we used the *B. subtilis* strain BSA115, characterized by stable IPTG-mediated induction of σ^B expression and lack of negative regulation of σ^B activity, due to a frameshift mutation in *rsbW* (see Material and Methods section). Unexpectedly, an induction of σ^B with IPTG resulted in a transient activity of β-galactosidase as indicated in Figure 5.2. Using mathematical modelling to compare different hypotheses lead to the conclusion of an instability of either mRNA or protein as potential causes for the transient activity as demonstrated in Figure 5.3. Subsequent Northern and Western-blot experiments confirmed proteolytic decay as the cause for the decrease in β-galactosidase signal (Figure 5.4). The transient activity in BSA115 resembles the transient activity observed in experiments in a wild-type *B. subtilis* strain (BSG56) containing an intact σ^B regulation. I tested whether proteolytic decay is at least partially responsible for transient β-galactosidase dynamics in the wild type by adapting the 'post-transcriptional instability' model to experimental observations in BSG56. Indeed, the results indicate that σ^B-induced β-galactosidase instability is a process with potential contributions to the adaptive behavior of β-galactosidase in the

wild-type. Two questions remain open: i) Is the increase in β-galactosidase proteolysis specific to the recombinant β-galactosidase? and ii) How can the different stresses that activate the σ^B-related general stress response diversify the expression of σ^B-dependent genes?

Results by Reeves et al. [2007] point to the importance of the ClpP protease for the regulation of σ^B activity. A *clpP* mutant strain results in lasting σ^B activation measured with β-galactosidase activity from a *ctc::lacZ* fusion [Reeves et al. 2007]. This leads to the assumption that ClpP could be associated with the turnover of σ^B dependent components that result in a deactivation of σ^B in the wild type [Reeves et al. 2007]. However, further experiments performed by us revealed that ClpP did not affect the stability of β-galactosidase. Hence, different proteolytic mechanisms may lead to a reduction in σ^B dependent β-galactosidase activity in our experimental setup. Similarly, our results stress the importance of induced proteolysis, albeit now it is the reporter protein β-galactosidase being targeted for degradation. In our experiments, transcriptional activity of σ^B is not diminished while the reporter signal still decreased. The previous list of possible mechanisms that could explain the transient nature of the σ^B response is neither complete nor are those mechanisms mutually exclusive. Further work is required to quantify and discriminate each contribution and to uncover new modes of regulation.

5.8. A wider context of transient responses

The mechanisms I study to explain the experimentally observed transient adaptive-like dynamics are derived from established biological processes associated with bacterial stress response. An analysis about all possible topologies that can result in adaptive dynamics was performed by Ma et al. [2009]. The authors found only two configurations for robust adaptation given suitable parameter combinations: integral feedback (buffered negative feedback), and incoherent feedforward. The 'transcription inhibition' and the 'σ^B proteolysis' models are examples for integral feedbacks, while the 'post-transcriptional instability' model is an example for an incoherent feedforward loop. According to Ma et al. [2009], there are few biological cases where incoherent feedforward loops are used to achieve adaptation. Although I do find such a motif explaining our observations, the wild-type regulation of σ^B-mediated general stress response is better known for its use of integral feedback regulation via anti-sigma factor RsbW [Benson and Haldenwang 1993a] and phosphatase RsbX [Völker et al. 1995a]. Thus, the observation by Ma et al. [2009] remains valid: adaptation generated by incoherent feedforward loops is rare.

5.9. Conclusions

The research focus with respect to σ^B-mediated general stress response has been on its activation whereas less information is available about mechanisms of the shut-off of σ^B activity. Using β-galactosidase to investigate σ^B deactivation is complicated since this protein is prone to degradation particularly in the context of overproduction (this study) and heat shock [Mogk et al. 1996]. Several mechanisms can contribute to the transient response of σ^B-dependent transcription: 1) silencing of σ^B by subsequent response strategies, 2) adaptivity caused by negative feedbacks, and 3) increased proteolytic instability after σ^B activation. Silencing of σ^B by subsequent response strategies could be an inevitable event of differentiation and adaptation processes of *B. subtilis* following deteriorating environmental conditions. Activation of processes, like sporulation or biofilm formation, could inhibit activity of σ^B much like they modulate activity of competence and chemotaxis [Liebal et al. 2010; Msadek 1999]. Subsequently, transcriptional activity of σ^B declines. Several studies have promoted the hypothesis that negative feedbacks within the partner switch regulation of σ^B result in its adaptive behavior [Igoshin et al. 2007; Scott et al. 2000; Völker et al. 1995a]. Activation of σ^B leads to increased expression of the anti-sigma factor RsbW and the phosphatase RsbX resulting in an increase in RsbV phosphorylation. This in turn releases RsbW to sequester and mute σ^B. This mechanism can result in a decline of σ^B-dependent transcriptional activity as well. Locke et al. [2011] studied how the σ^B system uses noise in combination with a kinase-phosphatase pair (RsbW-RsbP) to adjust stress response activation frequency. These authors are able to explain the transient dynamics they observe, only with the RsbW negative feedback and they disregard changes in YFP stability. Transient dynamics are generated in our β-galactosidase system via increased degradation following σ^B activation, and this offers an additional mechanism to generate or exaggerate transients.

Chapter 6

Final remarks

How does an organism perceive its environment? How do bacteria process information and regulate gene expression? The general stress response, and particularly the stressosome, enables us to learn about the organism-environment interface. The stressosome is a sensor of environmental information in the cytoplasm and processes information to regulate an appropriate response. The original stimuli are varying in their nature: stressosome responses have been observed upon exposure to stresses such as heat, osmolytes (NaCl), ethanol, and UV light [de Been et al. 2011; Hecker et al. 2007]. However, only for UV light was the mechanism of signal perception identified [Möglich and Moffat 2007]. This raises the question of how the other, seemingly non-related, stressors activate the stressosome. There is increasing evidence that ethanol, heat, and NaCl have a common physiological effect on *B. subtilis*: the generation of reactive oxygen species (ROS) [Höper et al. 2004; Mols and Abee 2011; Reder et al. 2012]. These results directly lead to the question whether ROS participate in an intermediary signalling step between environmental stresses and the stimulation of the stressosome.

ROS are generated by the premature leakage of electrons to oxygen during electron transport in aerobic respiration, which is particularly caused by the stressosome stressors ethanol, heat, and NaCl [Mols and Abee 2011]. Not only are ROS a common consequence of different stresses, but my results additionally reveal an identical activation profile in the signal-response behaviour for ethanol and NaCl [Liebal et al. 2013]. The cellular response to 3 % ethanol is as pronounced as that to 488 mM NaCl, presumably because these stresses produce the same amount of secondary oxidative stress and ROS. How ROS activate the stressosome is still unknown. *B. subtilis* specific peptides are believed to be involved, because the transplantation of the σ^{B} operon from *B. subtilis* to *E. coli* fails to conserve stressosome activation following ethanol or heat shock [Scott et al. 1999].

Although it is still a matter of debate whether the different stressors ethanol, heat, and NaCl act on a common intermediate, the Collapse Hypothesis of *Chapter 4* and all ensuing events are stressor-independent. These events are derived from the general properties of the geometric structure of the stressosome being either a truncated icosahedron (vertices as proteins), a pentakis dodecahedron (faces as proteins), or a regular icosahedron (edges as protein dimers), depending on the viewpoint. Common to these geometries is their property to allow three protein dimers (triangles) to perform motions - the collapse - that conserve the dimensions and distances of the geometry. The application of the Collapse Hypothesis to the stressosome provides an explanation for the communication between the signal perception by the N-terminus of RsbR to the RsbS-associated protein RsbT. These structural rearrangements prime RsbT to phosphorylate its target RsbR and subsequently RsbS, ultimately causing RsbT to dissociate. In order to switch the stressosome to its pre-stimulus condition, RsbS-P and RsbR-P need to be dephosphorylated to allow RsbT reassociation, and to cease RsbT kinase stimulation [Hecker and Völker 2001; Hecker et al. 2007; Price 2002]. During the resetting of the stressosome, a faster dephosphorylation of RsbS is observed compared to that of RsbR, thus allowing the reassociation of RsbT to a stressosome containing a still-phosphorylated RsbR. Slow RsbR dephosphorylation is reproduced in the monomer-stressosome model described in *Chapter 3*, where I also show that the phosphatase RsbX does not dephosphorylate RsbR for mild and medium stress insults. As a consequence, reassociated RsbT is stimulated by RsbR-P, causing the repeated phosphorylation of RsbS. The RsbR-P dephosphorylation is the slowest event in the signalling pathway, and by regulating its rate, the cell modulates the response duration. In conclusion, the stressosome output is independent of the quality and duration of the original signal.

With ROS being a shared consequence of ethanol, heat, and NaCl stress, it is not surprising that the transcriptomic responses are highly similar. I use the word 'highly', because the transcriptomic profiles of heat, ethanol, and salt are more comparable than the profiles of 266 other widely differing environmental conditions tested by Nicolas et al. [2012]. The physiological effects of ROS include the perturbation of the NAD^+/NADH balance, the redox-system, and disulfide bridges [Mols and Abee 2011]. Among the many stress responses activated by σ^B is the expression of proteases for the degradation of chemically altered proteins [Gottesman 2003]. Several σ^B-dependent proteases have been identified already [Price et al. 2001; Reeves et al. 2007], and the results of *Chapter 5* provide evidence that a protease is responsible for the degradation of the heterologous protein β-galactosidase. These results confirm the importance of proteases during the stress response, but they also caution against the use of the heterologous reporter protein β-galactosidase.

Computational models of the different signal processes in *B. subtilis* have helped to answer unresolved questions and to state new ones [Liebal et al. 2010]. Models that integrate the complete environmentally activated σ^B-dependent general stress response are within reach. In *Chapters 3* and *4* of this thesis, I provide the first computational models for stressosome activation by environmental factors. By reproducing a wide range of experimental data, these models faithfully capture stimulation by ethanol, heat, and NaCl, although they omit the partner-switching cascade of direct σ^B release. This partner-switching mechanism and its activation during energy stress was modelled independently by Igoshin et al. [2007] and Locke et al. [2011]. A full reproduction of σ^B-dependent stress response requires a combination of the stressosome and partner-switch models. However, hybrid modelling approaches are necessary, because although differential equations are beneficial for modelling the partner-switch, they are incapable of capturing the structural properties of the stressosome.

The models I present for the stressosome add to the foundation of models to come that integrate the σ^B response into the global environmental signalling landscape. This is possible for *B. subtilis* because it has only slightly more than 30 two-component systems per cell [Kunst et al. 1997], which are the primary means of bacteria to sense the environment [Mitrophanov and Groisman 2008]. As a soil generalist, how much does *B. subtilis* need to know about its environment, and how much information can be gathered in soil at all? Answering these questions will help classify bacteria, and enable us to determine lifestyles based on genomic information. However, this information extends beyond bacteria: we learn about our environment. Life means sensation, and bacteria are the most widely distributed sensors. By uncovering bacterial adaptation strategies, we learn more about the challenges and diversity in niches like hydrothermal vents in oceans, the valleys of Antarctica, or even our metazoan bodies that happen to be substrates for a bacterial success story.

Chapter 7

Bibliography

D. Acehan, X. Jiang, D. Morgan, J. Heuser, X. Wang, and C. Akey. Three-dimensional structure of the apoptosome: implications for assembly, procaspase-9 binding, and activation. *Mol Cell*, 9(2):423–432, 2002.

B. Adiwijaya, P. Barton, and B. Tidor. Biological network design strategies: discovery through dynamic optimization. *Mol BioSyst*, 2(12):650–659, 2006.

C. Aguilar, H. Vlamakis, A. Guzman, R. Losick, and R. Kolter. KinD Is a Checkpoint Protein Linking Spore Formation to Extracellular-Matrix Production in *Bacillus subtilis* Biofilms. *mBio*, 1(1):e00035–10, 2010.

S. Akbar, C. Kang, T. Gaidenko, and C. Price. Modulator protein RsbR regulates environmental signalling in the general stress pathway of *Bacillus subtilis*. *Mol Microbiol*, 24(3):567–578, 1997.

S. Akbar, T. Gaidenko, C. Kang, M. O'Reilly, K. Devine, and C. Price. New family of regulators in the environmental signaling pathway which activates the general stress transcription factor σB of *Bacillus subtilis*. *J Bacteriol*, 183(4):1329–38, 2001.

R. Alves and M. Savageau. Comparative analysis of prototype two-component systems with either bifunctional or monofunctional sensors: differences in molecular structure and physiological function. *Mol Microbiol*, 48(1):25–51, 2003.

L. Aravind and E. Koonin. The STAS domaina link between anion transporters and antisigma-factor antagonists. *Curr Biol*, 10(2):53–55, 2000.

M. Avila-Perez, K. Hellingwerf, and R. Kort. Blue light activates the *sigma*B-dependent stress response of *Bacillus subtilis* via YtvA. *J Bacteriol*, 188(17):6411–14, 2006.

M. Avila-Perez, J. Vreede, Y. Tang, O. Bende, A. Losi, W. Gartner, and K. Hellingwerf. In Vivo Mutational Analysis of YtvA from *Bacillus subtilis*: Mechanism of Light Activation of the General Stress Response. *J Biol Chem*, 284(37):24958–64, 2009.

U. Bai, I. Mandic-Mulec, and I. Smith. SinI modulates the activity of SinR, a developmental switch protein of *Bacillus subtilis*, by protein-protein interaction. *Genes Dev*, 7 (1):139–48, 1993.

J. Bancroft, G. Hills, and R. Markham. A study of the self-assembly process in a small spherical virus formation of organized structures from protein subunits in vitro. *Virology*, 31(2):354–79, 1967.

V. Barbe, S. Cruveiller, F. Kunst, P. Lenoble, G. Meurice, A. Sekowska, D. Vallenet, T. Wang, I. Moszer, C. Medigue, et al. From a consortium sequence to a unified sequence: the *Bacillus subtilis* 168 reference genome a decade later. *Microbiology*, 155 (6):1758–75, 2009.

A. Benson and W. Haldenwang. Characterization of a regulatory network that controls sigma B expression in *Bacillus subtilis*. *J Bacteriol*, 174(3):749–757, 1992.

A. Benson and W. Haldenwang. *Bacillus subtilis* SigmaB is regulated by a binding protein (RsbW) that blocks its association with core RNA polymerase. *Proc Natl Acad Sci USA*, 90(6):2330–2334, 1993a.

A. Benson and W. Haldenwang. Regulation of SigmaB levels and activity in *Bacillus subtilis*. *J Bacteriol*, 175(8):2347–2356, 1993b.

A. Benson, A. Stevenson, and W. Haldenwang. Mutations in *Bacillus subtilis* which influence the activity of a promoter recognized by a minor form of rna polymerase (e_crB). *Genetics and Biotechnology of Bacilli*, 3:13–21, 1989.

R. Berka, J. Hahn, M. Albano, I. Draskovic, M. Persuh, X. Cui, A. Sloma, W. Widner, and D. Dubnau. Microarray analysis of the *Bacillus subtilis* K-state: genome-wide expression changes dependent on ComK. *Mol Microbiol*, 43(5):1331–1345, 2002.

D. Bischoff and G. Ordal. *Bacillus subtilis* chemotaxis: a deviation from the *Escherichia coli* paradigm. *Mol Microbiol*, 6(1):23–28, 1991.

I. Bischofs, J. Hug, A. Liu, D. Wolf, and A. Arkin. Complexity in bacterial cell–cell communication: Quorum signal integration and subpopulation signaling in the *Bacillus subtilis* phosphorelay. *Proc Natl Acad Sci USA*, 106(16):6459–64, 2009.

H. Bisswanger. *Enzyme Kinetics: Principles and Methods*. Wiley-VCH, 2002.

F. Blattner, G. Plunkett III, C. Bloch, N. Perna, V. Burland, M. Riley, J. Collado-Vides, J. Glasner, C. Rode, G. Mayhew, et al. The complete genome sequence of *Escherichia coli* K-12. *Science*, 277(5331):1453–62, 1997.

J. Bornhorst and J. Falke. Quantitative analysis of aspartate receptor signaling complex reveals that the homogeneous two-state model is inadequate: development of a heterogeneous two-state model. *J Mol Biol*, 326(5):1597–1614, 2003.

S. Boylan, A. Redfield, M. Brody, and C. Price. Stress-induced activation of the sigma B transcription factor of *Bacillus subtilis*. *J Bacteriol*, 175(24):7931–7937, 1993.

A. Briegel, D. Ortega, E. Tocheva, K. Wuichet, Z. Li, S. Chen, A. Müller, C. Iancu, G. Murphy, M. Dobro, et al. Universal architecture of bacterial chemoreceptor arrays. *Proc Natl Acad Sci USA*, 106(40):17181–86, 2009.

G. Briggs and J. Haldane. A note on the kinetics of enzyme action. *Biochem J*, 19(2): 338–39, 1925.

M. Brigulla, T. Hoffmann, A. Krisp, A. Völker, E. Bremer, and U. Völker. Chill Induction of the SigB-Dependent General Stress Response in *Bacillus subtilis* and Its Contribution to Low-Temperature Adaptation. *J Bacteriol*, 185(15):4305–4314, 2003.

R. Bruinsma, W. Gelbart, D. Reguera, J. Rudnick, and R. Zandi. Viral self-assembly as a thermodynamic process. *Phys Rev Lett*, 90(24):248101, 2003.

J. Buescher, W. Liebermeister, M. Jules, M. Uhr, J. Muntel, E. Botella, B. Hessling, R. Kleijn, L. Le Chat, F. Lecointe, et al. Global Network Reorganization During Dynamic Adaptations of *Bacillus subtilis* Metabolism. *Science*, 335(6072):1099–1103, 2012.

B. Burnley and J. Cox. Dynamic polyhedral models of globular proteins. *J Theor Biol*, 229(2):197–208, 2004.

B. Burnley and J. Cox. An efficient biomimetic assembly of a macroscopic polyhedral shell from identical subunits. *Mater Sci Eng C*, 25(4):529–540, 2005.

V. Buttani, A. Losi, T. Eggert, U. Krauss, K. Jaeger, Z. Cao, et al. Conformational analysis of the blue-light sensing protein YtvA reveals a competitive interface for LOV-LOV dimerization and interdomain interactions. *Photochemical and photobiological sciences*, 6(1):41–49, 2007.

D. Caspar and A. Klug. Physical principles in the construction of regular viruses. *Cold Spring Harbor Symposia on Quantitative Biology*, 27:1–24, 1962.

D. Cazorla, J. Feliu, and A. Villaverde. Variable specific activity of *Escherichia coli* β-galactosidase in bacterial cells. *Biotechnol Bioeng*, 72(3):255–260, 2001.

M. Cebecauer, M. Spitaler, A. Sergé, and A. Magee. Signalling complexes and clusters: functional advantages and methodological hurdles. *J Cell Sci*, 123(3):309–320, 2010.

Y. Chai, F. Chu, R. Kolter, and R. Losick. Bistability and biofilm formation in *Bacillus subtilis*. *Mol Microbiol*, 67(2):254–63, 2007.

A. Chastanet, D. Vitkup, G.-C. Yuan, T. Norman, J. Liu, and R. Losick. Broadly heterogeneous activation of the master regulator for sporulation in *Bacillus subtilis*. *Proc Natl Acad Sci USA*, 107(18):8486–91, 2010.

C. Chen, R. Lewis, R. Harris, M. Yudkin, and O. Delumeau. A supramolecular complex in the environmental stress signalling pathway of *Bacillus subtilis*. *Mol Microbiol*, 49 (6):1657–69, 2003.

C. Chen, M. Yudkin, and O. Delumeau. Phosphorylation and RsbX-dependent dephosphorylation of RsbR in the RsbR-RsbS complex of *Bacillus subtilis*. *J Bacteriol*, 186 (20):6830–36, 2004.

F. Chu, D. Kearns, S. Branda, R. Kolter, and R. Losick. Targets of the master regulator of biofilm formation in *Bacillus subtilis*. *Mol Microbiol*, 59(4):1216–1228, 2005.

J. Claverys and L. Håvarstein. Cannibalism and fratricide: mechanisms and raisons d'être. *Nat Rev Microbiol*, 5(3):219–229, 2007.

J. Cohen. Mathematics is biology's next microscope, only better; biology is mathematics' next physics, only better. *PLoS Biol*, 2(12):e439, 2004.

L. Cuccia, R. Lennox, and F. Ow. Molecular modeling of fullerenes with modular origami. *Abstr Pap Am Chem S*, 208:26–31, 1994.

S. D'Amico, T. Collins, J. Marx, G. Feller, and C. Gerday. Psychrophilic microorganisms: challenges for life. *EMBO Rep*, 7(4):385–89, 2006.

B. Davis, H. Wen, and J. Ting. The inflammasome NLRs in immunity, inflammation, and associated diseases. *Annu Rev Immunol*, 29:707–735, 2011.

M. de Been, C. Francke, R. Siezen, and T. Abee. Novel {sigma} b regulation modules of gram-positive bacteria involve the use of complex hybrid histidine kinases. *Microbiology*, 157(1):3–12, 2011.

H. de Jong, J. Geiselmann, G. Batt, C. Hernandez, and M. Page. Qualitative simulation of the initiation of sporulation in *Bacillus subtilis*. *B Math Biol*, 66(2):261–299, 2003.

I. de Jong, J. Veening, and O. Kuipers. Heterochronic phosphorelay gene expression as a source of heterogeneity in *Bacillus subtilis* spore formation. *J Bacteriol*, 192(8):2053–67, 2010.

O. Delumeau, S. Dutta, M. Brigulla, G. Kuhnke, S. Hardwick, U. Völker, M. Yudkin, and R. Lewis. Functional and Structural Characterization of RsbU, a Stress Signaling Protein Phosphatase 2C. *J Biol Chem*, 279(39):40927–37, 2004.

O. Delumeau, C. Chen, J. Murray, M. Yudkin, and R. Lewis. High-Molecular-Weight Complexes of RsbR and Paralogues in the Environmental Signaling Pathway of *Bacillus subtilis*? *J Bacteriol*, 188(22):7885–92, 2006.

D. Dubnau and R. Losick. Bistability in bacteria. *Mol Microbiol*, 61:564–72, 2006.

A. Dufour and W. Haldenwang. Interactions between a *Bacillus subtilis* anti-sigma factor (RsbW) and its antagonist (RsbV). *J Bacteriol*, 176(7):1813–1820, 1994.

J. Dworkin. Transient genetic asymmetry and cell fate in a bacterium. *Trends Genet*, 19 (2):107–112, 2003.

J. Dworkin and R. Losick. Developmental commitment in a bacterium. *Cell*, 121(3): 401–409, 2005.

A. Earl, R. Losick, and R. Kolter. Ecology and genomics of *Bacillus subtilis*. *Trends Microbiol*, 16(6):269–275, 2008.

J. Edwards and B. Palsson. The *Escherichia coli* MG1655 in silico metabolic genotype: its definition, characteristics, and capabilities. *Proc Natl Acad Sci USA*, 97(10):5528–33, 2000.

M. Elowitz and S. Leibler. A synthetic oscillatory network of transcriptional regulators. *Nature*, 403(6767):335–338, 2000.

J. Errington. Regulation of endospore formation in *Bacillus subtilis*. *Nat Rev Microbiol*, 1(2):117–126, November 2003.

M. Espinosa, E. Garcia, and J. Fernaud. Mathematical approach to the stimulation of the competence development in *Bacillus subtilis*. *J Theor Biol*, 67(1):155–74, 1977.

C. Eymann, S. Schulz, K. Gronau, D. Becher, M. Hecker, and C. Price. In vivo phosphorylation patterns of key stressosome proteins define a second feedback loop that limits activation of *Bacillus subtilis* σB. *Mol Microbiol*, 80(3):798–810, 2011.

A. Fadda, A. Fierro, K. Lemmens, P. Monsieurs, K. Engelen, and K. Marchal. Inferring the transcriptional network of *Bacillus subtilis*. *Mol. BioSyst.*, 5:1840–1852, 2009.

P. Fawcett, P. Eichenberger, R. Losick, and P. Youngman. The transcriptional profile of early to middle sporulation in *Bacillus subtilis*. *Proc Natl Acad Sci USA*, 97(14): 8063–68, 2000.

Y. Feng, R. Jernigan, and A. Kloczkowski. Orientational distributions of contact clusters in proteins closely resemble those of an icosahedron. *Proteins: Struct , Funct , Bioinf*, 73(3):730–741, 2008.

A. Feucht, L. Abbotts, and J. Errington. The cell differentiation protein SpoIIE contains a regulatory site that controls its phosphatase activity in response to asymmetric septation. *Mol Microbiol*, 45(4):1119–1130, 2002.

A. Francez-Charlot, J. Frunzke, C. Reichen, J. Ebneter, B. Gourion, and J. Vorholt. Sigma factor mimicry involved in regulation of general stress response. *Proc Natl Acad Sci USA*, 106(9):3467–3472, 2009.

M. Fujita, J. González-Pastor, and R. Losick. High-and low-threshold genes in the Spo0A regulon of *Bacillus subtilis*. *J Bacteriol*, 187(4):1357–68, 2005.

T. Gaidenko, X. Yang, Y. Lee, and C. Price. Threonine phosphorylation of modulator protein RsbR governs its ability to regulate a serine kinase in the environmental stress signaling pathway of *Bacillus subtilis*. *J Mol Biol*, 288(1):29–39, 1999.

T. Gaidenko, T. Kim, A. Weigel, M. Brody, and C. Price. The blue-light receptor YtvA acts in the environmental stress signaling pathway of *Bacillus subtilis*. *J Bacteriol*, 188 (17):6387–95, 2006.

T. Gaidenko, X. Bie, E. Baldwin, and C. Price. Substitutions in the Presumed Sensing Domain of the *Bacillus subtilis* Stressosome Affect Its Basal Output but Not Response to Environmental Signals. *J Bacteriol*, 193(14):3588–97, 2011.

T. Gaidenko, X. Bei, E. Baldwin, and C. Price. Two surfaces of a conserved interdomain linker differentially affect output from the RST sensing module of the *Bacillus subtilis* stressosome. *J Bacteriol*, 194:3913–21, 2012.

L. Garrity and G. Ordal. Chemotaxis in *Bacillus subtilis*: how bacteria monitor environmental signals. *Pharmacol Ther*, 68(1):87–104, 1995.

D. Gillespie. Exact stochastic simulation of coupled chemical reactions. *J Phys Chem*, 81 (25):2340–61, 1977.

A. Goelzer, F. Brikci, I. Martin-Verstraete, P. Noirot, P. Bessieres, S. Aymerich, and V. Fromion. Reconstruction and analysis of the genetic and metabolic regulatory networks of the central metabolism of *Bacillus subtilis*. *BMC Syst Biol*, 20(1):20, 2008.

S. Gottesman. Proteolysis in bacterial regulatory circuits. *Annu Rev Cell Dev Biol*, 19: 565 – 587, 2003.

D. Gracias, M. Boncheva, O. Omoregie, and G. Whitesides. Biomimetic self-assembly of helical electrical circuits using orthogonal capillary interactions. *Appl Phys Lett*, 80: 2802–04, 2002.

N. Grover, E. Eidelstein, and L. Koppes. Bacterial shape maintenance: an evaluation of various models. *J Theor Biol*, 227(4):547–559, 2004.

T. Gurry, O. Kahramanoğulları, and R. Endres. Biophysical mechanism for Ras-nanocluster formation and signaling in plasma membrane. *PloS ONE*, 4(7):e6148, 2009.

W. Haldenwang. The sigma factors of *Bacillus subtilis*. *Microbiol Rev*, 59(1):1–30, 1995.

L. Hamoen, W. Smits, A. Jong, S. Holsappel, and O. Kuipers. Improving the predictive value of the competence transcription factor (ComK) binding site in *Bacillus subtilis* using a genomic approach. *Nucleic Acids Res*, 30(24):5517–28, 2002.

L. Hamoen, G. Venema, and O. Kuipers. Controlling competence in *Bacillus subtilis*: shared use of regulators. *Microbiology*, 149(1):9–17, 2003.

M. Hecker and U. Völker. General stress response of *Bacillus subtilis* and other bacteria. *Adv Microb Physiol*, 44:35–91, 2001.

M. Hecker, J. Pane-Farre, and U. Völker. SigB-Dependent General Stress Response in *Bacillus subtilis* and Related Gram-Positive Bacteria. *Annu Rev Microbiol*, 61:215–236, 2007.

J. Helmann, M. Wu, P. Kobel, F. Gamo, M. Wilson, M. Morshedi, M. Navre, and C. Paddon. Global transcriptional response of *Bacillus subtilis* to heat shock. *J Bacteriol*, 183 (24):7318–28, 2001.

J. Herrou and S. Crosson. Function, structure and mechanism of bacterial photosensory LOV proteins. *Nat Rev Microbiol*, 9:713–23, 2011.

D. Höper, U. Völker, and M. Hecker. Comprehensive Characterization of the Contribution of Individual SigB-Dependent General Stress Genes to Stress Resistance of *Bacillus subtilis*. *J Bacteriol*, 187(8):2810–26, 2004.

S. Hou, R. Larsen, D. Boudko, C. Riley, E. Karatan, M. Zimmer, G. Ordal, and M. Alam. Myoglobin-like aerotaxis transducers in Archaea and Bacteria. *Nature*, 403(6769):540–544, 2000.

P. Hugenholtz, B. Goebel, and N. Pace. Impact of culture-independent studies on the emerging phylogenetic view of bacterial diversity. *J Bacteriol*, 180(18):4765–74, 1998.

D. Iber. A quantitative study of the benefits of co-regulation using the spoIIA operon as an example. *Mol Syst Biol*, 2(43), 2006.

O. Igoshin, C. Price, and M. Savageau. Signalling network with a bistable hysteretic switch controls developmental activation of the F transcription factor in *Bacillus subtilis*. *Mol Microbiol*, 61(1):165–184, 2006.

O. Igoshin, M. Brody, C. Price, and M. Savageau. Distinctive Topologies of Partner-switching Signaling Networks Correlate with their Physiological Roles. *J Mol Biol*, 369 (5):1333–52, 2007.

O. Igoshin, R. Alves, and M. Savageau. Hysteretic and graded responses in bacterial two-component signal transduction. *Mol Microbiol*, 68(5):1196–1215, 2008.

G. Indelicato, P. Cermelli, D. Salthouse, S. Racca, G. Zanzotto, and R. Twarock. A crystallographic approach to structural transitions in icosahedral viruses. *J Math Biol*, 64(5):745–773, 2011.

S. Jabbari, J. Heap, and J. King. Mathematical Modelling of the Sporulation-Initiation Network in *Bacillus subtilis* Revealing the Dual Role of the Putative Quorum-Sensing Signal Molecule PhrA. *B Math Biol*, pages 1–31, 2010.

F. Jacob and F. Monod. Genetic regulatory mechanisms in the synthesis of protein. *J Mol Biol*, 3:318, 1961.

J. Jeong, J. Snay, and M. Ataai. A mathematical model for examining growth and sporulation processes of *Bacillus subtilis*. *Biotechnol Bioeng*, 35(2):160–184, 1990.

M. Jurk, M. Dorn, and P. Schmieder. Blue Flickers of Hope: Secondary Structure, Dynamics and Putative Dimerisation Interface of the Blue-Light Receptor YtvA from Bacillus subtilis. *Biochemistry*, 50(38):8163–71, 2011.

S. Kalman, M. Duncan, S. Thomas, and C. Price. Similar organization of the sigB and spoIIA operons encoding alternate sigma factors of *Bacillus subtilis* RNA polymerase. *J Bacteriol*, 172(10):5575–5585, 1990.

C. Kang, M. Brody, S. Akbar, X. Yang, and C. Price. Homologous pairs of regulatory proteins control activity of *Bacillus subtilis* transcription factor sigma (b) in response to environmental stress. *J Bacteriol*, 178(13):3846–53, 1996.

D. Kearns, F. Chu, S. Branda, R. Kolter, and R. Losick. A master regulator for biofilm formation by *Bacillus subtilis*. *Mol Microbiol*, 55(3):739–749, 2004.

B. Kholodenko, J. Hancock, and W. Kolch. Signalling ballet in space and time. *Nat Rev Mol Cell Biol*, 11(6):414–426, 2010.

A. Kierzek, L. Zhou, and B. Wanner. Stochastic kinetic model of two component system signalling reveals all-or-none, graded and mixed mode stochastic switching responses. *Mol BioSyst*, 6(3):531–542, 2010.

A. Kiester and K. Sahr. Planar and spherical hierarchical, multi-resolution cellular automata. *J Comp Env Urb Sys*, 32(3):204–213, 2008.

T.-J. Kim, T. Gaidenko, and C. Price. *In vivo* phosphorylation of partner switching regulators correlates with stress transmission in the environmental signaling pathway of *Bacillus subtilis*. *J Bacteriol*, 186(18):6124–32, Sep 2004a.

T.-J. Kim, T. Gaidenko, and C. Price. A Multicomponent Protein Complex Mediates Environmental Stress Signaling in *Bacillus subtilis*. *J Mol Biol*, 341(1):135–150, 2004b.

K. Kobayashi. Gradual activation of the response regulator DegU controls serial expression of genes for flagellum formation and biofilm formation in *Bacillus subtilis*. *Mol Microbiol*, 66(2):395–409, 2007.

A. Koch. The growth kinetics of *Bacillus subtilis*. *Antonie van Leeuwenhoek*, 63(1):45–53, 1992.

C. Kristich and G. Ordal. *Bacillus subtilis* CheD is a chemoreceptor modification enzyme required for chemotaxis. *J Biol Chem*, 277(28):25356–62, 2002.

E. Krüger, U. Völker, and M. Hecker. Stress induction of *clpC* in *Bacillus subtilis* and its involvement in stress tolerance. *J Bacteriol*, 176(11):3360–3367, 1994.

F. Kunst, N. Ogasawara, I. Moszer, A. Albertini, G. Alloni, V. Azevedo, M. Bertero, P. Bessieres, A. Bolotin, S. Borchert, et al. The complete genome sequence of the gram-positive bacterium *Bacillus subtilis*. *Nature*, 390(6657):249–256, 1997.

S. Kuo. *Characterization of the Bacillus subtilis protein Obg*. PhD thesis, The University of Texas Health Science Center at San Antonio, 2007. URL `http://gradworks.umi.com/32/88/3288343.html`.

G. Leach. *Of Music, Mathematics, and Magic: Why Math is All Made Up and why it Works So Well*. PhD thesis, Eastern Illinois University, 2011. URL `http://thekeep.eiu.edu/cgi/viewcontent.cgi?article=1492&context=theses`.

M. Leisner, K. Stingl, J. Radler, and B. Maier. Basal expression rate of *comK* sets a 'switching-window' into the K-state of *Bacillus subtilis*. *Mol Microbiol*, 63(6):1806–1816, 2007.

M. Leisner, K. Stingl, E. Frey, and B. Maier. Stochastic switching to competence. *Curr Opin Microbiol*, 11(6):553–559, 2008.

M. Leisner, J.-T. Kuhr, J. Rädler, E. Frey, and B. Maier. Kinetics of genetic switching into the state of bacterial competence. *Biophys J*, 96(3):1178–1188, 2009.

M. Li and G. L. Hazelbauer. Core unit of chemotaxis signaling complexes. *Proc Natl Acad Sci USA*, 108(23):9390–95, 2011.

U. Liebal, T. Millat, I. de Jong, O. Kuipers, U. Völker, and O. Wolkenhauer. How mathematical modelling elucidates signalling in *Bacillus subtilis*. *Mol Microbiol*, 77(5): 1083–95, 2010.

U. Liebal, P. Sappa, T. Millat, L. Steil, G. Homuth, U. Völker, and O. Wolkenhauer. Proteolysis of beta-galactosidase following SigmaB activation in *Bacillus subtilis*. *Mol BioSyst*, 8(6):1806–14, 2012.

U. Liebal, T. Millat, J. Marles-Wright, R. Lewis, and O. Wolkenhauer. Simulations of stressosome activation emphasize allosteric interactions between RsbR and RsbT. *BMC Syst Biol*, 7(3), 2013.

B. Lindner, J. Garcia-Ojalvo, A. Neiman, and L. Schimansky-Geier. Effects of noise in excitable systems. *Phys Rep*, 392:321–424, 2004.

X. Liu, W. Jin, and E. Theil. Opening protein pores with chaotropes enhances Fe reduction and chelation of Fe from the ferritin biomineral. *Proc Natl Acad Sci USA*, 100(7):3653–58, 2003.

J. Locke, J. Young, M. Fontes, M. Jiménez, and M. Elowitz. Stochastic Pulse Regulation in Bacterial Stress Response. *Science*, 334(6054):366–69, 2011.

D. López and R. Kolter. Extracellular signals that define distinct and coexisting cell fates in *Bacillus subtilis*. *FEMS Microbiol Rev*, 34(2):134–149, 2009.

D. López, H. Vlamakis, and R. Kolter. Generation of multiple cell types in *Bacillus subtilis*. *FEMS Microbiol Rev*, 33(1):152–163, 2008.

A. Losi, E. Polverini, B. Quest, and W. Gärtner. First evidence for phototropin-related blue-light receptors in prokaryotes. *Biophys J*, 82(5):2627–34, 2002.

A. Losi, B. Quest, and W. Gärtner. Listening to the blue: the time-resolved thermodynamics of the bacterial blue-light receptor YtvA and its isolated LOV domain. *Photochem Photobiol Sci*, 2(7):759–66, 2003.

W. Ma, A. Trusina, H. El-Samad, W. Lim, and C. Tang. Defining Network Topologies that Can Achieve Biochemical Adaptation. *Cell*, 138(4):760–773, 2009.

H. Maamar and D. Dubnau. Bistability in the Bacillus subtilis K-state (competence) system requires a positive feedback loop. *Mol Microbiol*, 56(3):615–624, May 2005.

H. Maamar, A. Raj, and D. Dubnau. Noise in gene expression determines cell fate in *Bacillus subtilis*. *Science*, 317(5837):526–529, 2007.

J. Marles-Wright and R. Lewis. Stress responses of bacteria. *Curr Opin Struct Biol*, 17 (6):755–760, 2007.

J. Marles-Wright, T. Grant, O. Delumeau, G. Van Duinen, S. Firbank, P. Lewis, J. Murray, J. Newman, M. Quin, P. Race, et al. Molecular Architecture of the 'Stressosome', a Signal Integration and Transduction Hub. *Science*, 322(5898):92–96, 2008.

L. Martinez, A. Reeves, and W. Haldenwang. Stressosomes formed in *Bacillus subtilis* from the RsbR protein of *Listeria monocytogenes* allow sigmaB activation following exposure to either physical or nutritional stress. *J Bacteriol*, 192(23):6279–86, 2010.

M. Mesarović. *Systems theory and biology*. Springer, 1968.

T. Millat, S. Sreenath, R. Soebiyanto, J. Avva, K.-H. Cho, and O. Wolkenhauer. The role of dynamic stimulation pattern in the analysis of bistable intracellular networks. *Biosystems*, 92(3):270–281, June 2008.

J. Milne, D. Shi, P. Rosenthal, J. Sunshine, G. Domingo, X. Wu, B. Brooks, R. Perham, R. Henderson, and S. Subramaniam. Molecular architecture and mechanism of an icosahedral pyruvate dehydrogenase complex: a multifunctional catalytic machine. *EMBO*, 21(21):5587–98, 2002.

A. Mitrophanov and E. Groisman. Signal integration in bacterial two-component regulatory systems. *Genes Dev*, 22(19):2601–11, 2008.

A. Mitrophanov, T. Hadley, and E. Groisman. Positive autoregulation shapes response timing and intensity in two-component signal transduction systems. *J Mol Biol*, 401(4): 671–680, 2010.

G. Mittenhuber. A phylogenomic study of the general stress response sigma factor B of *Bacillus subtilis* and its regulatory proteins. *J Mol Microbiol Biotechnol*, 4:427–452, 2002.

A. Mogk, R. Hayward, and W. Schumann. Integrative vectors for constructing single-copy transcriptional fusions between *Bacillus subtilis* promoters and various reporter genes encoding heat-stable enzymes. *Gene*, 182(1-2):33–36, 1996.

A. Möglich and K. Moffat. Structural basis for light-dependent signaling in the dimeric LOV domain of the photosensor YtvA. *J Mol Biol*, 373(1):112–126, 2007.

M. Mols and T. Abee. Primary and secondary oxidative stress in *Bacillus*. *Environ Microbiol*, 13(6):1387–94, 2011.

M. Morohashi, Y. Ohashi, S. Tani, K. Ishii, M. Itaya, H. Nanamiya, F. Kawamura, M. Tomita, and T. Soga. Model-based Definition of Population Heterogeneity and Its Effects on Metabolism in Sporulating *Bacillus subtilis*. *J Biochem*, 142(2):183–91, 2007.

T. Msadek. When the going gets tough: survival strategies and environmental signaling networks in *Bacillus subtilis*. *Trends Microbiol*, 7(5):201–207, 1999.

E. J. Murray, T. B. Kiley, and N. R. Stanley-Wall. A pivotal role for the response regulator DegU in controlling multicellular behaviour. *Microbiology*, 155(1):1–8, 2009.

J. Murray, O. Delumeau, and R. Lewis. Structure of a nonheme globin in environmental stress signaling. *Proc Natl Acad Sci USA*, 102(48):17320–25, 2005.

S. Nakano, E. Küster-Schöck, A. Grossman, and P. Zuber. Spx-dependent global transcriptional control is induced by thiol-specific oxidative stress in *Bacillus subtilis*. *Proc Natl Acad Sci USA*, 100(23):13603 – 08, 2003.

P. Nannapaneni, F. Hertwig, M. Depke, M. Hecker, U. Mäder, U. Völker, L. Steil, and S. van Hijum. Defining the structure of the general stress regulon of *Bacillus subtilis* using targeted microarray analysis and random forest classification. *Microbiol*, 158(Pt 3):696–707, 2012.

K. Newberry, S. Nakano, P. Zuber, and R. Brennan. Crystal structure of the *Bacillus subtilis* anti-alpha, global transcriptional regulator, Spx, in complex with the α C-terminal domain of RNA polymerase. *Proc Natl Acad Sci USA*, 102(44):15839 – 44, 2005.

T. Nguyen, R. Bruinsma, and W. Gelbart. Elasticity theory and shape transitions of viral shells. *Phys Rev E*, 72(5):051923, 2005.

P. Nicolas, U. Mäder, E. Dervyn, T. Rochat, A. Leduc, N. Pigeonneau, E. Bidnenko, E. Marchadier, M. Hoebeke, S. Aymerich, et al. Condition-Dependent Transcriptome Reveals High-Level Regulatory Architecture in *Bacillus subtilis*. *Science*, 335(6072): 1103–06, 2012.

M. Ogura, H. Yamaguchi, K. Kobayashi, N. Ogasawara, Y. Fujita, and T. Tanaka. Whole-genome analysis of genes regulated by the *Bacillus subtilis* competence transcription factor ComK. *J Bacteriol*, 184(9):2344–51, 2002.

Y. Oh, B. Palsson, S. Park, C. Schilling, and R. Mahadevan. Genome-scale Reconstruction of Metabolic Network in *Bacillus subtilis* Based on High-throughput Phenotyping and Gene Essentiality Data. *J Biol Chem*, 282(39):28791, 2007.

J. Pane-Farre, R. Lewis, and J. Stülke. The RsbRST Stress Module in Bacteria: A Signalling System That May Interact with Different Output Modules. *J Mol Microbiol Biotechnol*, 9(2):65–76, 2005.

A. Petersohn, M. Brigulla, S. Haas, J. Hoheisel, U. Völker, and M. Hecker. Global Analysis of the General Stress Response of *Bacillus subtilis*. *J Bacteriol*, 183(19):5617–31, 2001.

P. Piggot and D. Hilbert. Sporulation of *Bacillus subtilis*. *Curr Opin Microbiol*, 7(6): 579–586, 2004.

C. Price. *Bacillus Subtilis and Its Closest Relatives: From Genes to Cells*, chapter General stress response, pages 369–384. American Society for Microbiology, 2002.

C. Price, P. Fawcett, H. Ceremonie, N. Su, C. Murphy, and P. Youngman. Genome-wide analysis of the general stress response in *Bacillus subtilis*. *Mol Microbiol*, 41(4):757–774, 2001.

A. Raj and A. van Oudenaarden. Nature, Nurture, or Chance: Stochastic Gene Expression and Its Consequences. *Cell*, 135(2):216–226, 2008.

C. Rao and G. Ordal. The Molecular Basis of Excitation and Adaptation during Chemotactic Sensory Transduction in Bacteria. *Contrib Microbiol*, 16:33–64, 2009.

C. Rao, J. Kirby, and A. Arkin. Design and Diversity in Bacterial Chemotaxis: A Comparative Study in *Escherichia coli* and *Bacillus subtilis*. *PLoS Biol*, 2:239–252, 2004.

C. Rao, J. Kirby, and A. Arkin. Phosphatase localization in bacterial chemotaxis: Divergent mechanisms, convergent principles. *Phys Biol*, 2:148–158, 2005.

A. Reder, D. Höper, C. Weinberg, U. Gerth, M. Fraunholz, and M. Hecker. The Spx paralogue MgsR (YqgZ) controls a subregulon within the general stress response of *Bacillus subtilis*. *Mol Microbiol*, 69(5):1104–1120, 2008.

A. Reder, U. Gerth, and M. Hecker. Integration of σb activity into the decision making process of sporulation initiation in *Bacillus subtilis*. *J Bacteriol*, 194(5):1065–74, 2011.

A. Reder, D. Höper, U. Gerth, and M. Hecker. The contribution of individual σB-dependent general stress genes to oxidative stress resistance of *Bacillus subtilis*. *J Bacteriol*, 194(14):3601–10, 2012.

J. Reed and B. Palsson. Thirteen years of building constraint-based in silico models of *Escherichia coli*. *J Bacteriol*, 185(9):2692–99, 2003.

A. Reeves, U. Gerth, U. Völker, and W. Haldenwang. ClpP modulates the activity of the *Bacillus subtilis* stress response transcription factor, σB. *J Bacteriol*, 189(17):6168–75, 2007.

A. Reeves, L. Martinez, and W. Haldenwang. Expression of, and in vivo stressosome formation by, single members of the RsbR protein family in *Bacillus subtilis*. *Microbiology*, 156(4):990–98, 2010.

M. Rey, P. Ramaiya, B. Nelson, S. Brody-Karpin, E. Zaretsky, M. Tang, A. de Leon, H. Xiang, V. Gusti, I. Clausen, et al. Complete genome sequence of the industrial bacterium *Bacillus licheniformis* and comparisons with closely related Bacillus species. *Genome Biol*, 5(10):r77, 2004.

E. Roberts, A. Magis, J. Ortiz, W. Baumeister, and Z. Luthey-Schulten. Noise Contributions in an Inducible Genetic Switch: A Whole-Cell Simulation Study. *PLoS Comput Biol*, 7(3):e1002010, 2011.

M. Santillán and M. Mackey. Quantitative approaches to the study of bistability in the *lac* operon of *Escherichia coli*. *J R Soc Interf*, 5(Suppl 1):S29, 2008.

M. Sargent. Control of cell length in *Bacillus subtilis*. *J Bacteriol*, 123(1):7–19, 1975.

M. Schaechter. Talmudic question 83. http://schaechter.asmblog.org/schaechter/2012/01/talmudic-question-83.html, 01 2012.

H. Schmidt and M. Jirstrand. Systems Biology Toolbox for MATLAB: a computational platform for research in systems biology. *Bioinformatics*, 22(4):514–515, February 2006. `http://www.sbtoolbox2.org`.

O. Schrögel and R. Allmansberger. Optimisation of the BgaB reporter system: determination of transcriptional regulation of stress responsive genes in *Bacillus subtilis*. *FEMS Microbiol Lett*, 153(1):237–243, 1997.

D. Schultz, P. Wolynes, E. Ben-Jacob, and J. Onuchic. Deciding fate in adverse times: Sporulation and competence in *Bacillus subtilis*. *Proc Natl Acad Sci USA*, 106(50): 21027–21034, 2009.

J. Scott, N. Smirnova, and W. Haldenwang. A *Bacillus*-Specific Factor Is Needed to Trigger the Stress-Activated Phosphatase/Kinase Cascade of σB Induction. *Biochem Biophys Res Commun*, 257(1):106–110, 1999.

J. Scott, T. Mitchell, and W. Haldenwang. Stress Triggers a Process That Limits Activation of the *Bacillus subtilis* Stress Transcription Factor σB. *J Bacteriol*, 182(5):1452–56, 2000.

I. Segel. *Enzyme Kinetics*. John Wiley and Sons, 1993.

I. Serebriiskii and E. Golemis. Uses of *lacZ* to study gene function: evaluation of β-galactosidase assays employed in the yeast two-hybrid system. *Anal Biochem*, 285(1): 1–15, 2000.

T. Shimizu, S. Aksenov, and D. Bray. A spatially extended stochastic model of the bacterial chemotaxis signalling pathway. *J Mol Biol*, 329(2):291–309, 2003.

J. Shin, M. Brody, and C. Price. Physical and antibiotic stresses require activation of the RsbU phosphatase to induce the general stress response in *Listeria monocytogenes*. *Microbiology*, 156(9):2660, 2010.

J. Shioi, S. Matsuura, and Y. Imae. Quantitative measurements of proton motive force and motility in *Bacillus subtilis*. *J Bacteriol*, 144(3):891–97, 1980.

T. Silhavy and J. Beckwith. Uses of *lac* fusions for the study of biological problems. *Microbiol Mol Biol Rev*, 49(4):398–418, 1985.

W. Smits, C. Eschevins, K. Susanna, S. Bron, O. Kuipers, and L. Hamoen. Stripping *Bacillus*: ComK auto-stimulation is responsible for the bistable response in competence development. *Mol Microbiol*, 56(3):604–614, 2005.

A. Sonenshein. Control of sporulation initiation in *Bacillus subtilis*. *Curr Opin Microbiol*, 3(6):561–566, 2000.

J. Speir, S. Munshi, G. Wang, T. Baker, and J. Johnson. Structures of the native and swollen forms of cowpea chlorotic mottle virus determined by X-ray crystallography and cryo-electron microscopy. *Structure*, 3(1):63–78, 1995.

F. Stavru, C. Archambaud, and P. Cossart. Cell biology and immunology of *Listeria monocytogenes* infections: novel insights. *Immun Rev*, 240(1):160–184, 2011.

G. Süel, J. Garcia-Ojalvo, L. Liberman, and M. Elowitz. An excitable gene regulatory circuit induces transient cellular differentiation. *Nature*, 440(7083):545–550, 2006.

G. Süel, R. Kulkarni, J. Dworkin, J. Garcia-Ojalvo, and M. Elowitz. Tunability and Noise Dependence in Differentiation Dynamics. *Science*, 315(5819):1716–1719, 2007.

H. Szurmant, M. Bunn, V. Cannistraro, and G. Ordal. *Bacillus subtilis* hydrolyzes CheY-P at the location of its action, the flagellar switch. *J Biol Chem*, 278(49):48611–16, 2003.

J. Tabor, T. Bayer, Z. Simpson, M. Levy, and A. Ellington. Engineering stochasticity in gene expression. *Mol BioSyst*, 4(7):754–761, 2008.

F. Tama and C. Brooks. Diversity and identity of mechanical properties of icosahedral viral capsids studied with elastic network normal mode analysis. *J Mol Biol*, 345(2): 299–314, 2005.

F. Tama and C. Brooks III. The mechanism and pathway of pH induced swelling in cowpea chlorotic mottle virus. *J Mol Biol*, 318(3):733–747, 2002.

Y. Tang, Z. Cao, E. Livoti, U. Krauss, K. Jaeger, W. Gärtner, and A. Losi. Interdomain signalling in the blue-light sensing and GTP-binding protein YtvA: A mutagenesis study uncovering the importance of specific protein sites. *Photochem Photobiol Sci*, 9(1):47–56, 2010.

M. Tegmark. The mathematical universe. *Found Phys*, 38(2):101–50, 2008.

M. Tindall, S. Porter, P. Maini, G. Gaglia, and J. Armitage. Overview of Mathematical Approaches Used to Model Bacterial Chemotaxis I: The Single Cell. *B Math Biol*, 70 (6):1525–1569, 2008.

R. Twarock. Mathematical virology: a novel approach to the structure and assembly of viruses. *Philos T Roy Soc A*, 364(1849):3357–73, 2006.

J. Tyson, K. Chen, and B. Novak. Sniffers, buzzers, toggles and blinkers: dynamics of regulatory and signaling pathways in the cell. *Curr Opin Cell Biol*, 15(2):221–231, Apr. 2003.

M. van der Horst, J. Key, and K. Hellingwerf. Photosensing in chemotrophic, non-phototrophic bacteria: let there be light sensing too. *Trends Microbiol*, 15(12):554–562, 2007.

H. van Vlijmen and M. Karplus. Normal mode analysis of large systems with icosahedral symmetry: Application to (Dialanine) in full and reduced basis set implementations. *J Chem Phys*, 115(2):691–98, 2001.

A. Varma and B. Palsson. Stoichiometric flux balance models quantitatively predict growth and metabolic by-product secretion in wild-type *Escherichia coli* w3110. *Appl Environ Microbiol*, 60(10):3724–3731, 1994.

A. Vaz and L. Vicente. A particle swarm pattern search method for bound constrained global optimization. *J Global Optim*, 39(2):197–219, 2007.

J. Veening, W. Smits, and O. Kuipers. Bistability, epigenetics, and bet-hedging in bacteria. *Annu Rev Microbiol*, 62:193–210, 2008a.

J.-W. Veening, O. Igoshin, R. Eijlander, R. Nijland, L. Hamoen, and O. Kuipers. Transient heterogeneity in extracellular protease production by *Bacillus subtilis*. *Mol Syst Biol*, 4:184, April 2008b.

J.-W. Veening, E. Stewart, T. Berngruber, F. Taddei, O. Kuipers, and L. Hamoen. Bet-hedging and epigenetic inheritance in bacterial cell development. *Proc Natl Acad Sci USA*, 105(11):4393–98, 2008c.

K. Vijay, M. Brody, E. Fredlund, and C. Price. A PP2C phosphatase containing a PAS domain is required to convey signals of energy stress to the SigmaB transcription factor of *Bacillus subtilis*. *Mol Microbiol*, 35(1):180–188, 2000.

H. Vlamakis, C. Aguilar, R. Losick, and R. Kolter. Control of cell fate by the formation of an architecturally complex bacterial community. *Genes Dev*, 22(7):945–53, 2008.

C. Voigt, D. Wolf, and A. Arkin. The *Bacillus subtilis sin* Operon An Evolvable Network Motif. *Genetics*, 169(3):1187–1202, 2005.

U. Völker, A. Dufour, and W. Haldenwang. The *Bacillus subtilis rsbU* gene product is necessary for RsbX-dependent regulation of sigmaB. *J Bacteriol*, 177(1):114–22, 1995a.

U. Völker, A. Völker, B. Maul, M. Hecker, A. Dufour, and W. Haldenwang. Separate mechanisms activate sigmaB of *Bacillus subtilis* in response to environmental and metabolic stresses. *J Bacteriol*, 177(13):3771–80, 1995b.

U. Völker, A. Völker, and W. Haldenwang. Reactivation of the *Bacillus subtilis* anti-sigma B antagonist, RsbV, by stress-or starvation-induced phosphatase activities. *J Bacteriol*, 178(18):5456–63, 1996.

U. Völker, T. Luo, N. Smirnova, and W. Haldenwang. Stress activation of *Bacillus subtilis* sigmaB can occur in the absence of the sigmaB negative regulator RsbX. *J Bacteriol*, 179(6):1980–84, 1997.

S. Weeratunga, S. Lovell, H. Yao, K. Battaile, C. Fischer, C. Gee, and M. Rivera. Structural studies of bacterioferritin B from Pseudomonas aeruginosa suggest a gating mechanism for iron uptake via the ferroxidase center. *Biochemistry*, 49(6):1160–75, 2010.

G. Whitesides and M. Boncheva. Beyond molecules: self-assembly of mesoscopic and macroscopic components. *Proc Natl Acad Sci USA*, 99(8):4769–74, 2002.

W. Whitman, D. Coleman, and W. Wiebe. Prokaryotes: the unseen majority. *Proc Natl Acad Sci USA*, 95(12):6578–83, 1998.

B. Willing, L. Antunes, K. Keeney, R. Ferreira, and B. Finlay. Harvesting the biological potential of the human gut microbiome. *BioEssays*, 33(6):414–18, 2011.

O. Wolkenhauer and M. Mesarović. Feedback dynamics and cell function: Why systems biology is called systems biology. *Mol BioSyst*, 1(1):14–16, 2005.

O. Wolkenhauer, H. Kitano, and K.-H. Cho. Systems Biology: Looking at Opportunities and Challenges in Applying Systems Theory to Molecular and Cell Biology. *IEEE Contr Syst Mag*, 23(4):38–48, August 2003.

X. Yang, C. Kang, M. Brody, and C. Price. Opposing pairs of serine protein kinases and phosphatases transmit signals of environmental stress to activate a bacterial transcription factor. *Genes Dev*, 10(18):2265–75, 1996.

R. Zandi, D. Reguera, R. F. Bruinsma, W. M. Gelbart, and J. Rudnick. Origin of icosahedral symmetry in viruses. *Proc Natl Acad Sci USA*, 101(44):15556–60, 2004.

S. Zhang, A. Reeves, R. Woodbury, and W. Haldenwang. Coexpression Patterns of σB Regulators in *Bacillus subtilis* Affect σB Inducibility. *J Bacteriol*, 187(24):8520–25, 2005.

U. Zuber and W. Schumann. CIRCE, a novel heat shock element involved in regulation of heat shock operon *dnaK* of *Bacillus subtilis*. *J Bacteriol*, 176(5):1359–63, 1994.

Appendix A

Simulations of RsbR-paralogue dynamics

Five paralogues of RsbR (RsbRA, -B, -C, -D, and YtvA) are present in *B. subtilis*. RsbR sense environmental signals, however, the paralogues RsbRC and RsbRD are also receptive to energy stress [Martinez et al. 2010]. For further characterisation, Akbar et al. [2001] studied the response of stressosomes composed only of RsbRC and RsbRD, of both of them (RsbRC+RD), and the wild-type (RsbRA+RB+RC+RD), during onset of stationary phase, Figure A1(A). In conclusion, each RsbR paralogue shows a different pre- and post-stimulus excitation. This phenotype was reproduced in the model (Figure A1(B)) by increasing the phosphorylation parameter of RsbS, *kphs*. The white circles represent the wild type, $kphs = 0.6$. The black circles in Figure A1(A) represent RsbD stressosomes, with a higher β-galactosidase activity. This is reproduced in the model by setting $kphs = 0.75$. The highest β-galactosidase activity was measured for RsbRC (squares, (A)). This was simulated by setting $kphs = 0.9$ (square, (B)). The mixture of RsbRC and RsbRD with energy insensitive RsbRA and RsbRB lowers the overall stressosome sensitivity. In the model this corresponds to a reduction of the RsbS phopshorylation rate from 0.9 to 0.6.

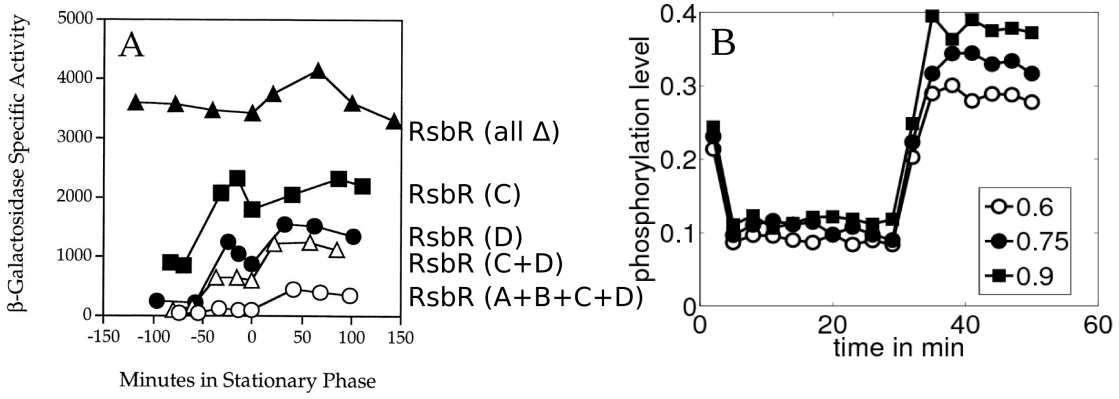

Figure A1: Stressosome activation over time during transition to stationary phase [Akbar et al. 2001], and increase of *kphs* in the model of the stressosome.

Appendix B

Triangle collapse parameter scan

The inspection of the solution space whilst changing two parameters allows to determine parameter combinations with biologically relevant or interesting dynamics. In Figure 4.6 of *Chapter 4*, I show parameter scans for the frequency of triangle collapse for different parameter values of r_{col} and *coop* in combination with r_{rlx}. Here, I show the remaining parameter combination between r_{col} and *coop* with the parameter $r_{rlx} = 0.9$. Following intuitive expectation, the fraction of collapsed triangles is lowest for small values of both r_{col} and *coop*, and an increase in their values raises the collapse fraction. The collapse fraction is lower for small values of r_{col}, because *coop* cannot complement the high value chosen for r_{rlx} in this condition (Figure 4.6(B)).

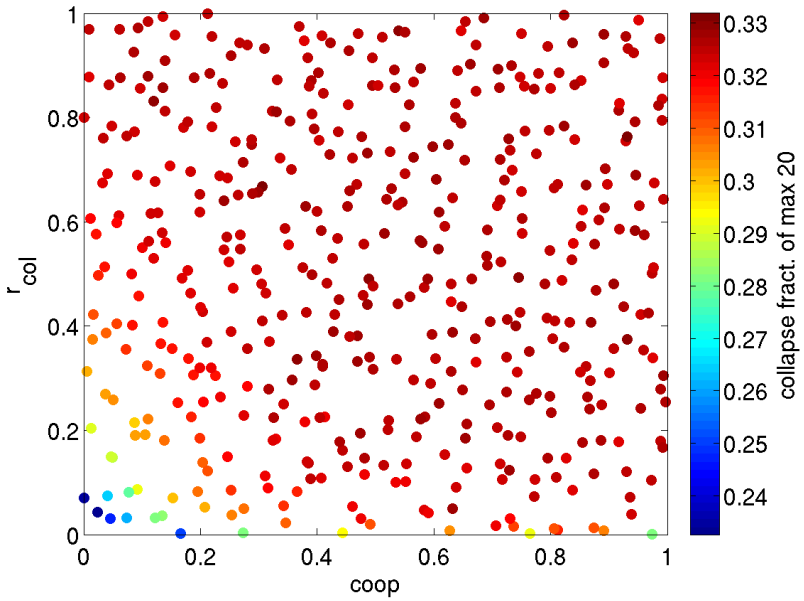

Figure B1: Triangle collapse fraction with different parameter values of *coop* and r_{col}.

Appendix C

Supporting information for σ^B protease expression

IPTG remains an active inducer

The experimental results of the IPTG induction of BSA115 show a transient peak of β-galactosidase activity (Figure 5.2 in *Chapter 5*). Among the possible explanations is breakdown or deactivation of IPTG. The experimental partners at the Ernst-Moritz-Arndt Universität in Greifswald tested the hypothesis by repeatedly adding IPTG to the reaction. The induction of σ^B was started by addition of IPTG to 1 mM final concentration at 100 min. Following, IPTG was added at regular time intervals to replenish any deactivated IPTG. The increased IPTG concentrations neither increased the β-galactosidase levels further nor did they prevent the activity drop at about 200 min.

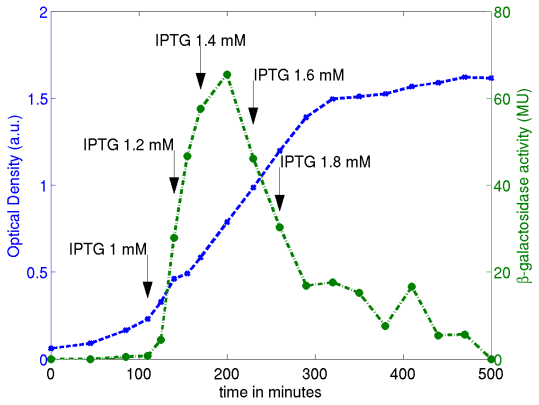

Figure C1: β-galactosidase activity and optical density of the repeated σ^B stimulation by IPTG.

Model for growth dependent β-galactosidase expression

In addition to the σ^B-dependent mechanisms I discuss in the main part (Figure 5.2, *Chapter 5*), I tested a model of a σ^B-independent, i.e. growth rate dependent, model of the activation of the protease Figure C1. The variable *Sgn* is an external signal for the expression of protease X. The growth rate dependent model is only plausible if the time for the activation of the parameter *Sgn* coincides with the transition of the culture to the stationary phase. However, this model fails to reproduce the data qualitatively for the following four reasons: 1) for an optimal fit of 1 mM IPTG, *Sgn* has to be active after 5 min of IPTG addition; 2) the final Miller Units differ according to the intensity of IPTG stimulation; 3) the peak delay for 0.1 mM IPTG is too low; and 4) the simulated β-galactosidase activity of 1 mM IPTG (cyan) is too high. In conclusion, growth transition effects are unlikely because the time of protease activation in the model for high IPTG is 5 min, whereas the experimental growth transitions is at about 60 min.

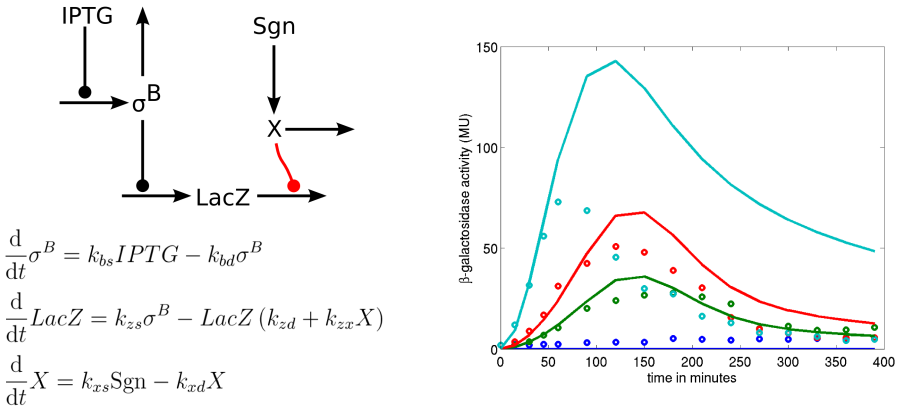

Figure C2: Schematic view, ODEs, and experimental fit of a model of σ^B independent β-galactosidase degradation.

Parameter	Value in $\frac{\mathrm{MU}}{\mathrm{min}}$	Parameter	Value in $\frac{\mathrm{MU}}{\mathrm{min}}$	optimal times for *Sgn* activation	
kbs	$1 \cdot 10^2$	*kzx*	$5 \cdot 10^{-5}$	IPTG in mM	time in min
kbd	$1.6 \cdot 10^{-2}$	*kxs*	6	0.1	95
kzs	$9 \cdot 10^{-7}$	*kxd*	$1.1 \cdot 10^{-9}$	0.2	90
kzd	$1.3 \cdot 10^{-7}$	*Sgn*	1 MU	1	5

Analysis of Parameter correlations

To ensure that the parameter estimation procedure is unique for each parameter, I performed a parameter correlation analysis for the 'transcription inhibition' (A), 'SigmaB proteolysis' (B) and 'prost-transcriptional instability' (C) models. Due to the small system sizes most parameters are uniquely identifiable without linear dependence on other parameters. Parameter correlations were determined on the basis of 500 parameter estimations for each model over all three IPTG-concentrations reproduced in Figure 5.2 in *Chapter 5*. Each estimation started with a randomized parameter set with a ten-fold range around the parameters values of Table 5.1. The procedure was performed with the SBToolbox2 [Schmidt and Jirstrand 2006], and the integrated particle swarm algorithm [Vaz and Vicente 2007].

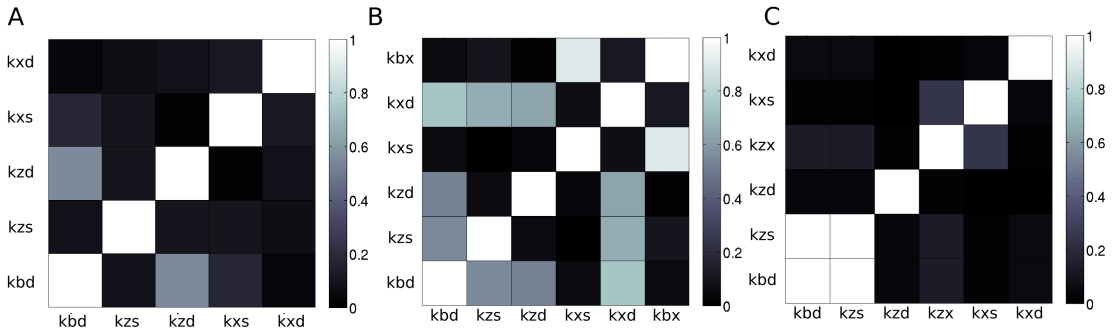

Figure C3: Absolute correlation of model parameters for (A) transcription inhibition, (B) SigmaB proteolysis, and (C) post-transcriptional instability.

Original publications and contributions

- **U.W. Liebal**, T. Millat, I. de Jong, O. Kuipers, U. Völker, and O. Wolkenhauer. How mathematical modelling elucidates signalling in *Bacillus subtilis* . *Mol Microbiol*, 77(5):1083-1095, 2010. doi: 10.1111/j.1365-2958.2010.07283.x

  Ulf Liebal conceived and designed the review. Ulf Liebal performed the literature search and wrote the paper. Ulf Liebal wrote the manuscript.

- **U.W. Liebal**, T. Millat, J. Marles-Wright, R.J. Lewis, and O. Wolkenhauer. Simulations of stressosome activation emphasize allosteric interactions between RsbR and RsbT. submitted, 07/2012.

  Ulf Liebal conceived and designed the research. Ulf Liebal generated and analysed the data. Ulf Liebal wrote the manuscript.

- **U.W. Liebal**, P.K. Sappa, T. Millat, L. Steil, G. Homuth, U. Völker, and O. Wolkenhauer. Proteolysis of β-galactosidase following σ^{B} activition in *Bacillus subtilis*. *Mol BioSyst*, 8(6):1806–14, 2012. doi: 10.1039/C2MB25031D

  Ulf Liebal participated in conceiving and designing the research, all experiments have been performed by Praveen K. Sappa. Ulf Liebal performed all simulations. Ulf Liebal wrote the manuscript.

- S. Nikolov, X. Lai, **U. Liebal**, O. Wolkenhauer, and J. Vera. Integration of Sensitivity and Bifurcation Analysis to Detect Critical Processes in a Model Combining Signalling and Cell Population Dynamics. *International Journal of Systems Science*, 41(1):81 105, 2009. doi: 10.1080/00207720903147746

  Ulf Liebal supported the sensitivity analysis. Ulf Liebal edited the manuscript.

Presentations

1. A computational stressosome model consolidates hypotheses about environmental activation of the SigmaB general stress response. *BaCell conference*, Dublin, Ireland, April 2012

2. The stressosome, spatial understanding of a signalling machine, *Int. workshop 'Modelling, Analysing and Exploring Spatial Dynamics of Cell Biological Systems'*, Rostock, October 2010

3. Models of the general stress response using the SBToolbox2 - can Sycamore substitute? *Sycamore User Meeting*, Heidelberg, Germany, June 2009

4. Mathematical modelling of the sigB mediated stress response and reporter protein instabilities in *B. subtilis*, *invited talk*, TU Berlin, Bioverfahrenstechnik, November 2009

5. SigmaB response is comparable between strains with and w/o anti-sigma factor RsbW. *B. subtilis day, invited talk*, Ernst-Moritz-Arndt Universität Greifswald, Inst. Functional Genomics, November 2009

6. Was verbindet Waschmittel, Hautkrebs, Alzheimer, Kraftstoff und Diabetis? *Lange Nacht der Wissenschaft*, Rostock, 2009/10

7. Computational Evolution of Regulatory Networks. *Biofusing Lecture Series*, KAIST, Daejeon, Rep. Korea, November 2008

8. Computer-Simulation in der Biomedizin-Forschung. *Lange Nacht der Wissenschaft*, Rostock, April 2008

Poster at international conferences

1. Liebal U., Millat T., Marles-Wright J., Lewis R., Wolkenhauer O. Protein diversity of the stressosome - Stress sensitivity and Response magnitude, *12th International Conference on Systems Biology*, Heidelberg/Mannheim, Germany, August 2011

2. Millat T., Rubenis O., Liebal U., Wolkenhauer O., de Jong I., Kuipers O. Automated analysis of flow cytometry data from heterogeneous bacterial populations, *12th International Conference on Systems Biology*, Heidelberg/Mannheim, Germany, August 2011

3. Liebal U., Sappa P.K., Millat T., Steil L., Völker U., Wolkenhauer O. Using a modelling approach to elucidate unexpected reporter gene signals for sigmaB activity in *B. subtilis*, *Conference on Systems Biology of Microorganisms*, Paris, France, March 2010

4. Millat T., Liebal U., Wolkenhauer O., de Jong I., Kuipers O. The dynamics of the phosphorelay and the initiation of sporulation in Bacillus subtilis - a systematic study, *11th International Conference on Systems Biology*, Edinburgh, UK, October 2010

5. Liebal U., Kim JR., Cho KH., Wolkenhauer O. Dynamic Behavior Determines the Design Strategy of Metabolic Regulation Networks, *10th International Conference on Systems Biology*, Stanford, USA, August 2009

6. Liebal U., Millat T., Sappa P.K., Hildisch H., Steil L., Völker U., Wolkenhauer O. Analysis of a Model of sigB Activation Following Glucose Starvation, *10th International Conference on Systems Biology*, Stanford, USA, August 2009

7. Liebal U., Schmidt H. Sensitivity Analysis based Adaptive Search-Space Reduction for Parameter Estimation Applications, *9th International Conference on Systems Biology*, Gothenburg, Sweden, August 2008

8. Lai X., Liebal U., Nikolov S., Wolkenhauer O., Vera J. Use of sensitivity analysis to detect critical biochemical processes in a mathematical model linking intracellular and cell population dynamics in erythropoiesis, *6th Conference on Computational Methods in Systems Biology*, Rostock-Warnemünde, Germany, October 2008

SYSTEMS BIOLOGY
BIOINFORMATICS
ROSTOCK

www.sbi.uni-rostock.de

Universität Rostock

Traditio et Innovatio

Protein Diversity of the Stressosome
Stress Sensitivity and Response Magnitude

Ulf Liebal[♭], **Thomas Millat**[♭], **Jon Marles-Wright**[♯], **Richard Lewis**[♯], **Olaf Wolkenhauer**[♭]

♭ Dept. of Systems Biology & Bioinformatics, University of Rostock, Rostock, Germany

♯ Inst. of Cell & Molecular Biosciences, Newcastle University, Newcastle-upon-Tyne, UK

The Stressosome protein complex integrates signals

- Prevalence: dispersed in bacterial clades (*Bacillus, Listeria, Streptomyces, Vibrio, Deinococcus*)
- Function: signal integration hub fed by sensors of physical stimuli e.g. light, EtOH, salt stress, chemical substances
- Structure: truncated icosahedron, radius of about 10 nm. R and S proteins form the backbone. Protein T associates reversibly with S. Each protein in the structure has three nearest neighbours. In total there are four combinations of neighbouring proteins (R1, R2, R3, and S1).
- Reactions: T phosphorylates R and S. Phosphorylated R (RP) stimulates kinase activity of T. Phosphorylated S (SP) repels kinase T from stressosome. SP inhibits T kinase activity. Free T activates stress response. There exist four R homologues.
- Activation: Signal perception increases the phosphorylation of R by unknown mechanisms.
- Research: What are the advantages of using four paralogues of R in the stressosome?

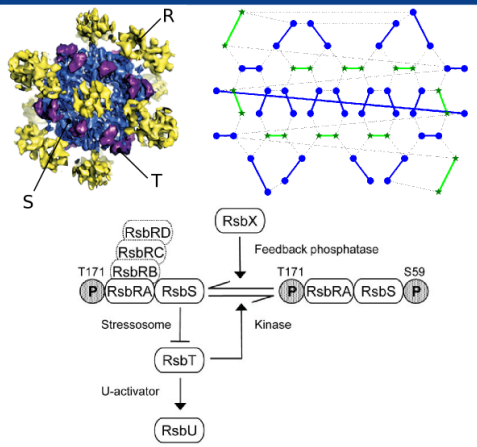

Model & Simulation

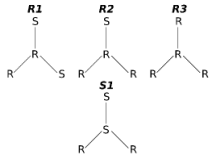

- Each protein is numbered together with a list of the three nearest neighbours.
- Initial condition: protein phosphorylation probability of 0.5.
- For each neighbourhood R1, R2, R3, and S1 the kinase T can be differently stimulated. Stimulation of phosphorylation depends on the number of RP and SP in the neighbourhood. An example for the probability of stimulation is given for R2:

phosphorylation of neighbours	probability of kinase T stimulation
{S,R,R}	{R}
{0,0,0}	{0}
{0,1,0}	{0.5}
{0,1,1}	{1}
{1,0,0}	{0}
{1,1,0}	{0}
{1,1,1}	{0}

Stimulation Transition Table (left): In the configuration R2 the central R has three neighbours {S,R,R}. If its S is phosphorylated {1,x,x} there is no stimulation of T. Only for one or two RP stimulation occurs (0.5 and 1).

- Other probabilistic parameters:

T activity: R —war:0.5 / peace:0.1→ RP

RP —0.02→ R

SP —1→ S

Magnitude and Sensitivity

- Phosphorylation of R3 regulates response magnitude.

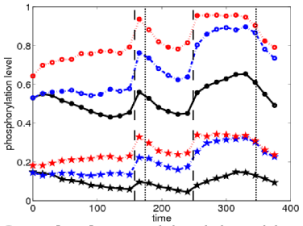

In a predictive simulation three values for the kinase activity of T on R proteins with R3 neighbourhood are tested (0.01-black, 0.1-blue, 1-red). Shown is total phosphorylation of R and S (circle and star) over time.

Conclusion: with rising kinase activity on R3 the magnitude of stress response increases likewise.

- Cooperativity of R2 regulates response sensitivity.

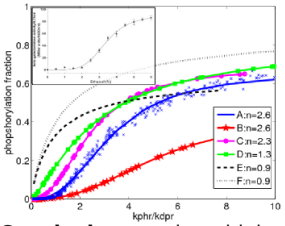

Here, cooperativity is the stimulation of kinase activity by RP. Different hypotheses can be tested by changing values in the *Stimulation Transition Table*. Shown is the steady state phosphorylation at various stresses.

Conclusion: sigmoidal shape reproduces experi-ments, cooperativity of R2 regulates signal sensitivity.

Novel insights to the Stressosome

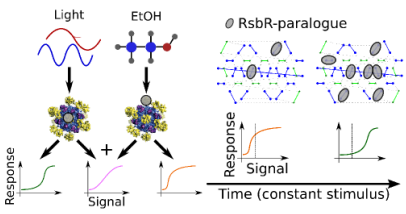

- The various homologues of R may be stimulated by different stresses.
- Stress response can be regulated by adjusting absolute kinase activity of T or cooperative effects of RP to stimulate kinase activity.
- Different protein positions are differently effective in changing dynamics (e.g. R3-magnitude or R2-sensitivity).
- Stressosome integrates signals: combination of stresses produce different outcomes than there action alone - fine tuned responses.
- Changing the stressosome composition over time to establish adaptivity: if at constant stress stimuli an R homologue is expressed with altered cooperativity that leads to reduced signal sensitivity, the stressosome could be muted.

SysMO Systems Biology of Microorganisms

bbsrc biotechnology and biological sciences research council

Bundesministerium für Bildung und Forschung

Ulf W. Liebal
Systems Biology & Bioinformatics
Institute of Computer Science
University of Rostock
ulf.liebal@uni-rostock.de

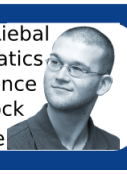

Elucidating Unexpected Reporter Signals for σ^B Activity in *B. subtilis*

Ulf W. Liebal ★ Praveen Kumar Sappa § Thomas Millat ★

Leif Steil § Uwe Völker § Olaf Wolkenhauer ★

Background

• The σ^B regulon confers *B. subtilis* with the ability to respond to various stress stimuli and adapts it for future stress incidents. Metabolic expenditures are reduced, in turn, expression of about 150 protective genes is activated.

• Starvation activates the anti-anti sigma factor RsbV that inhibits RsbW by complex formation. RsbW itself is the anti sigma factor of σ^B. Hence, an inhibition of RsbW results in release of σ^B and consequently in global expression changes. RsbW can phosphorylate RsbV thus inactivating it. The proteins RsbW and RsbV are transcribed by σ^B and it is assumed that increasing levels of RsbW lead to an inactivation of RsbV and to an adaptive σ^B response.

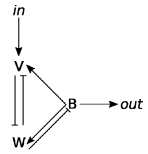

• To monitor different levels of σ^B-dependent expression, we modulated σ^B expression in a *rsbW* mutant via IPTG induction of a P_{spac} promotor cloned upstream of the σ^B. β-Gal activity of a *ctc::lacZ* fusion was used as reporter for σ^B dependent expression. Direct activation of σ^B in this strain (BSA115) is thought to activate reporter protein synthesis and dysfunctional feedback regulation should result is lasting β-Gal activity.

Surpise and Explanation

• Addition of IPTG induces expression of β-Gal, but activity is transient.
• Maximal β-Gal signal is independent of growth rate
• β-Gal decrease starts before transition to stationary phase for 1mM IPTG.
• All β-Gal signals drop to uninduced signal strength
• High σ^B activation → Strong β-Gal decrease
• Low σ^B activation → Weak β-Gal decrease

Models of the most simple three explanatory hypotheses are fitted to the experimental data to test how well each is able to reproduce the observations:

Transcription Inhibition

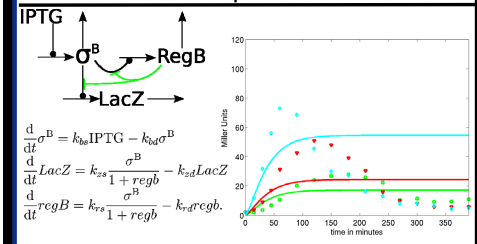

$$\frac{d}{dt}\sigma^B = k_{bs}\mathrm{IPTG} - k_{bd}\sigma^B$$
$$\frac{d}{dt}LacZ = k_{zs}\frac{\sigma^B}{1+regb} - k_{zd}LacZ$$
$$\frac{d}{dt}regB = k_{rs}\frac{\sigma^B}{1+regb} - k_{rd}regb.$$

✘ transient dynamics, adaptivity
✘ shifted peak positions
✘ comparable final state level

σ^B Proteolysis

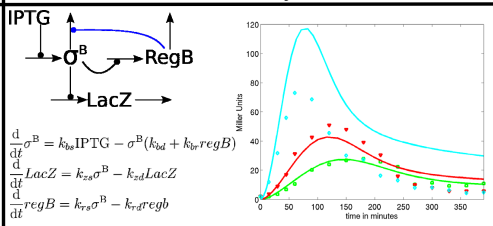

$$\frac{d}{dt}\sigma^B = k_{bs}\mathrm{IPTG} - \sigma^B(k_{bd} + k_{br}regB)$$
$$\frac{d}{dt}LacZ = k_{zs}\sigma^B - k_{zd}LacZ$$
$$\frac{d}{dt}regB = k_{rs}\sigma^B - k_{rd}regb$$

✓ transient dynamics, adaptivity
✓ shifted peak positions
✘ comparable final state level

β-Gal Proteolysis

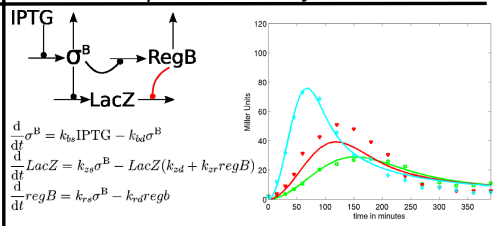

$$\frac{d}{dt}\sigma^B = k_{bs}\mathrm{IPTG} - k_{bd}\sigma^B$$
$$\frac{d}{dt}LacZ = k_{zs}\sigma^B - LacZ(k_{zd} + k_{zr}regB)$$
$$\frac{d}{dt}regB = k_{rs}\sigma^B - k_{rd}regb$$

✓ transient dynamics, adaptivity
✓ shifted peak positions
✓ comparable final state level

Adaptive σ^B behaviour

Hypothesis

Can β-Gal proteolysis contribute to the adaptive σ^B response in a wild type *B. subtilis*?:

1. Taking the β-Gal proteolysis model parameterized with BSA115 experiment as starting point.
2. Use of a previous experimental data of β-Gal in wt *B. subtilis*. σ^B response is activated by starvation at the transition to stationary phase.
3. Two parameters (IPTG, k_{zs}), that are independent of the putative protease dynamics, are allowed to vary during parameter estimation.

Result

The β-Gal proteolysis model (red) can fit a wt σ^B response with adaptive behaviour as well as a model that relies on negative feedback regulation including RsbW/V proteins (blue).

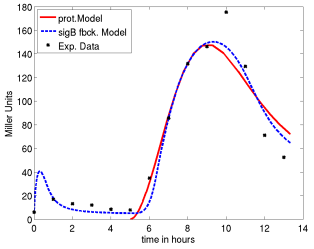

Conclusion

Therefore, the hypothesis can not be rejected and proteolysis of β-Gal can contribute to adaptivity in the wild type.

Conclusions and Perspectives

• *B. subtilis* BSA115 shows adaptive, transient dynamics of β-Gal following σ^B activation by IPTG. Modelling and Northern blot experiments suggest σ^B induced β-Gal proteolysis as the origin.

• σ^B induced proteolysis of β-Gal in BSA115 was assumed to occur also in *B. subtilis* wild type cells, raising the possibility that β-Gal instabilities might contribute to the transient nature of the σ^B response – testing the ability of the β-Gal proteolysis model to reproduce wild type adaptivity confirmed this assumption.

• Therefore, part of the adaptive dynamics of β-Gal reporter signal is due to induced protein proteolysis, questioning the applicability of β-Gal reporters.

• Research focus on σ^B has been on its activation and the cause of the transient response is not well known. Our results add proteolysis to the possible mechanisms:

1.

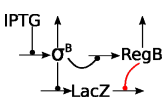

Induced proteolysis

2.

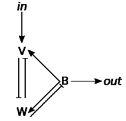

Negative feedback via anti and anti-anti sigma factors

3.

Silencing of σ^B by stress response strategies like sporulation

Affiliations, Contact & Acknowledgements

★ Systems Biology & Bioinformatics group, University of Rostock, Rostock, Germany

ulf.liebal@uni-rostock.de **www.sbi.uni-rostock.de**

§ Institute for Microbiology and Institute for Genetics and Functional Genomics, Ernst-Moritz-Arndt-University Greifswald, Greifswald, Germany

Funded by the SysMO-BaCell BMBF grant 0313978.

Federal Ministry of Education and Research

Universität Rostock Traditio et Innovatio

Analysis of a Model of σ^B Activation following Glucose Starvation

Ulf W. Liebal[†], Praveen Kumar Sappa[‡], Hendrikje Hildisch[‡], Thomas Millat[†], Leif Steil[‡], Michael Hecker[‡], Uwe Völker[‡], Olaf Wolkenhauer[†]

[†]University of Rostock, Systems Biology and Bioinformatics Group, Germany;
[‡]Ernst-Moritz-Arndt-University Greifswald, Institute for Microbiology and Institute for Genetics and Functional Genomics, Germany;

The Bacell-SysMO project

The SysMO project is a European transnational funding and research initiative on "Systems Biology of Microorganisms". The goal pursued by SysMO is to record and describe the dynamic molecular processes going on in unicellular microorganisms in a comprehensive way and to present these processes in the form of computerized mathematical models.

The objective of this project is an integrated understanding of the metabolic and genetic network that controls the transition from growth to glucose starvation, as shown in ***Fig. 1***. This transition is a fundamental ecophysiological response that serves as a scientific model for environmental signal integration and is pivotal for industrial fermentations of Bacillus that occur predominantly under nutrient starvation.

The σ^B regulon (***Fig. 2***) confers *B. subtilis* with the ability to respond to stress stimuli and adapts it for future stress incidents.

- Anti-sigma factor W binds B thereby precluding formation of RNA-polymerase holoenzyme. (*React.* 1)
- The affinity of V towards W (*React.* 2) is reduced by phosphorylation of V by W (*React.* 3).
- Following Glc-starvation VP dephosphorylation rate is increased resulting in V increase. (*React.* 4)
- V associates with W thereby reducing free W level. (*React.* 2)
- Reduced W level stimulates dissociation of WB complex. (*React.* 1)
- Increased levels of B (σ^B) associates with RNA-polymerase to induce expression of genes. (*React.* 5)
- Proteins and complexes are degraded with a first order mechanism (React 6)

1

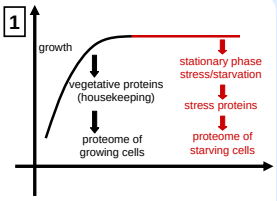

2

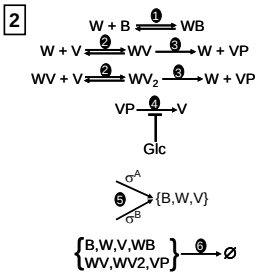

Direct Parameter Estimation Approach

3

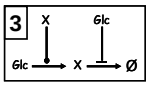

Glucose(Glc)-Biomass(X) model

Simulation of Glucose Starvation:
- *ctc::lacZ* reporter gene construct provides information on the transcriptionally active B level.
- Glc concentration is derived from the OD with a fitted model shown in ***Fig. 3***.

4

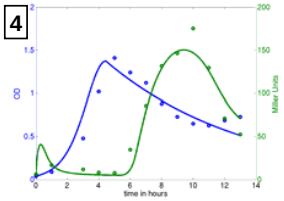

Interpretation of Simulations:
Parameter estimation process (***Fig. 4***) using sequentially particle swarm and simulated annealing optimization still allows for large possible parameter realizations with good fitting. The model-experiment relationship is therefore non-identifiable.
The simulations agree with the principles of general stress response outlined in the introduction.

Parameter Fitness Correlations

5

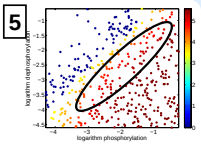

6

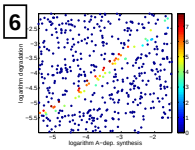

Goal:
determining parameter ranges that satisfy pre-defined observations for the fitness of stress response.
Fitness: low level of free B, high level of WB complex.

Procedure:
1. select two parameters & corresponding boundaries
2. randomly combine the two parameter values
3. evaluate the model fitness for each combination

Results:
phosphorylation and dephosphorylation: Antagonistic reactions, only a narrow parameter region is physiological feasible. (***Fig. 5***)
protein expression and degradation: Antagonistic reactions, but fitness is very sensitive on the balance of both reactions. (***Fig. 6***)

Transcriptomic Results for Regulon and Operon

7

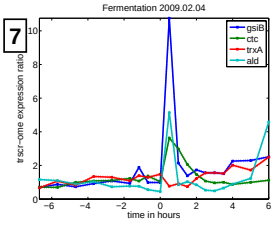

8

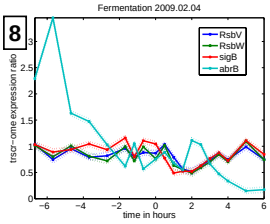

Transcriptome:
- activation of expression of the σ^B regulon during entry into starvation (***Fig. 7***).
- expression of the operon fails to increase (***Fig. 8***) despite the positive transcriptional feedback loop of σ^B on its operon.

Possible reason: sigma factor competition on the operon.

Conclusions and Perspectives

A model was developed that reproduces the available experimental data. However, the models are non-identifiable meaning that non-unique parameter sets can reproduce the data. To render the model identifiable, model reduction processes will be conducted to lump parameters and combine components. Additionally, we will gather more diverse data including concentrations of components in the regulation upstream of B-activation.

The fitness of parameter combinations shows high robustness of the system against changes in WV association rate. Considering pre-stress steady state fitness conditions will help to determine missing parameter values. Similar investigations will be conducted for possible steady state conditions during long lasting stress conditions.

Transcriptome results show that gene-specific sigma factor competition needs to be implemented in the models and that unknown post-transcriptional events modulate protein concentrations.

Universität Rostock Traditio et Innovatio

Contact: *Thomas.Millat@uni-rostock.de*

Systems Biology & Bioinformatics group
Department of Computer Science
University of Rostock, 18051 Rostock, Germany

www.SBI.uni-rostock.de Systems Biology & Bioinformatics

SPONSORED BY THE Federal Ministry of Education and Research

Dynamic behavior determines design strategies of regulation in metabolic networks

Ulf W. Liebal[1,*], Olaf Wolkenhauer[1]

Jeong-Rae Kim[2], Kwang-Hyun Cho[2,*]

*E-mail: ulf.liebal@uni-rostock.de, ckh@kaist.ac.kr

[1]University of Rostock, Department of Computer Science, 18051 Rostock, Germany
http://www.sbi.uni-rostock.de

[2]Department of Bio and Brain Engineering, Korea Advanced Institute of Science and Technology (KAIST), 335 Gwahangno, Yuseong-gu, Daejeon 305-701, Republic of Korea
http//:sbie.kaist.ac.kr

Enzyme activities are tightly regulated

Our goal is to uncover design principles of regulation of enzyme activity that optimize an objective function in a simple metabolic network. In metabolic networks enzyme activity is tightly regulated to adjust metabolite dynamics according to demands on the metabolism.

1

$$V_{max} = k_{kat} e$$

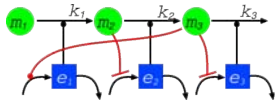

Enzyme activity is defined as a product of the enzyme catalytic rate constant and its total concentration. We examine the effect of the latter by transcriptional regulation. The basis is a simple metabolic network with three metabolites and three enzymes. Metabolites can activate (red line with circle) or inhibit (red line with bar) enzyme expression.

2

$$\frac{dm_2}{dt} = k_1 e_1 m_1 - k_2 e_2 m_2$$
$$\frac{de_2}{dt} = P(m, W) - k_d e_2$$

Rate equations for concentrations of metabolite M_2 and enzyme E_2. Metabolic reaction rate constants (k_1 to k_3) are randomly distributed on integers in the interval [1,10] for 50 independent combinations (*Metabolic Individuals*). The constant k_d is set to 1.

3

$$P(m, W) = \frac{1}{1 + \exp\left(-\sum_j W_j m_j\right)}$$

The function P controls synthesis of enzymes. It is a sigmoidal function with input of regulation quality (W_j:activating: +1, inhibiting: -1) and the metabolite concentration j that regulates. The output is the expression rate in an interval [0,1]. In case of no regulation the expression rate is 0.5.

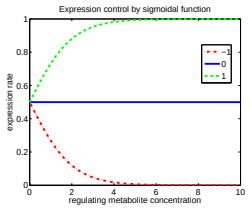

Quantification of effectiveness for all possible regulation strategies

4

$$W = \begin{pmatrix} 0 & 0 & 1 \\ 0 & -1 & 0 \\ 0 & 0 & -1 \end{pmatrix} \Rightarrow \begin{array}{c} \\ e_1 \\ e_2 \\ e_3 \end{array} \begin{array}{c} \begin{array}{ccc} m_1 & m_2 & m_3 \end{array} \\ \begin{pmatrix} 1 & 4 & 7 \\ 2 & 5 & 8 \\ 3 & 6 & 9 \end{pmatrix} \end{array}$$

Matrix W contains the regulation qualities of metabolites to enzymes. In the example above metabolite m_2 inhibits its degradation via e_2 while m_3 activates e_1 and inhibits e_3, coded with the ordinal numbers 5, 7 and 9 (cf. network in Box. 1).

5

The number of non-zero elements in the regulation matrix W indicates the number of regulations. We examine conditions with one, two and three regulations (non-zero elements in W). Based on a fitness objective the effectiveness of every regulation is rated for any of the 50 Metabolic Individuals (cf. Box 2).

# of combinations 1 regulation:	18
# of combinations 2 regulations:	144
# of combinations 3 regulations:	672

6

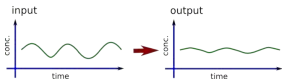

$$f = \frac{1}{k_{bg} + \mathrm{var}(m_3)} \cdot \frac{\mathrm{mean}(m_3)}{\mu}$$

$$\mathrm{var}(m_3) = \mathrm{variance}[m_3(t_{\frac{final}{2}}) : m_3(t_{final})]$$
$$\mathrm{mean}(m_3) = \mathrm{mean}[m_3(t_{\frac{final}{2}}) : m_3(t_{final})]$$

Among biological significant fitness functions we implemented the reduction of variation. We set m_1 to oscillate as a sinusoidal and tested m_3 of its capacity to reduce this oscillation. The first part of the fitness function penalizes an increase in variation. The second part in the function penalizes deviation from the m_3 concentration in a non-regulated network (μ).

Different network dynamics cause different regulations distribution

7 One regulation

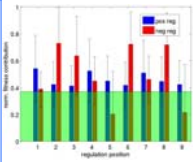

Bar plot of the regulation ordinals (cf. Box 4) and their fitness based on the equation in Box 6.
Green line indicates the limit for beneficial regulations, representing the sum of mean and standard deviation (s.d.) of a non-regulated network.
Most regulations are beneficial, albeit with a high s.d. To reduce s.d. we sub-divided the population into 13 individuals with and without accumulation in m_3 (cf. Box 1).

Low m_3 accumulation

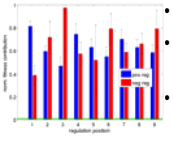

- Reduced s.d.
- All regulations are highly beneficial
- Blue bars decrease in rows of three, red bars increase

High m_3 accumulation

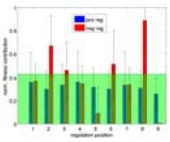

- High s.d.
- Few regulations are beneficial
- No obvious symmetries of regulations

8 Two regulations

We use the regulation roses to visualize two regulations. Lines connect the ordinal numbers of regulation whose thickness represents fitness.

Low m_3 accumulation | High m_3 accumulation

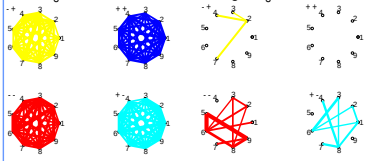

Low m_3 accumulation networks have comparable fitness values for all regulations, but to clearly distinguishable regulation strategies in m_3. For two regulations dynamic properties of the networks have higher impact on fitness than regulation quality.

9 Three regulations

The fitness for three regulation interactions is represented by the thickness of triangles.

Low m_3 accumulation | High m_3 accumulation

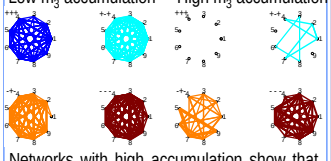

Networks with high accumulation show that contrasting regulations also have contrasting effects on the fitness. Many triple negative regulations can be used, while no triple positive regulation is >.25 of the highest fitness. Regulation -5, +7, -9 (orange line, cf. Box 1, 5) for high m_3 is particularly beneficial.

Results/Conclusions

We explored regulation distributions of simple metabolic networks (cf. Box 1) based on their capacity to reduce oscillation (cf. Box 6) and conclusions are restricted to this condition.

Dynamic properties and flow rate determine the distribution of optimal regulations:

• Networks that do not accumulate the tested metabolite m_3 have a wide choice of optimal regulations. These networks are characterized by low k_1 and high k_3 values. Reducing the inflow of oscillating substrate to the system allows for more regulation.

Regulation interactions have different effects compared to the individual regulation effects:

• The triple regulation interaction coded by ordinal numbers [-5, +7, -9] is highly beneficial (cf. Box 9). Each regulation in solitude is detrimental for the fitness (cf. Box 7).

Contrasting regulation schemes must not have contrasting fitness effects:

• For networks that accumulate the tested metabolite m_3 the interaction of two purely inhibitory regulations is beneficial, while the interaction of two activating regulations is detrimental (cf. Box 8). However, networks without m_3 accumulation show no substantial differences in regulation efficiencies for positive and negative regulation interactions.

Financial support

This work was supported by the National Research Foundation of Korea (NRF) grant funded by the Korea Ministry of Education, Science & Technology (MEST) through the Systems Biology grant (20090065567), the Nuclear Research grant (M20708000001-07B0800-00110), the 21C Frontier Microbial Genomics and Application Center Program (Grant 11-2008-10-004-00), and the WCU (World Class University) grant (R32-2008-000-10218-0), Systems biology infrastructure establishment grant provided by Gwangju Institute of Science&Technology in 2009, German Federal Ministry of Education and Research (BMBF)-BaCell-SysMO project (0313978F) and Deutscher Akademische Austauschdienst (DAAD)-grant (D/08/41437).

Sensitivity Analysis based Adaptive Search-Space Reduction for Parameter Estimation Applications

Ulf W. Liebal & Henning Schmidt
University of Rostock, Systems Biology and Bioinformatics group

Background

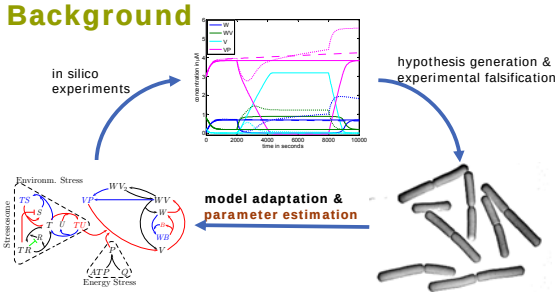

Modelling of biological systems is an iterative process. A common scenario is:

1. A model is built that reflects available experimental data.
2. New experimental data generated → the model is not able to explain the data.
3. Re-estimation of all parameters based on the new data?

Problems:
- many parameters
- different experiments and measurement data
- parameter unidentifiability

Current solutions use sensitivity based approaches for parameter selection:
- local SA, e.g. Dash et al.
- global SA, e.g. Jin et al.
- using SA with specific objective functions, e.g. Yue et al.

Goal: **Experiment specific adaptive identification of parameters responsible for divergent model-experiment behaviour!**
Residual and **S**ensitivity aided **i**terative **S**earch space **R**eduction: **RSiSR**

Method + Example

We consider a model of Thiamine uptake in *S. cerevisiae* (Ericson et al.). The example serves as a well known system; for the sake of demonstration of the method, simulated data is used with deviations in two parameters affecting Thiamine uptake.

Two exp. settings are investigated:
- 1st experiment: null-mutant for the Thiamine uptake
  →Experiment 1 - parameter estimation
- 2nd experiment: uptake of Thiamine is functional

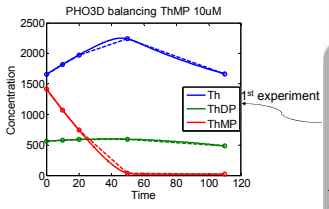

1st experiment

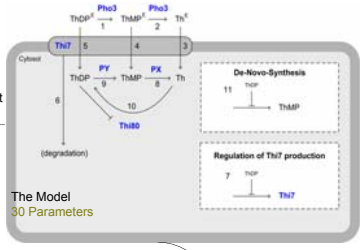

2nd experiment

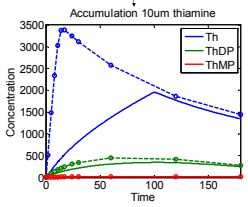

RSiSR procedure:

$$e(t,p) = y^m(t) - y(t,p)$$

residual — measured state (t) — model prediction (t)

$$\epsilon(p) = [e_1^1(t_1,p), e_1^1(t_2,p), ..., e_2^1(t_1,p), e_2^1(t_2,p), ..., e_1^2(t_1,p), ...]^T$$

stacked residuals vector

Taylor expansion for the error at Δp, assuming linear approximation and disregarding higher order terms.

$$\epsilon(p+\Delta p) = \epsilon(p) - \Omega\Delta p$$

$$-\frac{\partial}{\partial p}\epsilon(p) = \Omega = \begin{bmatrix} \frac{\partial y_1^1(t_1,p)}{\partial p_1} & \frac{\partial y_1^1(t_1,p)}{\partial p_2} & \dots & \frac{\partial y_1^1(t_1,p)}{\partial p_n} \\ \vdots & \vdots & & \vdots \\ \frac{\partial y_1^1(t_{m_1},p)}{\partial p_1} & \frac{\partial y_1^1(t_{m_1},p)}{\partial p_2} & \dots & \frac{\partial y_1^1(t_{m_1},p)}{\partial p_n} \\ \frac{\partial y_1^2(t_1,p)}{\partial p_1} & \frac{\partial y_1^2(t_1,p)}{\partial p_2} & \dots & \frac{\partial y_1^2(t_1,p)}{\partial p_n} \\ \vdots & \vdots & & \vdots \\ \frac{\partial y_1^2(t_{m_2},p)}{\partial p_1} & \frac{\partial y_1^2(t_{m_2},p)}{\partial p_2} & \dots & \frac{\partial y_1^2(t_{m_2},p)}{\partial p_n} \\ \vdots & \vdots & & \vdots \end{bmatrix}$$

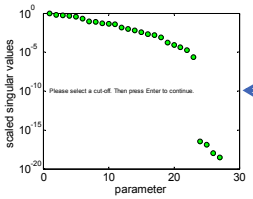

computing singular values of Ω allows identification of (almost) linearly dependent parameter sensitivities. These have to be eliminated to increase the information content of Ω.

Re-writing Taylor expansion for reduced sensitivity matrix and parameter vector.

$$\epsilon(p_{red} + \Delta p_{red}) \approx \epsilon(p_{red}) - \Omega_{red}\Delta p_{red}$$

setting l.h.s to zero and solving the equation for Δp_{red} .

$$\Delta p_{red} = (\Omega_{red}^T W \Omega_{red})^{-1} \Omega_{red}^T W \epsilon(p_{red})$$

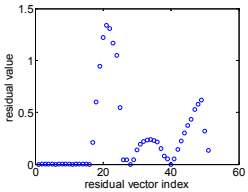

W, the weighting matrix, is user defined generated by choosing a threshold below which the significance of a residual increases the lower its value. This guarantees the conservation of already fitted experiments by raising their influence. The first 15 indices correspond to the well fitted experiment.

π_i is a measure that reflects the relative parameter change that is required to minimize the residual error. π_i forms the basis for a ranking for parameter estimation.

$$\pi_i = \Delta p_{red,i} \frac{1}{p_{red,i}}$$

The RSiSR ranking for weighted π_i in **log scale** shows four parameters that strongly determine the discrepancy of model and observation. Among those four identified parameters are the two parameters that are perturbed.

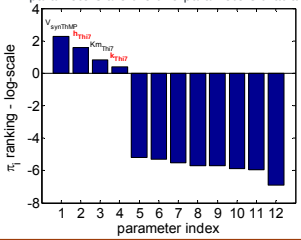

In a following parameter estimation the four top-scoring parameters would be estimated. This speeds up the parameter determination process and renders it more precise.

Conclusions

- Considerable reduction of search-space, identifying parameters important for un-fitted experiments
- Assumption of linearity => only an approximation
- Iterative use between different runs of parameter estimation
- Manual and eye inspection at the moment but can easily be automized
- Adaptable and improvable weight matrix
- Can be useful to determine parameters important for obtaining a desired response shape – potential use for drug target identification

Method soon available in the SBTOOLBOX2

Literature

Dash, R.; et al. (2008); *IEEE Trans. on Biomedical Engineering*
Ericsson, A., et. Al. (2008); *Essays in Biochemistry - Systems Biology*
Jin, Y., et al. (2007); *American Control Conference*
Schmidt, H., et al. (2006); *Bioinformatics*
Yue, H ., et al. (2006); *Molecular BioSystems*

Acknowledgments

BMBF – BaCell-SysMO Project
BMBF – Forsys Partner

Contact

Henning Schmidt
FORSYS Research Group hIMOsYS
Systems Biology and Bioinformatics
University of Rostock
Albert Einstein Str. 21
18059 Rostock, Germany
henning.schmidt@uni-rostock.de

Warum betrunkene Bakterien Wissenschaftlern viel über molekulare Prozesse in der Zelle verraten

Erschienen unter anderem in Profile-*Magazin der Universität Rostock, 2/2012, 12-13 und der* Ostseezeitung *am 03.04.2012. Text erstellt in Zusammenarbeit mit Wolfgang Thiel, Olaf Wolkenhauer und Ulrich Vetter.*

'Es ist mein Wunsch, das Leben von Bakterien, so gut es eben geht, zu erklären', sagt Ulf Liebal. Der 30-jährige Biochemiker der Universität Rostock hat in Halle studiert und seine Diplomarbeit, über die Wirkstoffproduktion in Bakterien, in Finnland geschrieben. Die Forschung im Labor sagt dem jungen Mann, der im Studentenorchester Fagott spielt, allerdings nicht so zu. Seiner Faszination, zu erfassen, wie aus kleinsten Molekülen ein komplexer Organismus entsteht, tut das aber keinen Abbruch. Deshalb ist sein Metier die noch junge Disziplin der Systembiologie der 'Biochemie am Computer' wie er sagt. Hier kombiniert er Methoden der experimentellen Biologie und der Bioinformatik mit mathematischen Modellierungsansätzen. So entsteht am Rechner ein Bild der Vorgänge innerhalb einer Zelle, der kleinsten biologischen Einheit, die sich selbst vermehren kann. Konkret erforscht Ulf Liebal, wie das im Boden lebende Bakterium Bazillus subtilis auf Stress reagiert, in diesem Falle, wenn es mit Alkohol in Berührung kommt. 'Ich untersuche also betrunkene Bakterien', beschreibt der junge Wissenschaftler seine Arbeit. Zwar wird im Laborversuch Alkohol bewusst eingesetzt, in der Natur allerdings gibt es mehrere Quellen, aus denen Alkohol entsteht und in den Boden sickert: beispielsweise faulende Früchte.

'Viele denken bei Bakterien an Krankheitserreger, die wir mit anti-bakteriellen Reinigungsmitteln aus unseren Häusern vertreiben', sagt Ulf Liebal. Das Bakterium, das er

untersucht, ist überall in der Umwelt anzutreffen. Es lebt im Boden und hilft den Pflanzen beim Wachstum, ist also kein Krankheitserreger. Wie gedeiht es im Boden und wie reagiert es auf die Umwelt? Das will der junge Forscher herausfinden. Es ist bekannt, dass ein Bakterium nach einem Stresserlebnis seine Zusammensetzung ändert. Die Untersuchungen mit Alkohol nutzt der 30-Jährige, um mehr über die Verknüpfung von Stresserlebnis und Zusammensetzung des Bakterium erfahren. So gibt es einen Einblick, welche Prozesse Bakterien im Menschen auslösen knnen, womit sich auch neue Möglichkeiten zum Beispiel zur Behandlung von Lebensmittelvergiftungen ergeben.

Alkohol stresst Bakterien, weil er wichtige Proteine beschädigt. Deshalb hat sich das Bakterium einen eigenen Alkoholtest entwickelt. Dieser Testsensor besteht aus 60 Proteinen, die geometrisch und symmetrisch aufgebaut sind. 'Das muss man sich in etwa wie einen Weihnachtsstern vorstellen', sagt der Forscher. Er hat mit einem einfachen Papiermodell diesen Sensor nachgebaut. 'Ich bin jetzt in der Lage, die Bewegungen des Proteins auf Tischmodellgröße nachzuempfinden'. So zeigt sich, dass es allgemeine Regeln für Bewegungen von geometrischen Strukturen gibt. Die sind vermutlich auch für den mikroskopisch kleinen Sensor in der Zelle gültig. Ulf Liebal gewinnt durch sein Modell einen besseren Einblick, wie das Bakterium auf Alkohol reagiert. Spürt eines von den 60 Proteinen Alkohol, dann bewegt sich das Protein und aktiviert damit andere in der Nachbarschaft. 'So kann wenig Alkohol schon eine große Reaktion in der Zelle auslösen. Ein kleines Geheimnis ist damit gelüftet', ist der junge Mann stolz. Für ihn sind Papier und Kreativität wichtiger geworden als teure Labore. Dennoch benutzt er Daten von Partner-Laboratorien, um seine Modelle an die Wirklichkeit anzupassen. Diese sind unentbehrlich, um die komplexen molekularen Anpassungsvorgänge vollständig zu erfassen.

Um die biologischen Organismen in ihrer Gesamtheit jedoch besser verstehen zu können, arbeiten Wissenschaftler verschiedener Fachrichtungen interdisziplinär eng zusammen. Die experimentellen Untersuchungen erfordern zudem so komplexe, aufwendige und teure La-

boreinrichtungen, dass ein einzelnes Labor dazu nicht in der Lage wäre. Die Gruppe um Professor Olaf Wolkenhauer in Rostock, zu der auch Ulf Liebal gehört, ist Teil einer großen internationalen Initiative, der sogenannten BaCell-SysMO, die sich zum Ziel gesetzt hat, das Bakterium nicht nur besser zu verstehen, sondern auch besser nutzen zu können. In Deutschland unterstützt das Bundesministerium für Bildung und Forschung (BMBF) neben den Wissenschaftlern in Rostock auch Forschergruppen in Greifswald, Göttingen, Erlangen, Braunschweig und Marburg. Im Ausland arbeiten Universitäten in Groningen, Manchester und Newcastle an den gleichen Zielen. 'Vernetzung, um Vernetzung aufzuklären. Das ist Systembiologie', sagt Professor Olaf Wolkenhauer.

Curriculum Vitae

Ulf Winfried Liebal

Nationality	German
Date of birth	15 September 1981
Place of birth	Magdeburg/Elbe, Germany

Education

07/2000	Abitur, Otto von Guericke Gymnasium, Magdeburg, Germany
09/2001 - 07/2006	Diplom Biochemie, Martin-Luther Universität Halle-Wittenberg, Halle/Saale, Germany
09/2003	Research internship at the Systems Biology Group, Max Planck Institute, Magdeburg, Germany
07/2004 - 10/2004	Research internship at Bioprocess Engineering Laboratory, Oulu University, Oulu, Finland
09/2006 - 12/2006	Research assistant at the Biocomputing Group, Dept. Biochemistry, Oulu University, Oulu, Finland
02/2007	Research internship at the Allan Wilson Institute, Massey University, Palmerston North, New Zealand
04/2007 - 08/2012	PhD at the Dept. of Systems Biology & Bioinformatics, Universität Rostock, Rostock, Germany
07/2008 - 11/2008	Visiting researcher at the Systems Biology Laboratory, KAIST, Daejeon, Republic of Korea

Selbstständigkeitserklärung

Hiermit bestätige ich, dass ich die vorliegende Arbeit selbstständig angefertigt habe. Ich versichere, dass ich nur die angegebenen Quellen und Hilfen in Anspruch genommen habe, und die den benutzten Werken wörtlich oder inhaltlich entnommenen Stellen als solche kenntlich gemacht habe.

Rostock, 27. Februar 2013 Ulf Liebal